ORGANIC SENSITIZERS AND LUMINOGENS FOR OPTOELECTRONIC DEVICES

A Dissertation Presented

by

ŞEBNEM BAYSEÇ

Submitted to Faculty of Mathematics and Natural Sciences of the
Bergische Universität Wuppertal in partial fulfillment
of the requirements for the degree of

DOCTOR DER NATURWISSENSCHAFTEN
(Dr. rer. nat.)

Wuppertal, May 2019

The PhD thesis can be quoted as follows:

urn:nbn:de:hbz:468-20190910-101746-5
[http://nbn-resolving.de/urn/resolver.pl?urn=urn%3Anbn%3Ade%3Ahbz%3A468-20190910-101746-5]

DOI: 10.25926/3txq-wa08
[https://doi.org/10.25926/3txq-wa08]

To My Beloved Family

This work was carried out during the period from January 2014 to November 2017 in the Department of Chemistry, Macromolecular Chemistry Group, Bergische Universität Wuppertal, under the supervision of Prof. Dr. Ullrich Scherf.

This Project has received funding from the European Community's Seventh Framework Programme (FP7/2007-2013) under the Grant Agreements nº 607585 project OSNIRO between 01.2014 to 01.2017 and from Bergische Universität Wuppertal Scholarship between 02.2017-11.2017.

1. **Reviewer: Prof. Dr. Ullrich Scherf**
2. **Reviewer: Prof. Dr. Levent Toppare**
3. **Reviewer: Dr. Christos Chochos**

“All my life through, the new sights of Nature
made me rejoice like a child.”

Marie Skłodowska Curie

ACKNOWLEDGEMENTS

Undertaking this Ph.D. has been a truly life experience for me. Here, I would like to take the opportunity to express my thankfulness to the people for their support and guidance.

Firstly and foremost, I would like to thank to my supervisor, Prof. Dr. Ullrich Scherf, for his support and guidance throughout this work. Moreover, I would like to mention my gratefulness to him for providing me the opportunity to do my Ph.D. in a European Commission project at his Macromolecular Chemistry Research Group in Bergische Universität Wuppertal.

I must specify my gratitude to Prof. Dr. Levent Toppare of the Middle East Technical University as my background from which this thesis stems, I acquired from his research group and also for his acting as a reviewer.

I greatly acknowledge the financial support from European Comission through the Marie Skłodowska-Curie ITN Fellowship Programme between 01.2014-01.2017 and Bergische Universität Wuppertal Scholarship between 02.2017-11.2017.

Through the project OSNIRO, I would like to thank every individual from each project partner for their valuable contributions. Additionally, I would like to thank to Dr. Christos Chochos from Advent Technologies SA, Assoc. Prof. Ergang Wang from Chalmers University of Technology and Prof. Dr. Franco Cacialli from University College London for welcoming me to their working groups during the secondments.

My sincere thanks to Dr. Sybille Allard for her valuable advices, comments, suggestions and support during this time period.

My special thanks to Kerstin Müller for all her help and support during my life in Germany.

I would also like to thank for the helpful discussions and technical support from Dr. Michael Forster, Dr. Eduard Preis, Anke Helfer and Sylwia Adamczyk.

I would like to thank Dr. Andrea Zampetti and Dr. Alessandro Minotto for their contribution to the application of the materials in Organic Electronic.

I owe my deepest thanks to all colleagues in Macromolecular Chemistry Research Group for the fruitful scientific discussions, helps and for get-togethers.

Furthermore, my lovely friend Dr. Gözde Öktem, I am grateful to have a friend like you! It baffles description, but from here I would like to thank you again for everything!

There is one person that I want to thank for every time and every condition he is always with me and supports me, my dear Fiancé; Mustafa Gemci. It would be unfair not to thank to his family and their supports. Thank you for everything you have done for me and Mustafa!

Last but not least, I would like to express my deep gratitude to my parents, Ceyla Nihal and Sedat Bayseç, and my little brother Korhan Bayseç for their support, love and encouragement. I am really lucky to have each of you!

ABSTRACT

ORGANIC SENSITIZERS AND LUMINOGENS FOR OPTOELECTRONIC DEVICES

ŞEBNEM BAYSEÇ

B.Sc., IZMIR INSTITUTE OF TECHNOLOGY

M.Sc., MIDDLE EAST TECHNICAL UNIVERSITY

Ph.D., BERGISCHE UNIVERSITÄT WUPPERTAL

Directed by: Professor Ullrich Scherf

Among the world of materials, organic semiconductors have attracted great attention due to their low cost, easy fabrication, and tunable properties. The development of high-performance organic materials over the past years have led to increase of their investigation and usage in optoelectronic field rapidly. So far, increasing the device efficiencies have been the main issue. From the chemist's point of view, tailoring the properties of materials by facile synthetic modifications to enhance the efficiency of the device and enlarging the application areas is a useful strategy.

In that respect, different synthetic strategies have been applied to reach the desired properties in this thesis. A variety of small molecules and polymers based on Boron-dipyrromethene (BODIPY) and Tetraphenylethylene (TPE) have been synthesized, characterized and properties of the materials with regard to their application in OFETs, fluorescent-based chemical sensors, and OLEDs have been demonstrated. In addition, this thesis provides an overview of recent developments in the field.

TABLE OF CONTENTS

Page

LIST OF TABLES

Table Page

LIST OF FIGURES

Figure Page

LIST OF SCHEMES

Scheme Page

CHAPTER 1

INTRODUCTION

1. General Introduction to Organic Semiconductors

In the early 1920s, Hermann Staudinger demonstrated the existence of macromolecules.[1,2] Due to his studies on the development of macromolecular chemistry, he was awarded Nobel prize in 1953. During the Nobel lecture, he stated, *"I sincerely hope that this great distinction will be the means whereby macromolecular chemistry will undergo further fruitful development."* [3] His pioneering research lead to the birth of polymer chemistry. However, functional polymeric materials did not gain much interest until the synthesis of electrically conducting (conjugated) polymers through halogen doping in 1977.[4-6] This discovery by Alan G. MacDiarmid, Alan J. Heeger, and Hideki Shirakawa was honored with Nobel Prize in 2000.[7-9] Conjugated materials possess the electronic properties of metals or semiconductors as well as mechanical properties of polymer materials.[10-16] Thanks to the combination of these features, utilization of organic materials in the development of electronic devices such as organic light emitting diodes (OLEDs), organic photovoltaic devices (OPVs), organic field effect transistors (OFETs) and chemical sensors, gained significant attention.[17-23]

1.1. Structure of Organic Semiconductors

Organic semiconductors can be defined as the materials which show semiconducting properties and are formed mainly from carbon and hydrogen atoms with a few heteroatoms like sulfur, oxygen, and nitrogen. This wide class of materials comprises π-bonded small molecules and polymers. Typical examples of organic semiconductors are depicted in Figure 1.1. These examples are widely studied on OPVs, OLEDs, and OFETs due to their high charge carrier mobility with very strong absorption and emission in the visible and Near-IR spectral range.[24-31]

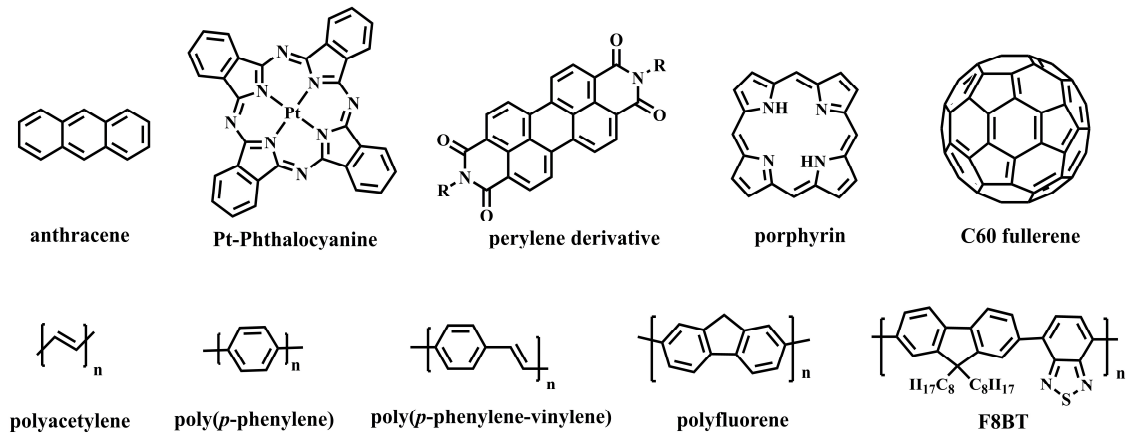

Figure 1.1 Chemical structures of common organic semiconductors.

1.2. Electronic Properties of Organic Semiconductors

1.2.1. π-conjugated systems

The electrical conductivity in organic semiconductors (small molecules and polymers) results from the conjugated π-electron system formed by the p_z orbitals of sp^2-hybridized C atoms in the molecule.[32] The overlap of the two p_z orbitals which forms π-bond as in ethene (Figure 1.2 (a) left), leads to the formation two π molecular orbitals named as bonding and anti-bonding π orbitals and showed with π and π* respectively (Figure 1.2 (a) right). The electrons in the p_z orbital are stabilized by occupying the lower energy π orbital. Similarly, the overlap of the two sp^2 orbitals forms bonding (σ) and anti-bonding (σ*) σ-orbitals with the σ orbitals lower in energy compared to their respective π-orbitals. In long polymer chains (polyacetylene) quasi-continuous bands of occupied and unoccupied states are formed due to the increasing number of sp^2 hybridized carbon atoms, with an energy gap between valence and conduction bands. Highest bonding π-orbital is named as the highest occupied molecular orbital (HOMO), and the lowest anti-bonding π*-orbital is named as the lowest unoccupied molecular orbital (LUMO) while the energy difference defined as band gap (E_g). The energy gap (E_g) reduces as the extent of conjugation increases (Figure 1.2 (b)). For organic semiconductors E_g is typically between ~1.2-3.5 eV depending on the chemical structure of the π-conjugated main chain (see Figure 1.1) and covers the infrared to ultraviolet region of the spectrum.

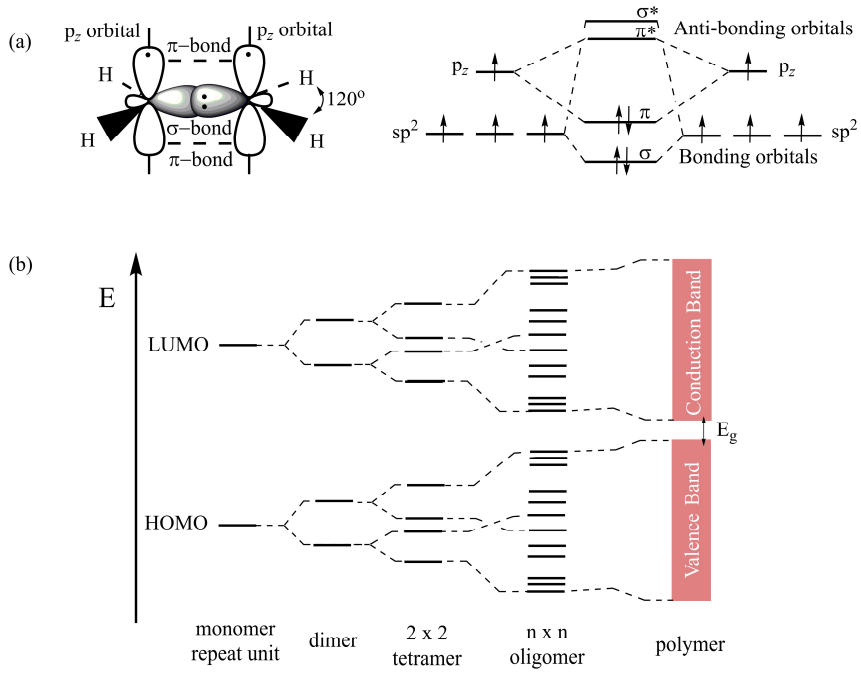

Figure 1.2 (a) Left: σ and π bonds in ethane. Right: Schematic representation of bonding and anti-bonding orbitals (b) Band formation from molecular repeat units in a π-conjugated polymer. (Resketched images.[33,34])

1.2.2. Excited states and charge transport

The electronic properties of a molecule strongly depend on the so-called conjugation length and the presence of electron donating or withdrawing groups. As the conjugation length increases, π-electron delocalization is extended which is described as resonance bonding. Thus, electrons are free to move along the carbon backbone with this resonance interactions and form electrical conductivity. However, in case of polymers, this process is often disrupted by intrinsic or dynamical defects. [35,36]

There are some effective methods that lead to charge carriers in organic semiconductors:

- ◊ Oxidation or reduction
- ◊ Charge injection
- ◊ Photoinduced charge transfer

In case of π-conjugated systems built up by aromatic repeat unit the ground state equilibrium geometry (benzoid-like geometry) of the molecule changes to quinoid-like geometry by bond alternation in the presence of a net charge. This distribution forms quasi-particles (electron or hole) known as polarons, that can move across the polymer chain and influence the charge transport. Additionally, they create mid-states in the energy gap

(Figure 1.3). Polarons can be either positive or negative; in case of radical cation, positive polarons are formed while negative polarons are formed in case of the radical anion. When two polarons of the same sign bound weakly, they forms bipolarons. As the lattice relaxation of two charges is stronger than one charge, mid-states in energy gap occur, even further away from valence and conduction band (Figure 1.3).

Neutral quasi-particles which are generated by photoexcitation are named as excitons. There are different types of excitons due to different binding energy between the electron and hole (Frenkel and Wannier-Mott excitons).[37] These excitons can decay radiatively or non-radiatively. The detailed explanation will be given in section 1.3. In donor-acceptor (D-A) systems there is an intermediate state named charge-transfer state (CT state). In this state, the exciton is an intermediate between Frenkel-type and Wannier-Mott-type excitons. In charge-transfer excitons, the electron and hole are separated but still tightly bound.

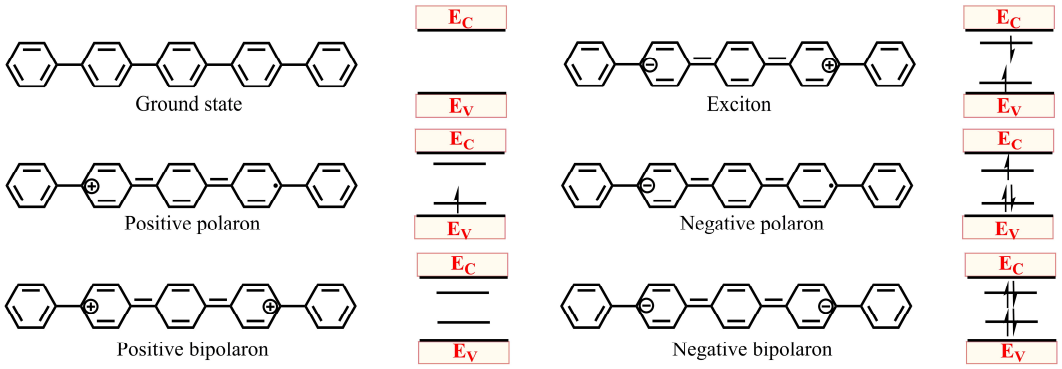

Figure 1.3 Illustration of structural changes of poly(p-phenylene) in the presence of a net charge and difference of mid-states in the energy gap.

1.3. Optical Properties of Organic Semiconductors

1.3.1. Jablonski diagram

As stated in the previous section, the excitons which are formed by photoexcitation can decay radiatively or non-radiatively. Light absorption and emission processes are often described using the so-called Jablonski diagram (Figure 1.4).

Due to absorption of a photon, the electron in the ground state S_0 is promoted to a corresponding vibrational levels of the excited state S_1 or S_2. This vertical transition from S_0 to S_1 is described as absorption, and it occurs in about 10^{-15}s. The excited electron (exciton) relaxes to the lowest vibrational level of excited state (Kasha's rule) by non-

radiative internal conversion (IC) process within 10^{-12} s. From the lowest vibrational level of excited state to ground state, the exciton relaxes by a non-radiative or radiative processes. The non-radiative and radiative processes are indicated with dashed and solid lines respectively in the Jablonski diagram (Figure 1.4).

The radiative relaxation process of the photoexcited conjugated systems is defined as photoluminescence (PL) and can occur in two ways: fluorescence and phosphorescence. If the exciton at the excited singlet state (S_1) is paired by the opposite spin electron at the ground-state (S_0), the emission of light is called fluorescence. Typical fluorescence lifetimes are near 10^{-8} s.

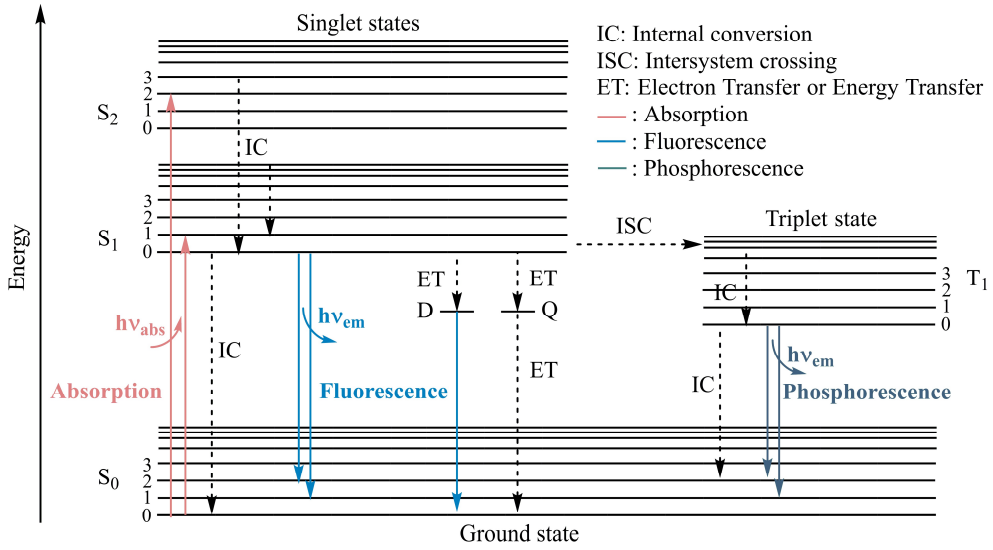

Figure 1.4 Jablonski diagram. Radiative and non-radiative decays are represented by solid and dashed lines respectively. Detailed information is reported in the text.

The exciton at the excited singlet state can also undergo a spin conversion to the triplet state (T_1) resulting in the same spin orientation as the ground-state. This conversion from S_1 to T_1 is named as intersystem crossing (ISC). Alternative relaxation process occurs between T_1 to S_0 which is called phosphorescence. Since this transition is spin-forbidden it occurs slower than fluorescence. The average lifetime of phosphorescence emission is between milliseconds to seconds (10^{-3} to 10^{0} s).[38]

Besides fluorescence, internal conversion, intersystem crossing and phosphorescence, the exciton at the excited singlet state (S_1) can be relaxed by electron or energy transfer (ET) to a fluorescence quenching defect or an acceptor molecule or analyte (Q) or an emissive defect (D).

1.3.2. Intra- and inter-chain interactions

Until now, the photophysical properties of a chromophore has been represented as an ideal sample which is dissolved in a good solvent and exhibited no other interactions with its surroundings. The primary photoexcitation of an ideal sample is an intrachain singlet exciton which migrates through the chromophore by a one-dimensional random path and relaxes back to the ground state by fluorescence or another deactivation process such as electron transfer to a quenching analyte or defect (Q/D).

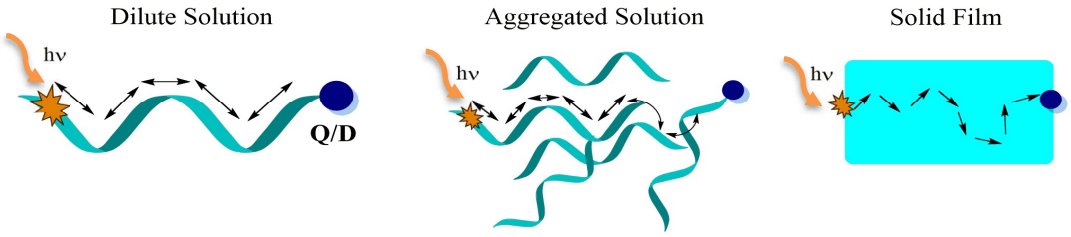

Figure 1.5 Representation of exciton migration of a chromophore in dilute solution, an aggregated solution, and a solid film.

However, two or more chromophores can interact and absorb or emit light in a cooperative manner. This interaction in the ground state forms a molecular complex named as aggregate. In aggregated solutions, interchain exciton migrations become possible due to the close distance between the chromophores. As the number of exciton migration pathway increase, exciton migration efficiency can be enhanced.[39,40]

In a solid film state, aggregates are placed in very close contact with many other chains. Therefore, excitons can move even more freely in a three-dimensional random path. This leads to more enhanced exciton migration efficiency before it relaxes.

1.4. Macromolecular Design

Tailoring organic semiconductors for specific applications and aims can be achieved by structural modifications of the conjugated backbone and the pendant side-chains. This modular approach provides an easy way to tune the physical and optical properties of the materials. In the following chapters of this thesis, different structural modifications are discussed to achieve distinct aims and applications by this approach. However, in this chapter, the general design principles due to electronic, optical and

morphological properties are going to be explained briefly which is essential to improve the performance of organic electronics.

1.4.1. Mobility

The performance of the devices extremely depends on the efficiency of charge carriers movement along the π-conjugated systems; in other words, the charge carrier mobility. High mobility is achieved by charges moving from molecule to molecule (intramolecular and intermolecular charge transport) without any trapping or scattering. Rigid and planar chains with few defects lead the overlap of orbitals (2D π-stacking) that makes well-suited to good charge transport.[41]

Crystallinity also leads to high mobility properties by minimizing the number of defects and supporting the stacking of chains which also facilitates inter-chain charge transport. Large crystalline domains can be achieved by annealing the film and by slow crystallization.[42-44] In preferred case, crystallization should be in the direction of charge transport that promotes band transport toward the electrodes. Sandberg *et al.* investigated[45] that in poly(3-hexylthiophene) (P3HT) the formation of π-π stacking parallel to the substrate is the favoured orientation in a thin film transistor. Furthermore, similar results were found for other regioregular conjugated polymers.[46]

1.4.2. Frontier molecular orbital (FMO) energy levels

The energy levels of materials, HOMO and LUMO, determine the electron donating and accepting tendencies. Different substituents in a given material affect these energy levels and directly influence the band gap. Electron donating groups tend to increase the HOMO level and decrease the band gap. Moreover, higher HOMO corresponds to lower ionization potential and lower energy necessary to extract an electron from the π-system. The electron withdrawing groups generally reduce the LUMO level and make the molecule more stable in air by increasing the energy needed to remove electrons from the LUMO. For the applications OLEDs and OFETs, suitable HOMO and LUMO energy levels are required to have efficient electron and hole injection from electrodes.

1.4.3. Conjugation length and band gap

The other principal way to modify the frontier orbital energies is enlarging the π-orbital systems.[47] This method is highly effective in reducing the band gap and increasing the HOMO energy level. In agreement with an increase of HOMO energy levels, the oxidation potential decreases as the conjugation length increases.[48-51]

The absorption maximum of the lowest energy transition is red-shifted in wavelength with increasing the conjugation length. The relationship is explained mathematically by Meier *et al.*[52] Their equations allow for a determination of the effective conjugation length (value for *n*), at which a property (e.g. the lowest energy absorption wavelength) saturates for a given repeated unit structure.

Another relationship between conjugation length and hopping conductivity is presented by Baughman and Shacklette.[53,54] The work showed that intra- and interchain conductivity varies with conjugation length.

For the application in OPVs, the energy difference between HOMO of donor and LUMO of acceptor significantly influence the open circuit voltage (V_{oc}) of devices. Additionally, the energy gap between LUMOs of donor and acceptor strongly effects the exciton dissociation. In case of OLEDs applications, the emitting colour can be tuned by conjugation length and by altering the energy gap between HOMO and LUMO.

1.4.4. Solubility

Conjugated materials are relatively rigid molecules due to the double bonds in their molecular structure which limits their flexibility and solubility. However, solubility is an essential parameter for organic materials due to the need for applicable low-cost processing techniques such as spin or spray casting, inkjet printing, and other roll-to-roll methods. In order to improve solubility, alkyl side chains are affixed to the backbone of the molecules. The material is becoming processible due to a disruption of π-π stacking interactions during dissolution by these side chains. Nevertheless, the material should have a significant π-π stacking interaction in the solid-state to maintain the desired optoelectronic properties.

The side chains show various effects depending on their type, shape (linear or branched) and length, therefore, they need to be chosen accordingly. While nonpolar alkyl chains allow solubility in and processability from organic solvents, side chains such as oligoether chains or carboxylate terminated alkyl chains provide solubility in and

processability also from polar solvents. Generally, longer and branched side chains improve solubility. However, the use of oversized side chains can cause too much steric hindrance that may disturb the conjugation of the backbone. Besides that, intermolecular packing and morphology are affected by the shape and length of the side chains and accordingly influence the device performance, especially for OFETs and OPVs.

1.5. Organic Electronics

The evaluation and development of organic semiconductors have been followed by the research on thin-film devices using these materials. The research has been aiming to minimize device size and electronic mismatch effects, increasing yield, simplifying the process, and reducing the manufacturing costs. As a result, small organic molecules and conjugated polymers start to become an integral unit in the progress of new electronic devices. Sensors, OLEDs, OPVs, OFETs, organic lasers, photodetectors, flexible displays, and batteries are the main application areas of organic electronics.

In this thesis, the synthesized polymers and small molecules are used in fluorescence-based chemical sensors, OFET and OLED applications. So, in the following these applications are briefly explained.

1.5.1. Organic field effect transistors

Field effect transistors (FETs) are the most important and the fundamental components in semiconducting devices. Organic and inorganic materials have been integrated into transistors. However, the possible low-cost fabrication, light-weight, flexibility, and compatibility with heat sensitive substrates such as plastics favoured the research on organic materials and their usage in FETs. The first pioneering research on OFETs started in 1983 by Ebisawa[55] and continued in 1986 with Tsumura's study[56] on OFETs based on polythiophene with the mobility of 10^{-5} $cm^2V^{-1}s^{-1}$. As a small-molecule semiconductor, pentacene was applied in OFETs and achieved high carrier mobility of 1.5 cm^2 $V^{-1}s^{-1}$ in 1997.[57] In the recent study of Huang and Bao, mobilities between 90~118 $cm^2V^{-1}s^{-1}$ were observed with the reproducible mobility up to 43 $cm^2V^{-1}s^{-1}$ which is the highest reported values for small-molecular organic semiconductors.[58]

In principle, an OFET consists of three elements: one semiconducting layer, one insulating layer (dielectric layer) and the electrical connections (gate (G), source (S), and drain (D)). The insulating layer separates the gate from the semiconducting layer, while the

source and drain contacts are directly connected to the semiconducting layer. When the voltage is applied to the gate, charges in the semiconducting layer are induced, and an electrical current is generated between source and drain.

FETs are divided into three categories based on the majority charge carriers; p-type (holes), n-type (electrons) and ambipolar. Additionally, different deposition orders of the device layers lead to different device architectures. According to the gate position and contact between drain/source and semiconducting layer, there are four possible device configurations (Figure 1.6) namely, (a) bottom-gate top-contact (BGTC), (b) bottom-gate bottom-contact (BGBC) which are mainly used for p-type materials, whereas (c) top-gate top-contact (TGTC), and (d) top-gate bottom-contact (TGBC) geometries are used for n-type and ambipolar OFETs to reduce the influence of oxygen and water.

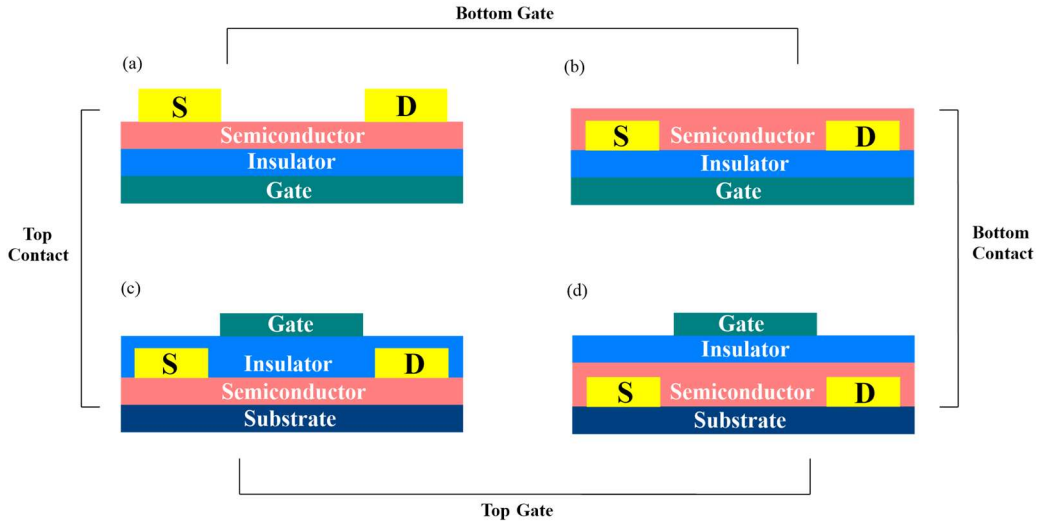

Figure 1.6 Device architectures of OFETs. (a) bottom-gate top-contact (b) bottom-gate bottom-contact (c) top-gate top-contact (d) top-gate bottom-contact.

In general, two electrical characterization methods applied on OFETs are:

1) To obtain output characteristics: Applying constant gate voltage (V_{GS}), scanning drain-source voltage (V_{DS}) and measuring drain-source current (I_{DS}) simultaneously. (Figure 1.7 a)
2) To obtain transfer characteristics: Applying constant drain-source voltage (V_{DS}/V_D), scanning gate voltage (V_{GS}/V_G) and measuring the drain-source current (I_{DS}). (Figure 1.7 b)

The key parameters for an OFET which uses novel materials are; charge carrier mobility (μ), current on/off ratio (I_{ON}/I_{OFF}), and threshold voltage (V_T). The charge carrier mobility (μ) is a bulk property of a material which brings a quantitative definition of the velocity of the charge carriers when an electric field is applied. The current on/off ratio (I_{ON}/I_{OFF}) is a measure of the quality of a transistor which is the ratio of the highest source-drain current to the minimal current when the gate voltage is increased gradually from 0 V upwards. The threshold voltage (V_T) is the gate voltage which is required for the formation of charge carriers in the conduction channel.

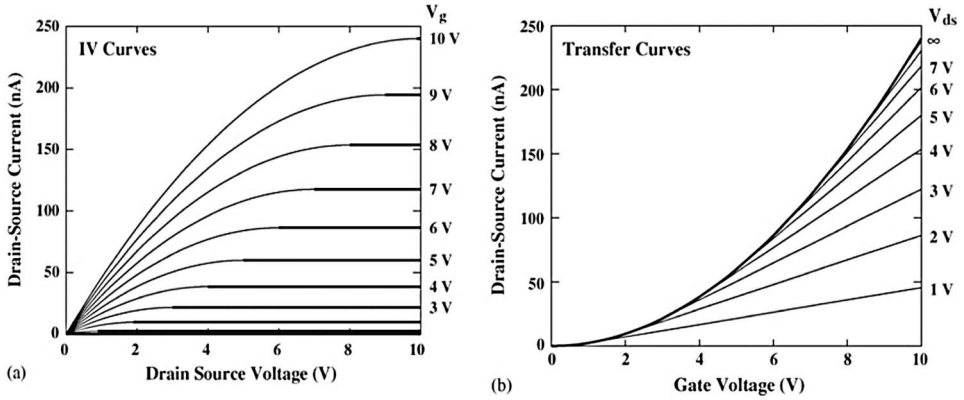

Figure 1.7 Representative characteristics of a typical OFET (a) output characteristic (b) transfer characteristic.[59]

1.5.2. Fluorescence-based chemical sensors

A sensor is a transducer that converts a physical or a (bio)chemical quantity into an electric or optical signal while detecting the measurand. In the design of chemical sensors, the selection of sensitive and selective materials with a low detection limit is a critical point. According to the highly sensitive optical change (fluorescence quenching or enhancement, wavelength shift) upon analyte binding, fluorescence-based sensors have gained significant importance. Among the fluorescent materials, conjugated polymers provide efficient electronic communication and an extended exciton migration, thereby amplifying the response signal, if compared to small molecules. This amplification was first proposed by Swager and Zhou[60] in 1995 as "molecular-wire" effect (Figure 1.8) using a poly(phenyleneethynylene) containing cyclophane-based receptors in comparison to individual receptor-chromophore phenylene ethyne chromophores.

There are several mechanisms which induce fluorescence quenching in fluorescence-based sensors such as photoinduced electron transfer, resonance energy transfer, electron exchange, etc.[61]

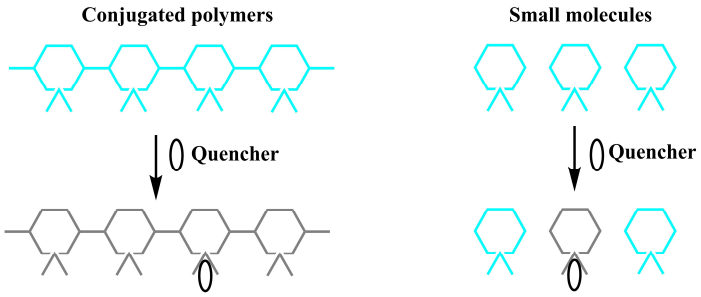

Figure 1.8 Illustration of the "molecular wire" theory.[60]

For example, interaction of the electron-deficient species and the electron-rich polymer backbone induces nonradiative excitation decay. One possible mechanism of the fluorescence quenching is illustrated in Figure 1.9. Upon the excitation of a conjugated polymer, an electron transfer from the valence band to conduction band can take place. The exciton can, thereby, migrate through the polymer. In the presence of the analyte, the electron is transferred to the low-lying LUMO of the analyte. Here, a significant fluorescence quenching occurs since the polymer-based excited state is disrupted and the polymer is no longer fluorescent. As a result, electron is transferred from the LUMO of the analyte to the valence band of the polymer accompanied by a non-radiative deactivation process.

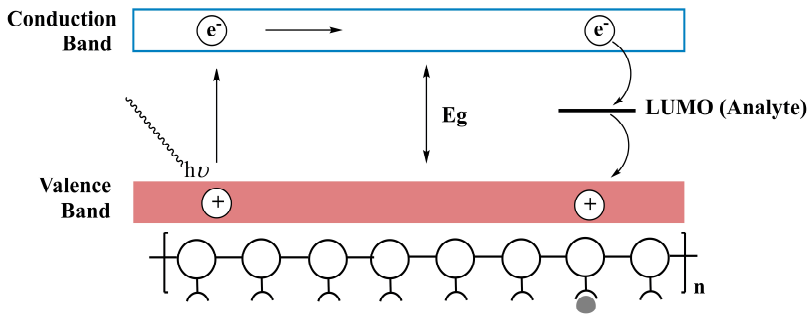

Figure 1.9 Band diagram representation of the exciton transport and electron transfer-induced fluorescence quenching in a fluorescence-based sensor.

1.5.3. Organic light emitting diodes

As a simple definition, organic light emitting diodes are electroluminescent devices composed of multiple organic layers between the electrodes. Organic light emitting diodes have been the focus of intense research in academia and industry over the last decades. With the recent advances in materials and engineering techniques, OLEDs have become the ideal candidates for next-generation display and solid-state lighting technologies. Even though the early device structure was reported in 1963 by Pope *et al.*[62], the breakthrough device performance was achieved by Tang and VanSlyke[63] in 1987. This improvement was achieved by using a two-layer organic stack of a hole transport layer (HTL) and an electron transport layer (ETL) between anode (ITO) and cathode (silver). Further remarkable progress in the OLED research came in 1998 by Forrest and Thompson with the introduction of phosphorescent emitters by using both singlet and triplet excited states' contribution to the luminescence[64].

The basic device configuration and working principle of an OLED is illustrated in Figure 1.10. When an external voltage is applied, electrons are injected from the cathode and holes are injected from the anode. While electrons are transported through the LUMO of the ETL, holes are transported through the HOMO of the HTL. Recombination of the transported electrons and holes via Coulomb interaction forms excitons. The light is emitted through a semitransparent anode or cathode of the device, when the excitons decay and release their energy by photon emission. In case of a radiative exciton decay electroluminescence (EL) occurs.

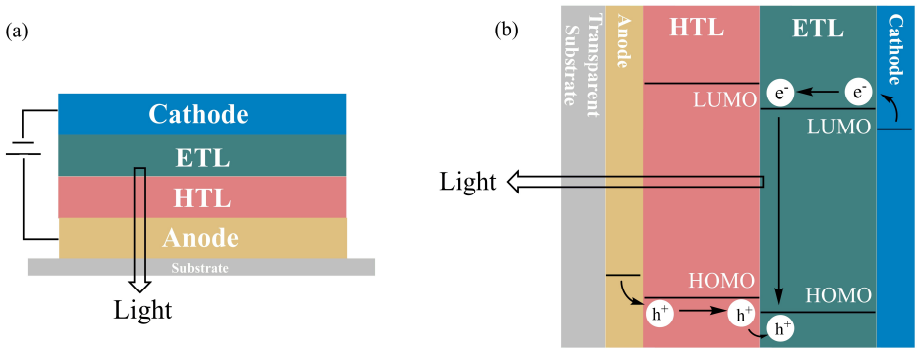

Figure 1.10 A basic OLED (a) device structure and (b) working principles.

An OLED is characterized according to optical and electrical properties as follows:

1) For electrical characterization; the direct relationship between current (I) and voltage (V) is used. This characterization allows to model OLEDs behaviour in an electrical circuit. (Figure 1.11 b)
2) Radiometry is used to measure the emitted light intensity from an OLED. This emission intensity is measured as radiance (R) (Wm^{-2}).
3) For electro-optical characterization; the radiance (R) emitted by OLED upon the forward voltage (V) is measured (Figure 1.11 b). In the presence of two emitters in an OLED, electroluminescence (EL) spectra measurements are used to differentiate the minority carrier current between emitting layers. Additionally, EL spectra measurements can record the spectral differences between photoluminescence (PL) and electrical excitation (Figure 1.11 a). The quantum efficiency of an OLED is the ratio of the number of emitted photons to the number of injected charge carriers (Figure 1.11c).

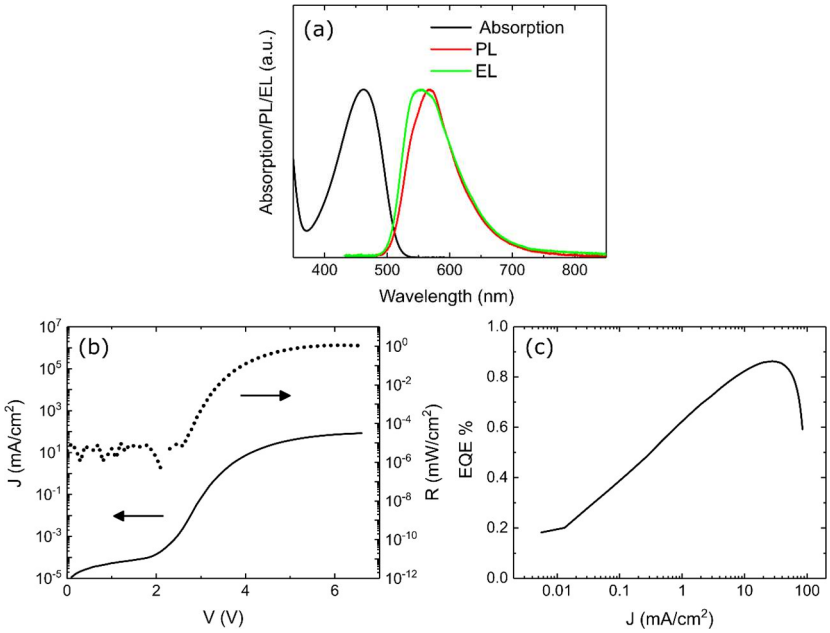

Figure 1.11 (a) Absorption, PL and EL spectra of F8BT from a 100 nm solid-state thin film, deposited from a 10 mg/mL toluene solution. (b) JVR characteristics and (c) EQE versus current density of an undoped F8BT OLED.[65]

1.6. Motivation and Aim of Work

The main focus of this thesis is the synthesis of new emissive materials by following two lines: (1) Structural modifications of BODIPY-based small molecules and polymers, and (2) Search for highly emissive polymers with Aggregation-Induced Emission (AIE), both with the focus on an optimization of the materials' properties.

Chapter 2 presents modifications of BODIPY dyes by fusion with aromatic rings at their "zig-zag" edge in order to shift the absorption into the NIR region. Such a strategy may help in overcoming the spectral mismatch in the solar energy conversion and provide additional benefits in sensing and detection applications. In this chapter the incorporation of NIR BODIPY derivative together with different donor units resulted in D-A type conjugated copolymers. The synthesized polymers were characterized optically and electrochemically. The polymers were tested as semiconductor layer in n-type OFET devices.

Chapter 3 shows a study on Aggregation-Induced Emission (AIE) properties of Poly(tetra-phenylethylene) (Poly(TPE)) derivatives. Many fluorophores show aggregation-caused quenching (ACQ) in the solid-state which limits their application. However, the AIE phenomenon can overcome the ACQ effect and enhance the solid-state fluorescence emission. The variation of the main chain arylene units (para- or meta-phenylene, phenylene-oxyphenylene), and of the aryl rotors was, hereby, investigated. The copolymer with the highest photoluminescence quantum yield in the solid-state was tested as sensing material for PL-quenching-based detection of nitroaromatic analytes.

Chapter 4 presents the combination of the AIE phenomenon and NIR emission in TPE-BODIPY derivatives. Thanks to this combination, high solid-state emission was achieved while conserving the optical properties of the chromophore species. This study provides a systematic investigation of substitution effects (alkyl substituents, number of TPE units) in small molecules and polymers. The remarkable solid-state emission properties of TPE-BODIPY small molecules were utilized in far red/NIR emitting and solution-processed OLEDs.

1.7. References

1. H. Staudinger, *Ber. Deut. Chem. Ges.* **1920**, *53*, 1073.
2. H. Staudinger, *Chem. Ztg.* **1953**,*77*, 679.
3. H. Staudinger, *Nobel Lectures, Chemistry 1942-1962*, **1953**, Elsevier Publishing Company: Amsterdam, 1964.
4. H. Shirakawa, E. J. Louis, A. G. MacDiarmid, C. K. Chiang, A. J. Heeger, *J. Chem. Soc. Chem. Commun.* **1977**, 578.
5. C. K. Chiang, C. R. Fincher, Y. W. Park, A. J. Heeger, H. Shirakawa, E. J. Louis, S. C. Gau, A. G. MacDiarmid, *Phys. Rev. Lett.* **1977**, *39*, 1098.
6. C. K. Chiang, M. A. Druy, S. C. Gau, A. J. Heeger, E. J. Louis, A. G. MacDiarmid, Y. W. Park, H. Shirakawa, *J. Am. Chem. Soc.* **1978**, *100*, 1013.
7. H. Shirakawa, *Angew. Chem. Int. Ed.* **2001**, *40*, 2575.
8. A. G. MacDiarmid, *Angew. Chem. Int. Ed*. **2001**, *40*, 2581.
9. A. J. Heeger, *Angew. Chem. Int. Ed.* **2001**, *40*, 2591.
10. J. L. Bredas, R. Silbey, Eds., Conjugated Polymers: The Novel Science and Technology of Highly Conducting and Nonlinear Optically Active Materials; *Kluwer Academic Publishers:* Boston, **1991**.
11. H. G. Kiess, D. Baeriswyl, Eds., Conjugated Conducting Polymers; *Springer-Verlag:* New York, **1992**.
12. N. N. Barashkov, A. Gunder, Fluorescent Polymers; *Ellis Horwood*: NewYork, **1993**.
13. W. R. Salaneck, I. Lundstrom, B. G. Ranby, Eds., Conjugated Polymers and Related Materials: The Interconnection of Chemical and Electronic Structure; *Oxford University Press:* New York, **1993**.
14. P. Bernier, S. Lefrant, G. Bidan, Eds., Advances in Synthetic Metals: Twenty Years of Progress in Science and Technology; *Elsevier:* New York, **1999**.
15. S. Roth, D. Carroll, One-Dimensional Metals: Conjugated Polymers, Organic Crystals, Carbon Nanotubes, 2nd ed.; *Wiley-VCH:* Weinheim, **2004**.
16. T. A. Skotheim, R. L. Elsenbaumer, J. R. Reynolds, Eds., Handbook of Conducting Polymers, 3rd ed.; *CRC Press:* New York, **2007**.
17. Y. J. Cheng, S. H. Yang, C. S. Hsu, *Chem. Rev.* **2009**, *109*, 5868.

18. A. C. Grimsdale, K. L. Chan, E. R. Martine, P. G. Jokisz, A. B. Holmes, *Chem. Rev*. **2009**, *109,* 897.
19. P. M. Beaujuge, J. R. Reynolds, *Chem. Rev*. **2010**, *110*, 268.
20. S. Gfines, H. Neugebauer, N. S. Sariciftci, *Chem. Rev*. **2007**, *107*, 1324.
21. D. T. McQuade, A. E. Pullen, T. M. Swager, *Chem. Rev*. **2000**, *100*, 2537.
22. T. M. Swager, *Acc. Chem. Res*. **1998**, *31*,201.
23. S. W. Thomas III, G. D. Joly, T. M. Swager, *Chem. Rev*. **2007**, *107*, 1339.
24. K. Müllen, U. Scherf, Organic light emitting devices; *Wiley Online Library*, **2006**.
25. G. Grem, G. Leditzky, B. Ullrich, G. Leising, *Adv. Mater*. **1992**, *4*, 36.
26. A. Kraft, A. Grimsdale, A. Holmes, *Angew. Chem*. **1998**, *37*, 402.
27. U. Scherf, E. List, *Adv. Mater*. **2002**, *14*, 477.
28. C. Brabec, U. Scherf, V. Dyakonov, Organic photovoltaics: materials, device physics, and manufacturing technologies; *John Wiley & Sons*, **2014**.
29. H. Hoppe, N. S. Sariciftci, *J. Mater. Chem*. **2006**, *16*, 45.
30. M. Caironi, Y.-Y. Noh, Large Area and Flexible Electronics; *Wiley-VCH*, **2015**.
31. J. Liu, H. Zhang, H. Dong, L. Meng, L. Jiang, L. Jiang, Y. Wang, J. Yu, Y. Sun, W. Hu, A. J. Heeger, *Nat. Commun.* **2015**, *6*, 10032.
32. S. Schols, Device architecture and materials for organic light-emitting devices; *Springer*, **2011**.
33. P. Kumar, Organic Solar Cells: Device Physics, Processing, Degradation, and Prevention; *CRC Press*: Boca Raton, FL, **2017**.
34. R. Gutzler, *Phys. Chem. Chem. Phys*. **2016**, *18*, 29092.
35. J. Cornil, D. Beljonne, J. P. Calbert, J. L. Bredas, *Adv. Mater.* **2001**, *13*, 1053.
36. E. Collini, G. Scholes, *Science*, **2009**, *323*, 369.
37. M. Pope, C. Swenberg, Electronic processes in organic crystals and polymers; *Oxford University Press*: New York **1999**.
38. J. R. Lakowicz, Principles of Fluorescence Spectroscopy, 2nd ed.; *Kluwer Academic/Plenum*: New York, **1999**.
39. I. A. Levitsky, J. Kim, T. M. Swager, *J. Am. Chem. Soc*. **1999**, *121*, 1466.
40. E. Hennebicq, G. Pourtois, G. D. Scholes, L. M. Herz, D. M. Russell, C. Silva, S. Setayesh, A. C. Grimsdale, K. Müllen, J. L. Brédas, D. Beljonne, *J. Am. Chem, Soc.* **2005**, *127*, 4744.

41. T. Nishinaga, Organic Redox Systems, 1st ed.; *John Wiley & Sons, Inc*: Hoboken, New Jersey, **2016**.
42. Y. Kim, S. Cook, S. M. Tuladhar, S. A. Choulis, J. Nelson, J. R. Durrant, D. D. C. Bradley, M. Giles, I. McCulloch, C. S. Ha, M. Ree, *Nat. Mater.* **2006**, *5*, 197.
43. I. McCulloch, M. Heeney, C. Bailey, K. Genevicius, I. MacDonald, M. Shkunov, D. Sparrowe, S. Tierney, R. Wagner, W. Zhang, M. L. Chabinyc, R. J. Kline, M. D. McGehee, M. F. Toney, *Nat. Mater*. **2006**, *5*, 328.
44. R. J. Kline, M. D. McGehee, M. F. Toney, *Nat. Mater*. **2006**, *5*, 222.
45. H. G. O. Sandberg, G. L. Frey, M. N. Shkunov, H. Sirringhaus, R. H. Friend, M. M. Nielsen, C. Kumpf, *Langmuir* **2002**, *18*, 10176.
46. B. S. Ong, Y. Wu, Y. Li, P. Liu, H. Pan, *Chem. Eur. J.* **2008**, *14*, 4766.
47. J. Gierschner, J. Cornil, H. J. Egelhaaf, *Adv. Mater*. **2007**, *19*, 173.
48. J. J. Apperloo, J. M. Raimundo, P. Frère, J. Roncali, R. A. J. Janssen, *Chem. Eur. J*. **2000**, *6*, 1698.
49. J. J. Apperloo, L. B. Groenendaal, H. Verheyen, M. Jayakannan, R. A. J. Janssen, A. Dkhissi, D. Beljonne, R. Lazzaroni, J. L. Brédas, *Chem. Eur. J.* **2002**, *8*, 2384.
50. C. Lin, T. Endo, M. Takase, M. Iyoda, T. Nishinaga, *J. Am. Chem. Soc*. **2011**, *133*, 11339.
51. M. Turbiez, P. Frère, J. Roncali, *J. Org. Chem*. **2003**, *68*, 5357.
52. H. Meier, U. Stalmach, H. Kolshorn, *Acta Polym.* **1997**, *48*, 379.
53. R. H. Baughman, L. W. Shacklette, *Phys. Rev. B*, **1989**, *39*, 5872.
54. R. H. Baughman, L. W. Shacklette, *J. Chem. Phys*. **1989**, *90*, 7492.
55. F. Ebisawa, T. Kurokawa, S. Nara, *J. Appl. Phys.***1983**, 54, 3255.
56. A. Tsumura, H. Koezuka, T. Ando, *Appl. Phys. Lett*. **1986**, *49*, 1210.
57. D. J. Gundlach, Y. Y. Lin, T. N. Jackson, S. F. Nelson, D. G. Schlom, *IEEE Electr. Device L.* **1997**, *18*, 87.
58. Y. Yuan, G. Giri, A.L. Aynzer, A.P. Zoombelt, S.C. Mannsfeld, J. Chen, D. Nordlund, M.F. Toney, J. Huang, Z. Bao, *Nat. Commun*. **2014**, *5*, 3005.
59. H. L. Gomes, G. Nisato, D. Lupo, S. Ganz, Eds., Organic Field Effect transistors: Organic and Printed Electronics (pp. 147-198); *Pan Standford Publishing*: Singapore, **2016**.
60. Q. Z. Zhou, T. M. Swager, *J. Am. Chem. Soc*., **1995**, *117*, 12593.

61. J. R. Lakowicz, Principles of Fluorescence Spectroscopy; *Springer*: Singapore, **2006**.
62. M. Pope, H. P. Kallmann, P. J. Magnante, *J. Chem. Phys*. **1963**, *38*, 2042.
63. C. W. Tang, S. A. VanSlyke, *Appl. Phys. Lett*. **1987**, *12*, 913.
64. M.A. Baldo, D.F. O'Brien, Y. You, A. Shoustikov, S. Sibley, M. E. Thompson, S. R. Forrest, *Nature* **1998**, *395*, 151.
65. S. Baysec, A. Minotto, P. Klein, S. Poddi, A. Zampetti, S. Allard, F. Cacialli, U. Scherf, *Sci. China Chem.* **2018**, *61*, 932.

CHAPTER 2

RING-FUSED BODIPY-BASED POLYMERS

2.1. Introduction

Near-Infrared (NIR) absorbing and emitting π-conjugated organic materials have great potential in optoelectronic devices which serve for civilian and defense applications such as thermal imaging, health monitoring, optical communication, chemical/biological sensing.[1,2] During the development of new materials, well-understood structure-property-relationship should result in better device performances.

BODIPY gained a lot of attention during the last years due to their outstanding structural and optoelectronic properties like easily modifiable molecular backbone[3] which enables to reach the NIR region easily, large molar absorption coefficient[4] (40000 to 110000 $M^{-1}cm^{-1}$), high fluorescence quantum yield[5], and excellent chemical and photochemical stability[6].

To this end, NIR-absorbing organic materials have been synthesized, based on anthracene-fused BODIPY units that are incorporated into novel copolymers with different types of electron-rich comonomer unit as linkers. In addition to the synthesis, this study presents the investigation of optical and electronic properties of the resulting low band gap copolymers which exhibit absorption bands up to 1200 nm. Finally, the semiconducting properties of these copolymers were explored in n-channel OFETs.

In the following sections of the introduction, an overview to the BODIPY fluorophore, strategies to achieve absorbing in the NIR region and recent progresses in the literature about OFET applications are briefly explained.

2.1.1. General overview on Boron-dipyrromethene (BODIPY) as a fluorophore

BODIPY fluorophores are a class of dye molecules, referring to 4,4-difluoro-4-bora-3a,4a-diaza-*s*-indacene in IUPAC nomenclature. The structure is formed by the complexation of BF_2 with dipyrromethene. The formed N-B-N bridge at the dye molecule

forces planarity of the π-electrons system where the positive charge is delocalized between the two nitrogen atoms at this bridge as illustrated resonance structure in Figure 2.1 (b). The structure of BODIPY dye and its functional positions are shown in Figure 2.1 (a).

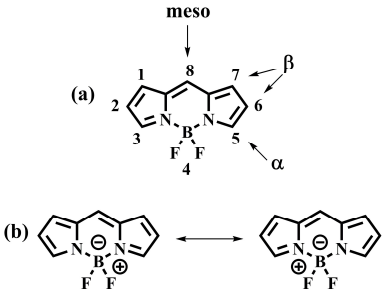

Figure 2.1 (a) The structure of BODIPY core and its IUPAC numbering system, (b) The two equivalent zwitterionic resonance structures of BODIPY.

The BODIPY dye and its derivatives have extraordinary photophysical properties like sharp absorption and emission peaks, high fluorescence quantum yields, high molar extinction coefficients, insensitivity to solvent polarity and pH, thermal-, chemical- and photochemical stabilities. Figure 2.2 shows the unsubstituted BODIPY core's absorption and emission spectra.[7]

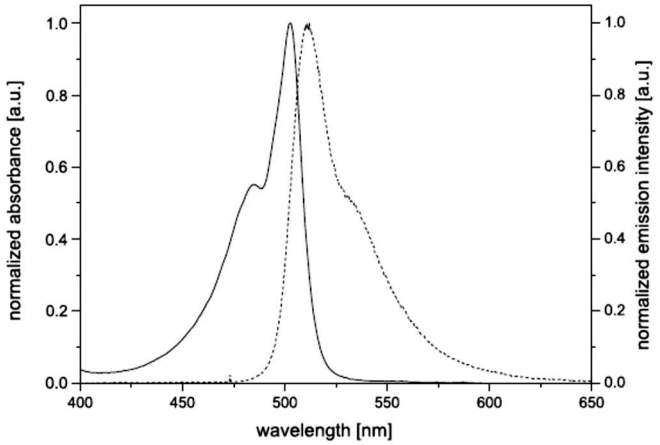

Figure 2.2 Normalized absorption and emission of the unsubstituted BODIPY core in dichloromethane (DCM).[7]

Owing to these properties, BODIPY dye gains significant importance and its derivatives are applied in a variety of applications, such as solar cells[8-11], chemical sensors[12-14], laser dyes[15], fluorescent switches[16,17], photodynamic therapy[18].

2.1.2. General methodologies to the synthesis of BODIPY

The BODIPY dyes were first synthesized in 1968 by Treibs and Kreuzer.[19] In terms of the general synthetic method of a symmetric BODIPY core, there are two distinct ways which are based on methods of porphyrin chemistry.[20]

The first synthetic pathway (Scheme 2.1) uses pyrroles and aldehydes in the presence of an acid as the catalyst. As the intermediate dipyrromethane compounds are unstable and sensitive to light and air, the reactions generally take place as a one-pot reaction. The dipyrromethane compounds are oxidized with 2,3-dichloro-5,6-dicyano-1,4-benzoquinone (DDQ) or *p*-chloranil in order to form dipyrromethenes. The oxidant is chosen according to the reactivity of dipyrromethanes.[3,21,22] DDQ is a much stronger oxidant compared to *p*-chloranil and is used for dipyrromethanes which are highly substituted and only oxidizable under harsh conditions. The BODIPY framework forms after the addition of a base (a tertiary amine) and boron trifluoride diethyl etherate ($BF_3 \cdot OEt_2$) as Lewis acid. Even though this method requires one more step compared to the second one to form dipyrromethene, it is still more direct and convenient.

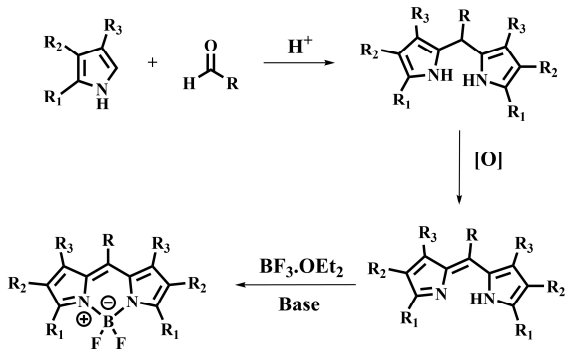

Scheme 2.1 Condensation of aldehydes with pyrrole to form BODIPY framework.

The second pathway (Scheme 2.2) uses pyrroles and highly reactive acyl compounds (acid chloride[23], anhydride[24] or ortoester[25]). The intermediate acylpyrrole compounds react with the excess pyrrole in an acidic environment to form dipyrrins. As in the first reaction pathway, the addition of excess base and borontrifluoride diethyl etherate ($BF_3 \cdot OEt_2$) yields the BODIPY dye. The advantage of this method is that the formation of dipyrromethene occurring in a single process. However, the conversion is not always complete which makes the purification difficult.

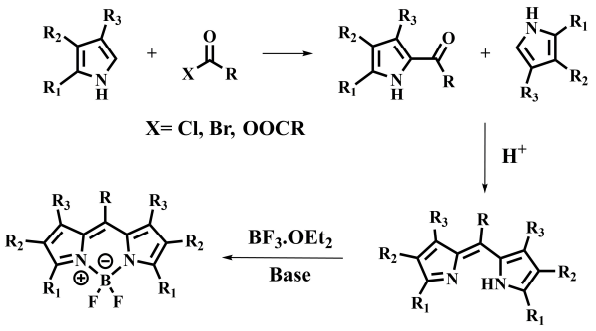

Scheme 2.2 Condensation of acyl compound with pyrrole to form BODIPY framework.

The synthesis of asymmetric BODIPY dyes were obtained by the MacDonald coupling approach. The synthetic pathway (Scheme 2.3) starts with the acid-catalyzed condensation of a keto pyrrole with an α-unsubstituted pyrrole which gives the desired dipyrromethene intermediate.[20] This intermediate is isolated as a salt and undergoes a complexation reaction with $BF_3 \cdot OEt_2$ in the presence of a base to form a BODIPY structure. The main advantage of this method is the possibility to incorporate various substituents on the pyrrole ring that yields different functional groups on the BODIPY dye.

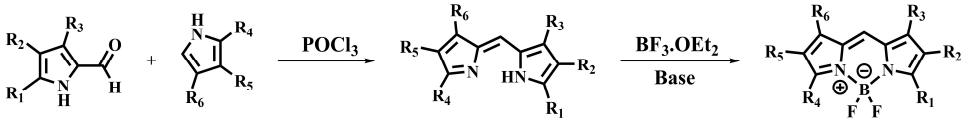

Scheme 2.3 Synthesis of asymmetric BODIPY core from keto pyrroles.

As seen in the schemes 2.1, 2.2, 2.3, the substitution of the carbonyl compound determines the functionality of meso position, while the substitution of the pyrrole compound induces a rise of peripheral groups at the 1-3 and 5-7 positions on the BODIPY dye. According to this, proper synthetic strategies allow functionalizing the BODIPY dye efficiently for different applications.

2.1.3. General properties and strategies for BODIPY-based far-red and NIR dyes

The development of new materials that absorb or emit in the far-red and near-infrared (NIR) regions is the point of interest by many different fields as the application areas ranging from medical or biological to optoelectronics.[2,26] The far-red and NIR regions are located between 650 and 2500 nm of the spectrum. This means nearly 50% of the energy from the sun comes as NIR radiation. As well as providing higher efficiency by overcoming

the spectral mismatches for solar energy conversion, NIR absorbers are effective in heat-ray blocking.[27] Moreover, being in the 650-900 nm "optical window" offers less interference, low light scattering and deep penetration for sensing and detection applications in biological samples.[28]

Among all NIR materials, dye-based structures promise efficient light absorption, chemical stability, robustness against light, heat, water, and pH.[2] Next to its excellent properties, BODIPY dyes allow easy and diverse chemical modification to reach the desired NIR spectral region compared to other chromophores. The design strategies can be summarized in the following categories:

i) Extending the π- conjugation length and decreasing the resonance energy
ii) Attaching strong electron-donating groups
iii) Attaching fused and rigid ring systems
iv) Replacement of C8 with N to form aza-BODIPYs

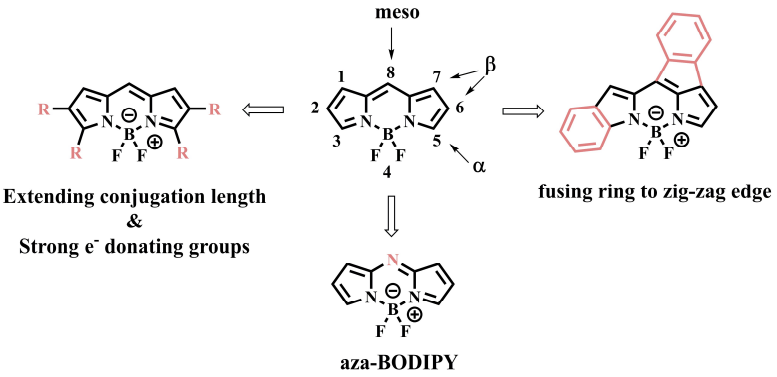

Scheme 2.4 Schematic illustration of modification strategies towards NIR-absorbing BODIPYs.

Studies on structure-property relationships of BODIPYs shows that the introduction of amine, oxygen or sulfur-containing groups to the α-position of BODIPY afford a significant bathochromic shift of absorption and emission with a decrease (in general) in photoluminescence (PL) quantum yield compared to the parent BODIPY. The strong electron donating nature of these groups reduce the band gap by increasing the electron density of the BODIPY and cause a usually 70-100 nm red-shift of absorption and emission. To investigate this effect in 1999 Burgess and coworkers synthesized a series of α-substituted BODIPY molecules with aryl substituents.[29] The synthesized molecules (Figure

2.3) showed bathochromic shifts of the long wavelength absorption bands. However, the fluorescence quantum yields of these molecules came up significantly lower than that of the corresponding alkyl-substituted dyes.

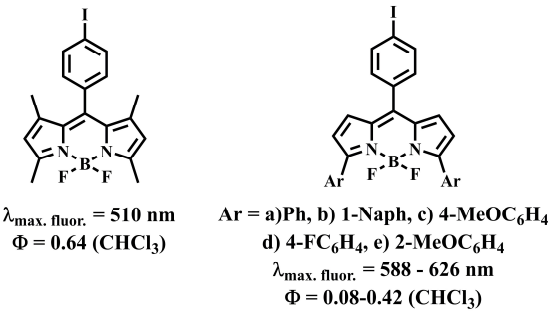

Figure 2.3 Effect of functionalization with e^- donating group of BODIPY from α-positions.

Another study on the introduction of aryl groups to the α-positions of BODIPY was reported by Yu and coworkers.[30] Here, the π-conjugation with substituent in 3- and 5-position leads to a bathochromic shift of absorption and emission with a decrease in PL quantum yield with respect to the relevant BODIPY parents. However, an extension of conjugation length from the same position with vinyl substituents (Figure 2.4) resulted in a lower decrease in PL quantum yield as the parent BODIPY as well as to the already mentioned bathochromic shifts of the absorption bands.

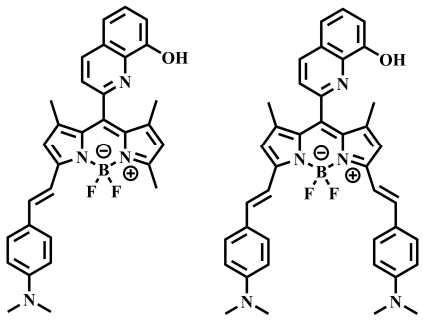

Figure 2.4 Functionalization with vinyl substituents of BODIPY in α-positions.

The extension of the conjugation system by fusion with aryl or heteroaryl groups is more effective compared to a simple substitution of the BODIPY core in order to induce red-shift in absorption and emission (Figure 2.5). In the study of Ziessel and coworkers[31],

1,2- and 6,7-ring-fused BODIPY compounds showed a noticeable absorption and emission shift into the NIR region in compared to the parent BODIPY core. Heteroaryl fusion in 2,3- and 5,6-positions of BODIPY have resulted in such bathochromic shift too, but coupled with a higher fluorescence quantum yields and higher molar absorptivities compared to an aryl fusion.[32,33]

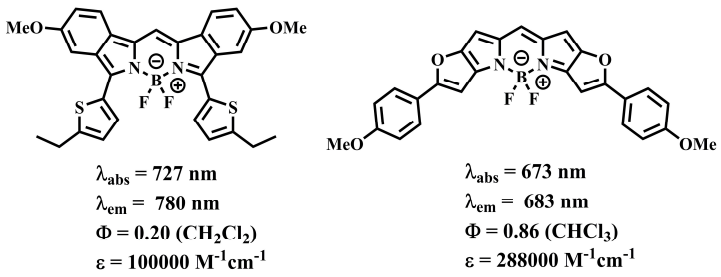

λ_{abs} = 727 nm
λ_{em} = 780 nm
Φ = 0.20 (CH_2Cl_2)
ε = 100000 $M^{-1}cm^{-1}$

λ_{abs} = 673 nm
λ_{em} = 683 nm
Φ = 0.86 ($CHCl_3$)
ε = 288000 $M^{-1}cm^{-1}$

Figure 2.5 Effect of aryl and heteroaryl fusion on BODIPY from different positions.

Fusing rings at the zig-zag edge (1,7,8- positions) of the BODIPY core is another successful approach to reach the desired bathochromic shift. To generate a proper push-pull structure, Wu and co-workers have developed an intramolecular oxidative cyclodehydrogenation strategy to fuse electron-rich groups to the BODIPY core.[34,35] By using this approach, anthracene-, perylene- and porphyrin-fused BODIPY dyes with NIR absorption/emission and high stability have been synthesized (Figure 2.6).[34,36] The absorption spectra of these molecules show a unique broad absorption band in the long-wavelength region which was proposed by the researchers as evidence for the existence of intramolecular charge transfer or aggregation (intermolecular interaction). Due to these features, these structures showed low fluorescence quantum yields.

The last strategy is forming "aza-BODIPY" by replacing the carbon atom at meso position of BODIPY core with a nitrogen atom. Aza-BODIPY dyes were first reported in 1940s[37], but received particular attention in 2002 by the research of O'Shea and co-workers.[38] Besides their remarkable properties such as high molar extinction coefficients and high fluorescence quantum yield, aza-BODIPYs are typically red and NIR fluorophores since the energetic positions of their orbital levels are affected and accordingly the band gap is reduced by the presence of the nitrogen's lone pair electrons. Similar to the BODIPY core, the absorption spectra of aza-BODIPY also strongly depends on the type of substituents and π-conjugation extension. Introduction of an electron-donating group at 3- and 5- positions[38,39], replacing the phenyl rings with thiophene rings[40,41] or attaching

alkynyl groups[41] generate further bathochromic shift compared to the conventional 1,3,5,7-tetraaryl aza-BODIPY (Figure 2.7).

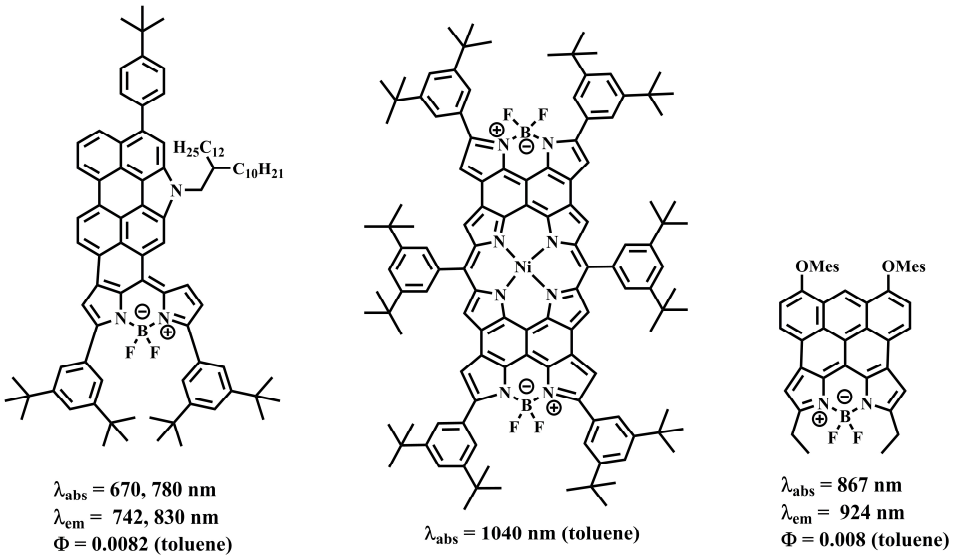

Figure 2.6 Aromatic units fused at the zig-zag edge of BODIPY dyes.

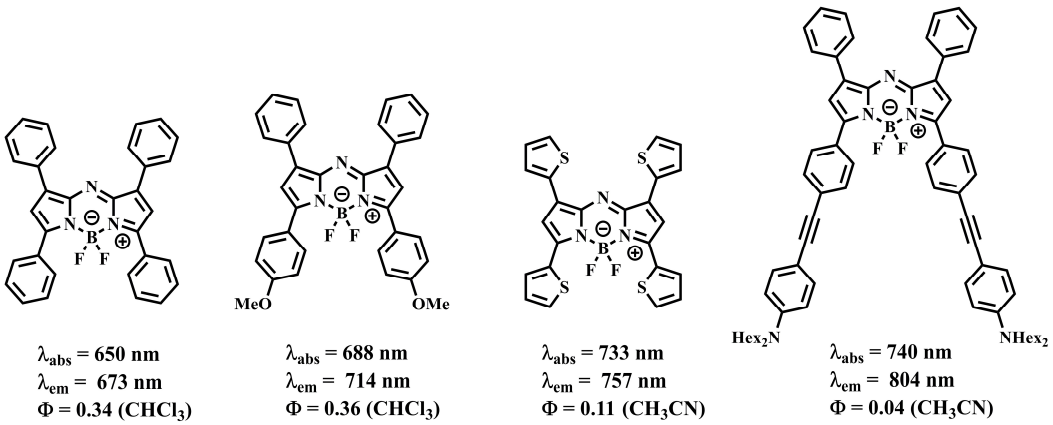

Figure 2.7 Effect of substituents on aza-BODIPYs.

Similarly, fusing rigid rings results in stable fluorophores with moderate fluorescence quantum yield and red-shifted absorption and emission due to more efficient π-conjugation.[42] The study of Kobayashi shows the effect of ring fusing and the electron donating group effect for α-substituted aza-BODIPYs. The dimethyl amino substituents provide a significant red-shift in absorption and emission, however, they strongly reduce the fluorescence quantum yield (Figure 2.8).

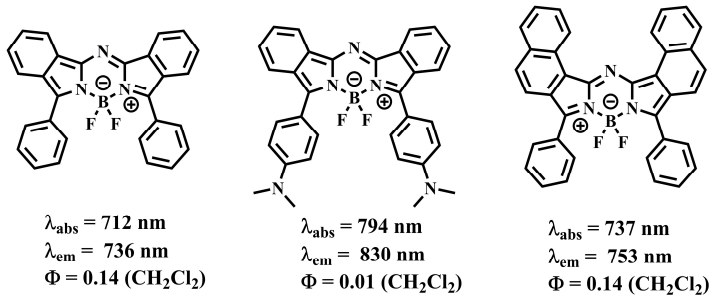

Figure 2.8 Ring-fused aza-BODIPYs.

In 2005, Carreira and Zhao investigated the effect of conformational restriction on aza-BODIPY's optical properties.[43,44] (Figure 2.9) In this study, it is reported that while the conformational restriction causes an absorption shift to longer wavelengths, the position of the substituents at the fused-rings also affects the photophysical properties. The electron-donating groups on the 2,3- and 5,6-fused-ring tend to cause further red-shift whereas additional electron-donating groups on the 1- and 7-positioned aryl rings result in a slight hypsochromic shift and slightly higher fluorescence quantum yield.

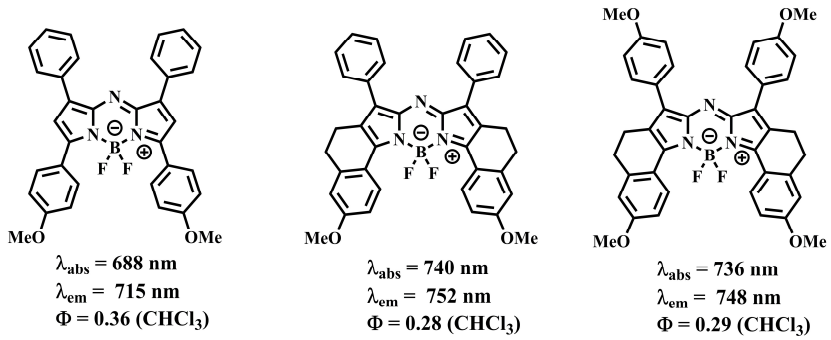

Figure 2.9 Conformationally restricted aza-BODIPYs.

2.1.4. BODIPY-based materials for organic field effect transistors

Among the optoelectronic devices, organic field effect transistors (OFETs) emerged as an alternative to the conventional inorganic counterparts by providing cost-effectiveness, compatibility with flexible substrates, and large area processability.[45-48] As explained in Chapter 1, performance of organic transistors depends on the solid-state charge transport characteristics of the semiconductor materials. Among the organic semiconductor materials, BODIPY is an attractive lead structure with promising properties, yet the charge transport properties are less investigated as compared to the photophysical properties.[49-61]

The OFET charge carrier mobilities of red-NIR absorbing/emitting BODIPY-based polymers and small molecules vary between 10^{-9}-10^{-1} $cm^2/V{\cdot}s$.[49, 51-54, 58-61]

In 2011, Thayumanavan and co-workers presented four D-A type copolymers and a homopolymer incorporating a BODIPY core (Figure 2.10).[51] The homopolymer as well as copolymers with quinoxaline (**Qx**) and benzothiadiazole (**BzT**) show a p-type charge transport behaviour while copolymers with naphthalene-tetracarboxylic diimide (**NDI**) and perylene-tetracarboxylic diimide (**PDI**) show n-type behaviour in thin film transistor devices. The incorporation of the donor units **Qx** and **BzT** to the polymer backbone decreased the hole mobility compared to the homopolymer, and on the other hand, **PDI** incorporation increased the mobility by one order of magnitude.

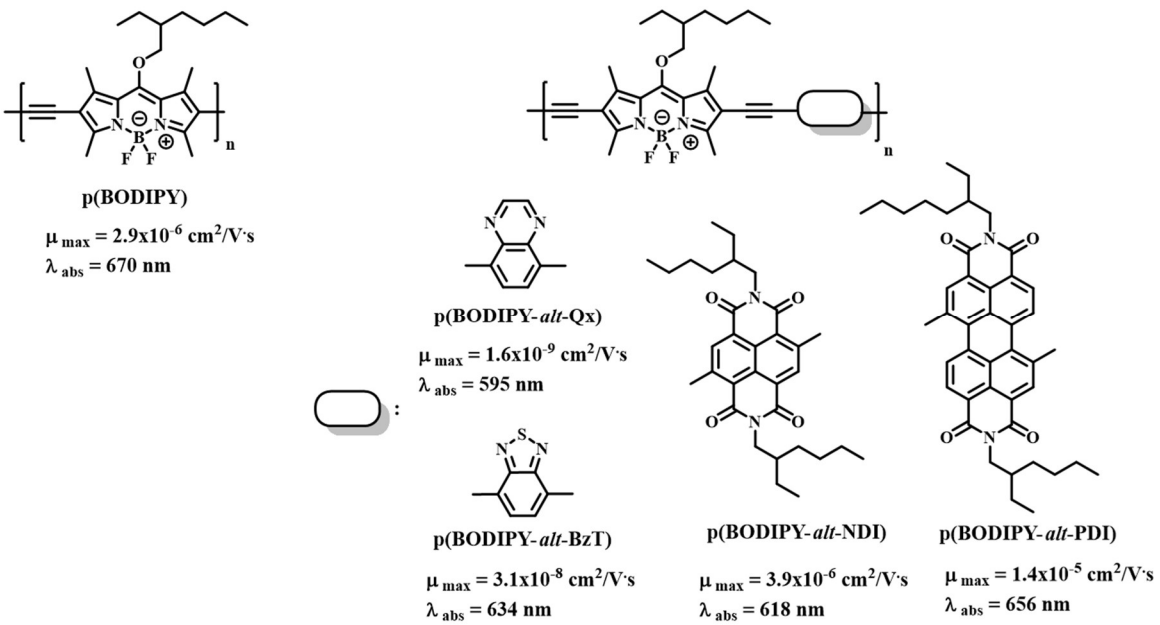

Figure 2.10 Structures of BODIPY-based homo- and copolymers with OFET mobilities.

Usta et al. (2013) have synthesized four BODIPY-thiophene copolymers and explored their organic field-effect transistor (OFET) performances.[53] All polymers have shown p-type behaviour (Figure 2.11). From the polymers, **P3** showed a hole mobility of 0.17 $cm^2/V{\cdot}s$ which is still the highest mobility among the BODIPY-based polymer semiconductors. The researchers have indicated that improved π-conjugation in the polymer backbone, proper electronic structure, and optimized film morphology have resulted in the remarkable charge carrier mobility in the OFETs.

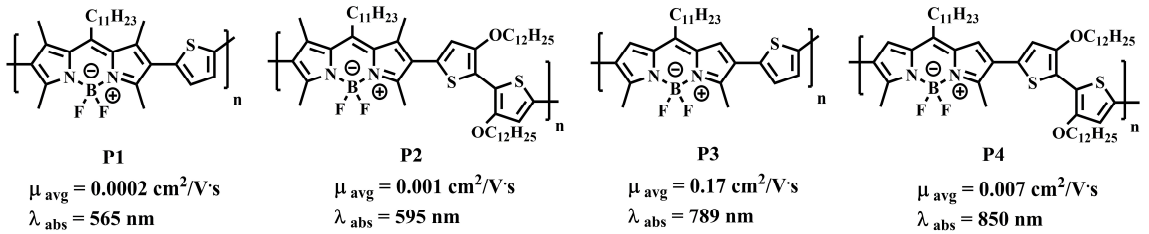

Figure 2.11 Chemical structures of BODIPY-thiophene copolymers with OFET mobilities.

In another work of Thayumanavan and co-workers (2014), three NIR-absorbing A-D-A type small molecules containing terminal BODIPY unit were presented (Figure 2.12).[54] Despite the incorporation of the strong central donor units, all small molecules have shown n-type behaviour with electron mobilities in the order of 10^{-5} $cm^2/V{\cdot}s$.

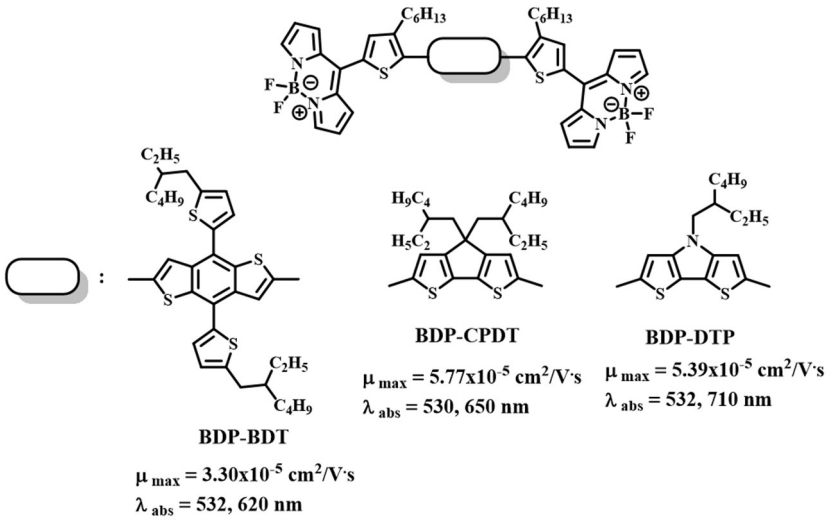

Figure 2.12 Chemical structures of BODIPY-based A-D-A small molecules with OFET mobilities.

Another set of NIR-absorbing small molecules, used as active layer in OFETs, was presented by the Ziessel Group.[52,60] From these studies, compounds **TB2** and **6** (Figure 2.13) showed moderate electron and hole mobilities. They concluded that these mobilities are result of a planar organization of the dye molecules with strong intermolecular interactions and short distances between neighboring molecules in the solid-state.

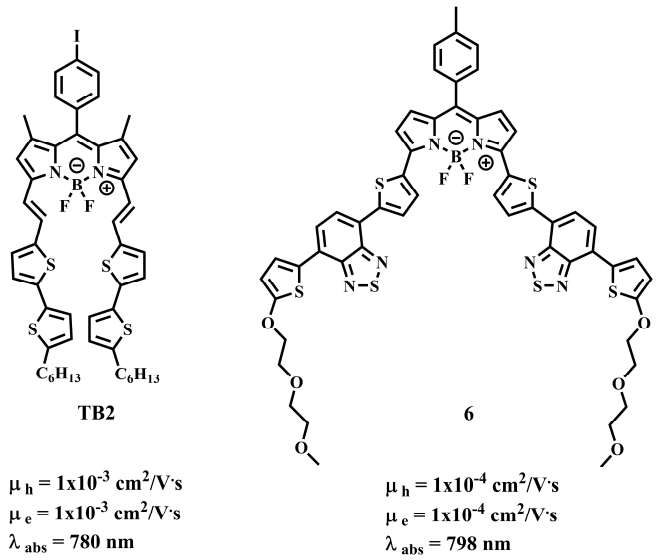

Figure 2.13 Chemical structures of ambipolar NIR-absorbing small molecules with OFET mobilities.

In the recent work of Squeo et al. in 2018, the influence of the positions of alkyl chains at the quarterthiophene linkers in BODIPY-based alternating copolymers on the hole mobility was investigated (Figure 2.14).[59] The study reveals that a head to head (HH) or tail to tail (TT) orientation of the didodecyl side chains in the two central thiophene rings of the quarterthiophene unit cause a significant difference in device performance. The TT positioned molecule **BODIPY-qT*i*** had better device performance than HH positioned molecule **BODIPY-qT*o*** due to the less steric hindrance in the polymer backbone.

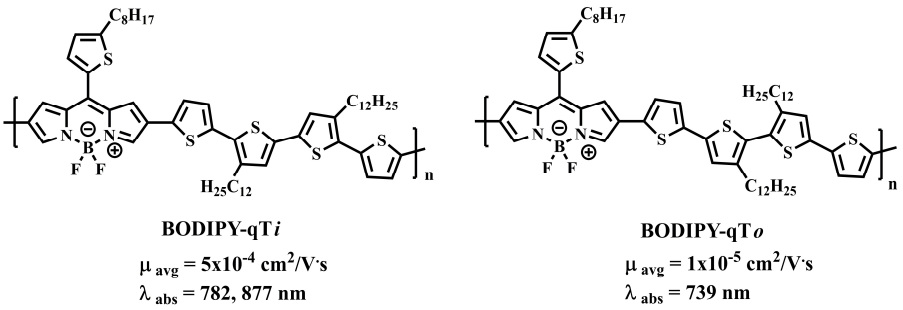

Figure 2.14 Chemical structure of NIR-absorbing D-A conjugated polymers with OFET mobilities.

All in all, even although the measurements of charge transport parameters in field-effect transistors are done under specific and different conditions, the results give enough insight about the relationship between the molecular structure and charge transport properties. Based on the results of polymers and small molecules in literature, it can be

concluded that, the molecular architecture (D-A-D, A-D-A in small molecules or D-A in polymers) affects the OFET type (p- or n-type). Moreover, molecular packing and surface morphology also have strong influence on charge mobility and device performance.

2.2. Results and Discussions

2.2.1. Synthesis of ring-fused BODIPY-based polymers

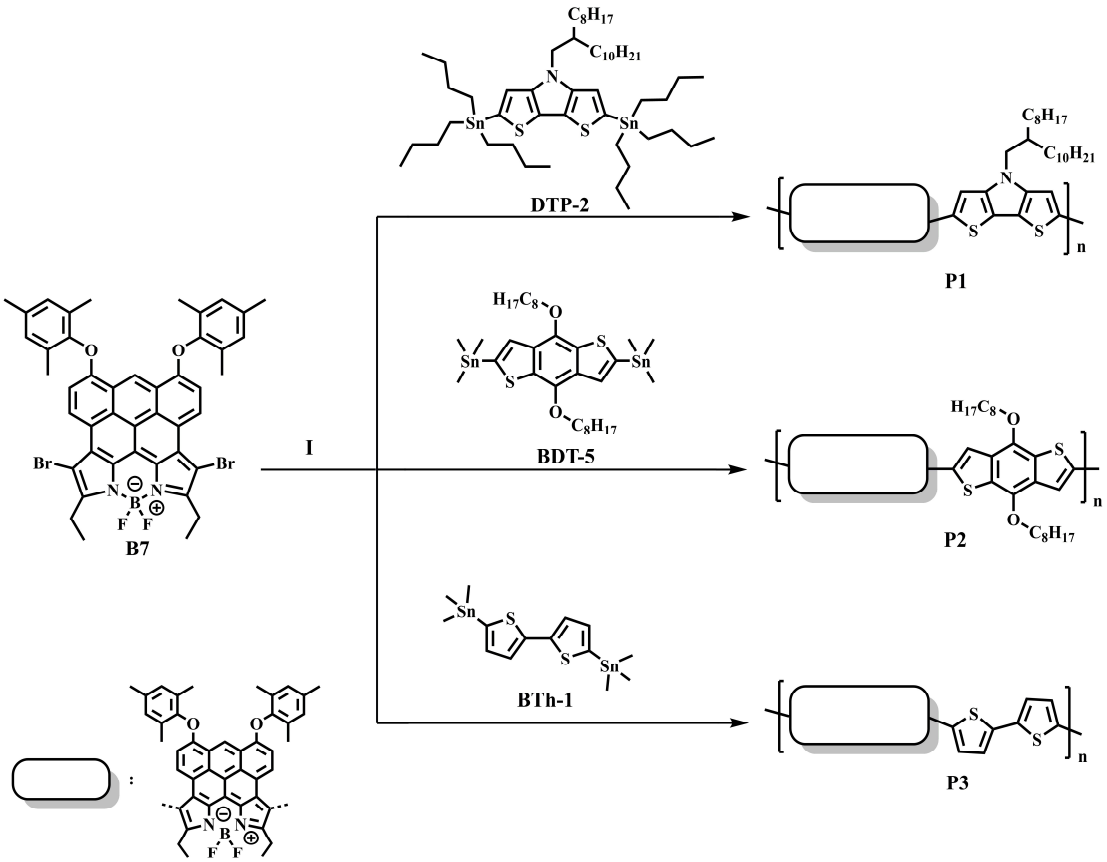

Scheme 2.5 Synthetic route for ring-fused BODIPY-based polymers via Stille cross-coupling. (I: $Pd(PPh_3)_4$, DMF:toluene,120 °C)

The dibrominated ring-fused BODIPY building block **B7**[62-66] and the distannylated donor monomers **DTP-2**[67], **BDT-5**[68], **BTh-1**[69] were synthesized according to the literature. The detailed procedures are explained in the experimental section. The ring-fused BODIPY-based polymers **P1**, **P2**, and **P3** were prepared in a microwave-assisted Stille cross-coupling as shown in Scheme 2.5. The polymerizations were carried out with dibrominated ring-fused BODIPY compound **B7** and the corresponding distannylated donor comonomers (**DTP-2**, **BDT-5**, **BTh-1**) in dimethylformamide (DMF)/toluene mixture (1:3) at 120 °C for 40 min., in the presence of tetrakis(triphenylphosphine)

palladium(0) ($Pd(PPh_3)_4$) as the catalyst. The polymers were isolated by reduction of solvent volume followed by precipitation into methanol. The crude polymers were purified by Soxhlet extraction. The final product resulted as dark green solids with yields ($CHCl_3$ fraction) of 65%, 61% and 64% for **P1**, **P2** and **P3** ($CHCl_3$ fractions) respectively. The chemical structures of the monomers were confirmed by nuclear magnetic resonance (NMR) spectroscopy and mass spectrometry (detailed information at experimental section). The chemical structures of obtained polymers were also confirmed by NMR spectroscopy (detailed information at experimental section), and the average molecular weights and polydispersity indexes were estimated by gel permeation chromatography (GPC). (Table 2.1).

Table 2.1 Polymerization results for polymers.

	Yield [%]	M_n [kg/mol]	M_w [kg/mol]	PDI
P1	65	7.1	22.0	3.1
P2	61	19.6	91.1	4.6
P3	63	5.1	6.3	1.3

2.2.2. Photophysical properties

The effect of fusing rings to the BODIPY core on the photophysical properties has been discussed in section 2.1.3. Regarding the ring-fused BODIPY compound (Figure 2.6, the compound positioned on the right of the figure), in 2011 the Wu group has verified a significant bathochromic shift in the absorption after the cyclodehydrogenation reaction of the meso-anthracene substituted BODIPY precursor.[65] The cyclodehydrogenation reaction resulted in an extended π-conjugation around the BODIPY core. Thereby, the long wavelength absorption of the meso-anthracene substituted BODIPY precursor which displays characteristic absorption bands of respective BODIPY and anthracene is shifted from 520 nm to 826 nm for the designed structure ring-fused BODIPY.

By designing a larger conjugation system, the bathochromic spectral shift of ring-fused BODIPY can be further enhanced. With this aim, the ring-fused BODIPY core was incorporated into polymers with different donor structures as in the Scheme 2.5.

The absorption spectra of the designed polymers were recorded in $CHCl_3$ and as spin-coated films are shown in Figure 2.15. All polymers show a very similar absorption pattern from UV to NIR. The polymers in solution show absorption maxima at 316 and 403

nm for **P1**, 305 and 403 nm for **P2**, and 300 and 403 nm for **P3** in the UV-Vis range and a broad absorption band between 500 and 1000 nm with maxima at 663, 764 and 844 nm for **P1**, 665, 757 and 836 nm for **P2**, and 666, 756 and 832 nm for **P3**. In the case of spin-coated films of **P1**, **P2**, and **P3**, a slight red-shift of 10 to 20 nm is observed. The shifts were attributed to some aggregation in the solid-state. In comparison to the ring-fused BODIPY monomers (**7**) from the literature[65] (λ_{max} in NIR region = 826 nm), extending the π-conjugation in 2- and 6- position through polymerization with the comonomers **DTP**, **BDT**, and **BTh** provides a ~20 nm bathochromic spectral shift and enhances the absorption in the NIR region. Considering the low degree of polymerization for **P1**, **P2** and **P3**, slightly higher bathochromic shifts could be attainable with longer chains.

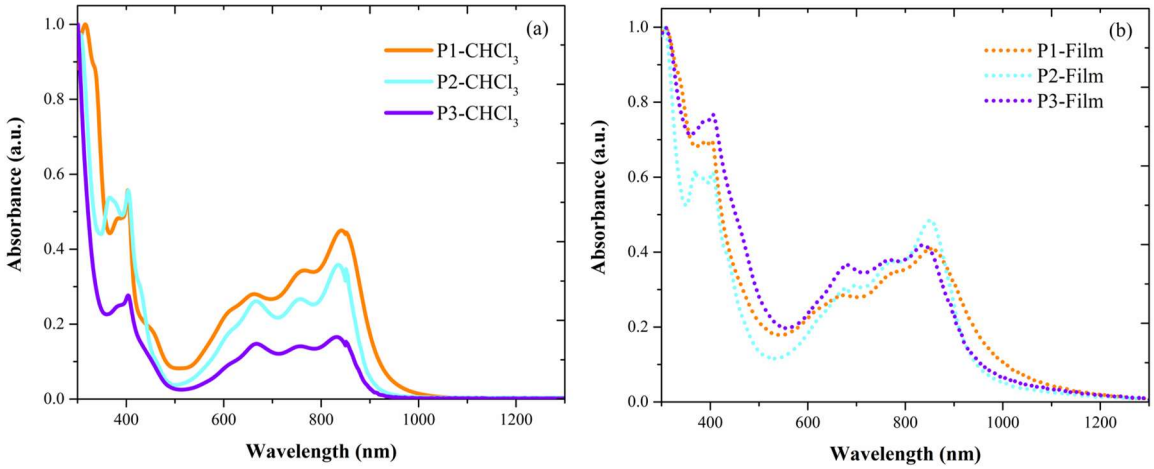

Figure 2.15 Absorption spectra of **P1**, **P2**, and **P3** (a) in $CHCl_3$ solution (10^{-5} M), (b) in spin-coated film.

The optical band gaps of **P1**, **P2**, and **P3** were estimated according to the correlation of energy and wavelength by using the low energy onset of the thin film absorption band (band gap energy (E_g)= h×C/λ where h: Planks constant (6.626×10^{-34} Joules.sec), C: Speed of light (3.0×10^{-8} meter/sec), λ: Cut off wavelengths). Regarding the energy levels, the highest occupied molecular orbital (HOMO) energy was measured by atmospheric pressure photoelectron spectroscopy (AC-2 method), and the lowest unoccupied molecular orbital (LUMO) energy was calculated by subtracting HOMO level from the band gap. The optical data and the electronic levels are summarized in Table 2.2.

According to the estimated band gaps and energy levels, all polymers have a low band gap and deep-lying HOMO energy levels. Among the polymers, **P1** has the lowest

band gap due to the relatively high HOMO energy level caused by the strong donor unit **DTP**.

Table 2.2 Photophysical properties of **P1**, **P2**, and **P3**. ([a] measured by atmospheric pressure photoelectron spectroscopy (AC-2 method), [b] LUMO=HOMO(AC-2)+$E_{g(opt)}$, [c] calculated from low energy onset of thin film absorption band)

	λ_{max}^{sol} [nm]	λ_{max}^{film} [nm]	HOMO [a] [eV]	LUMO [b] [eV]	E_g^{opt} [c] [eV]
P1	844	855	-5.26	-4.11	1.15
P2	836	852	-5.41	-4.13	1.28
P3	832	842	-5.34	-4.11	1.23

2.2.3. Electrochemical properties

The electrochemical properties of **P1**, **P2** and **P3** were investigated by cyclic voltammetry in 0.1 M tetrabutylammonium perchlorate (TBAP)/$CHCl_3$ solution. According to the voltammograms in Figure 2.16 (a), **P1** exhibits a quasi-reversible oxidation peak at $E_{p,a}^{ox}$ = 1.00 V and $E_{p,c}^{ox}$ = 0.77 V ($E_{1/2}^{ox}$ = 0.89 V), **P2** and **P3** exhibited an irreversible oxidation at $E_{p,a}^{ox}$ = 1.30 V and $E_{p,c}^{ox}$ = 0.29 V ($E_{1/2}^{ox}$ = 0.80 V) for **P2**, $E_{p,a}^{ox}$ = 1.19 V and $E_{p,c}^{ox}$ = 0.19 V ($E_{1/2}^{ox}$ = 0.69 V) for **P3**. On the other hand, all polymers exhibited reversible reduction peaks (Figure 2.16 (b) **P1**: $E_{p,a}^{red}$ = -0.40 V and $E_{p,c}^{red}$ = -0.49 V, $E_{1/2}^{red}$ = -0.45 V, **P2**: $E_{p,a}^{red}$ = -0.54 V and $E_{p,c}^{red}$ = -0.62 V, $E_{1/2}^{red}$ = -0.58 V, **P3**: $E_{p,a}^{red}$ = -0.50 V and $E_{p,c}^{red}$ = -0.57 V, $E_{1/2}^{red}$ = -0.54 V) which corresponds to n-type doping properties of these polymers.

HOMO and LUMO energy levels were calculated using the onset of the corresponding oxidation and reduction potential against standard calomel electrode (SCE) according to the formula[70]; $E_{HOMO/LUMO}$ = -(4.7 + $E_{on}^{ox/red}$) eV. Additionally, the electronic band gaps of **P1**, **P2**, and **P3** were calculated from these HOMO and LUMO levels. The results are summarized in Table 2.3. The HOMO values and band gaps (E_g) obtained by the cyclic voltammetry are in good agreement with the corresponding optical values. By comparison to the ring-fused BODIPY[65] monomer (in the literature compound named as **7**) (Table 2.3), the copolymerization with the donor comonomers yields copolymers with deeper lying HOMO and LUMO levels. The LUMO levels decrease more than the HOMO levels, resulting in a narrowed band gap. Among the polymers, **P1** has the highest HOMO

energy level caused by the incorporation of the strong donor unit **DTP**, in agreement with the previously outlined optical result.

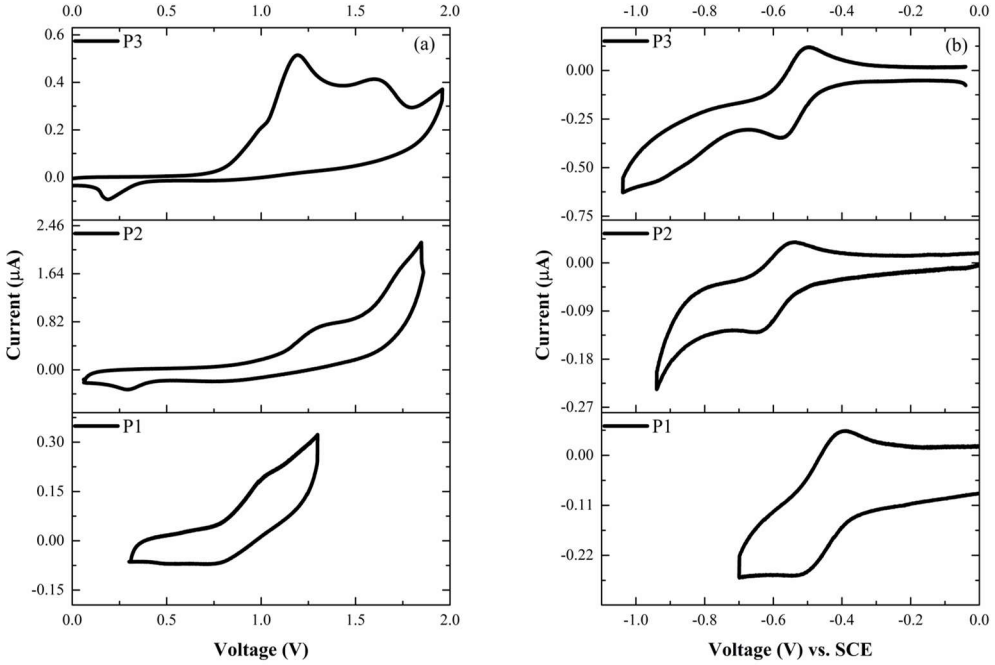

Figure 2.16 Cyclic voltammograms of **P1**, **P2**, and **P3** during (a) oxidation, (b) reduction.

Table 2.3 Summary of the electrochemical properties of **P1**, **P2**, and **P3**. ([a] $E^{ox/red}_{onset}$ vs SCE, [b] $E^{ox/red}_{onset}$ vs Fc^{+}/Fc)

	E^{ox}_{onset} [V]	E^{red}_{onset} [V]	HOMO [eV]	LUMO [eV]	E_g^{elec} [eV]
P1	0.81[a]	-0.37[a]	-5.51	-4.33	1.18
P2	1.04[a]	-0.52[a]	-5.74	-4.18	1.56
P3	0.92[a]	-0.46[a]	-5.62	-4.24	1.38
7[65]	0.57[b]	-0.97[b]	-5.30	-3.88	1.42

2.2.4. Charge transport properties: OFET measurements

The charge transport properties of **P1**, **P2**, and **P3** were investigated in OFET devices in cooperation with the group of Professor Franco Cacialli from London Centre for Nanotechnology, UCL. The charge carrier mobilities were estimated in bottom-gate bottom-contact (BGBC) device configuration using Au as source and drain electrodes as shown in Figure 2.17.

According to the CV results in the previous section, **P1**, **P2**, and **P3** showed typical n-type charging properties (see the reversible reduction peaks). Thus, the OFET structure needs to be prepared accordingly. In n-type OFETs, in order to open the channel, positive

bias must be applied. In this way electrons are collected at the semiconductor-insulator interface. For this purpose, a superficial treatment was done to the SiO_2 insulator layer with octadecyltrichlorosilane (OTS). This enable the electron mobility of the materials to be measured. Each polymer was spin-coated directly from a 10 mg/mL solution in toluene on top of the silicon/SiO_2 substrates.

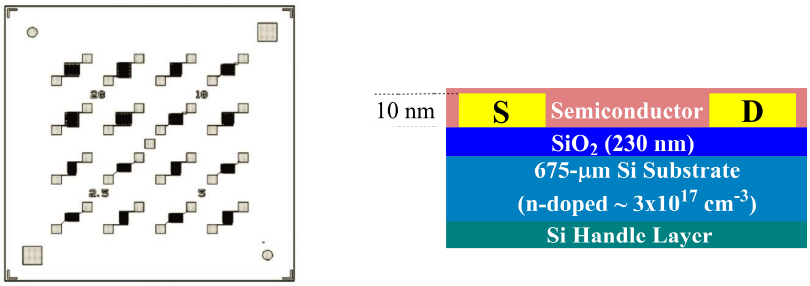

Figure 2.17 Layout of the substrate.

Only the OFETs incorporating copolymer **P2** exhibited a clear output characteristic, as shown in Figure 2.18. As observed with the optical microscope (shown in Figure 2.19), the films of **P1** and **P3** exhibit a non-homogeneous morphology compared to that of **P2**. These non-homogeneous features can probably affect the percolation of the charge when the channel is formed. This may be related to the low molecular weights of **P1** and **P3** (see Table 2.1).

Additionally, as the electrical response is not consistent in the transfer characteristics of **P2**, the mobility (μ) has been extrapolated, but further measurements are needed to confirm this value. Due to this reason, the parameters such as threshold voltage and I_{ON}/I_{OFF} ratio are not reported. However, the electron mobility (μ) calculated from the electrical features of **P2** is ~ 10^{-9} cm^2/Vs. Unfortunately, this mobility is low compared to those usually measured in organic semiconductors (> 10^{-4} cm^2/Vs).

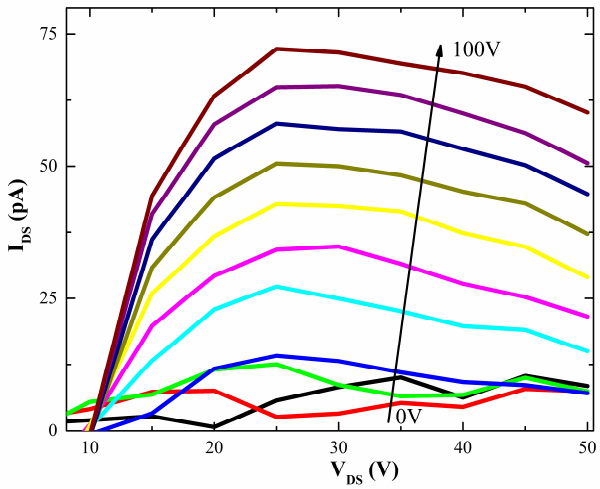

Figure 2.18 Output characteristics of OFET incorporating **P2**.

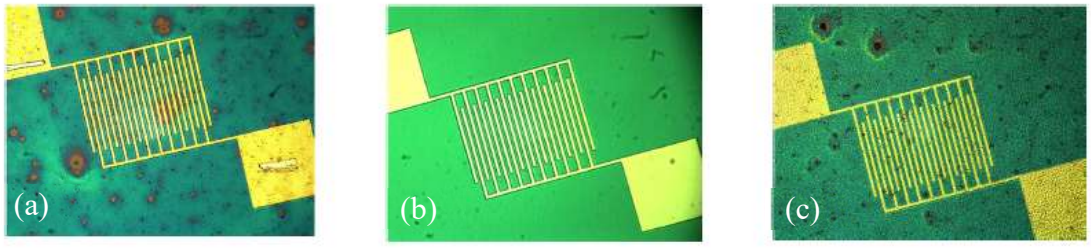

Figure 2.19 Optical microscope images of n-OFETs incorporating (a) **P1**, (b) **P2**, (c) **P3**.

2.3. Conclusion

In summary, three ring-fused BODIPY dye-containing π-conjugated polymer materials have been successfully synthesized based on the Stille cross-coupling polymerization reaction with varied distannyl comonomers as the donor units. The optical and electrochemical properties have been investigated. In the design of an enlarged conjugation system, a moderate bathochromic spectral shift into the NIR region is achieved compared to ring-fused BODIPY monomer. According to the optical and electrochemical measurements, **P1**, **P2**, and **P3** show deep-lying HOMO and LUMO levels and low band gaps. It is observed that among the donor units, **DTP** is the strongest donor unit which provides a relatively deep-lying HOMO level. Additionally, the electron transport properties were investigated in n-type thin-film transistor devices. Among the polymers, only the **P2** showed satisfying film morphology after deposition, its electron mobility is calculated as ~10^{-9} cm^2/Vs.

2.4. Experimental

2.4.1. Materials and instrumentation

All starting materials and reagents were obtained from commercial suppliers and used without further purification. Dry solvents were bought from Acros. All reactions were carried out under argon atmosphere by Schlenk techniques, if not specified otherwise.

NMR spectra were recorded on a Bruker AVANCE 400 or AVANCE III 600. Gel permeation chromatography (GPC) measurements were carried out on a PSS/Agilent SECurity GPC System equipped with polystyrene gel columns using chloroform as eluent. APLI (Atmospheric Pressure Laser Ionization) and APCI (Atmospheric Pressure Chemical Ionization) measurements were carried out on Bruker Daltronik Bremen with micrOTOF Gas chromatography coupled with mass spectrometry (GC-MS) measurements were recorded on either a GC17AQP5050 or a 7890GC gas chromatograph from Shimadzu with 5975C MS detector from Agilent Technologies. Matrix Assisted Laser Desorption Ionisation (MALDI) measurements were carried out using a Bruker Reflex TOF at the Max Planck Institute for Polymer Research in Mainz. UV-visible absorption spectra were recorded on a Jasco V-670 spectrometer. The HOMO (highest occupied molecular orbital) levels were estimated on a Surface Analyzer MODEL AC-2 from RIKEN, given as the threshold where photoelectron emission first occurs. **CV Measurements:** Cyclic voltammetry (CV) measurements of the polymers were performed on a standard three-electrode electrochemical cell with a polished Pt disk as working electrode, Pt wire as counter electrode and Ag/AgCl (1 M KCl) as the reference electrode attached to a VersaSTAT 4 electrochemical workstation in dry chloroform with 0.1 M tetrabutylammonium perchlorate (TBAP) as the supporting electrolyte at a scan rate of 0.1 V/s for polymers. Fc/Fc^+ was used as an internal reference. The onset potentials were determined from the intersection of two tangents drawn at the rising current and background current of the cyclic voltammogram. **OFET Measurements:** The transistors were prepared using n-doped silicon substrates ($3 \cdot 10^{17}$ cm^{-3}), provided with OFET structures patterned on top with four different channel lengths (2.5, 5, 10 and 20 μm), as shown in Figure 2.17. The substrates have been purchased from Fraunhofer IPMS. All transistors have a channel width of 10 mm and a common gate contact located on the bottom of the chip. N-doped silicon substrates were cleaned by acetone and isopropyl alcohol (IPA). Then each substrate was passivated by treatment with octadecyltrichlorosilane

(OTS) at 1500 rpm for 60 sec. Thermal annealing was done at 100 ºC for 1 h. The surfaces were rinsed by IPA and the polymers were spin-coated at 1500 rpm for 60 s. from a 10 mg/mL solution in toluene.

2.4.2. Synthesis of monomers for ring-fused BODIPY-based polymers

2.4.2.1. Synthesis of the ring-fused BODIPY building block

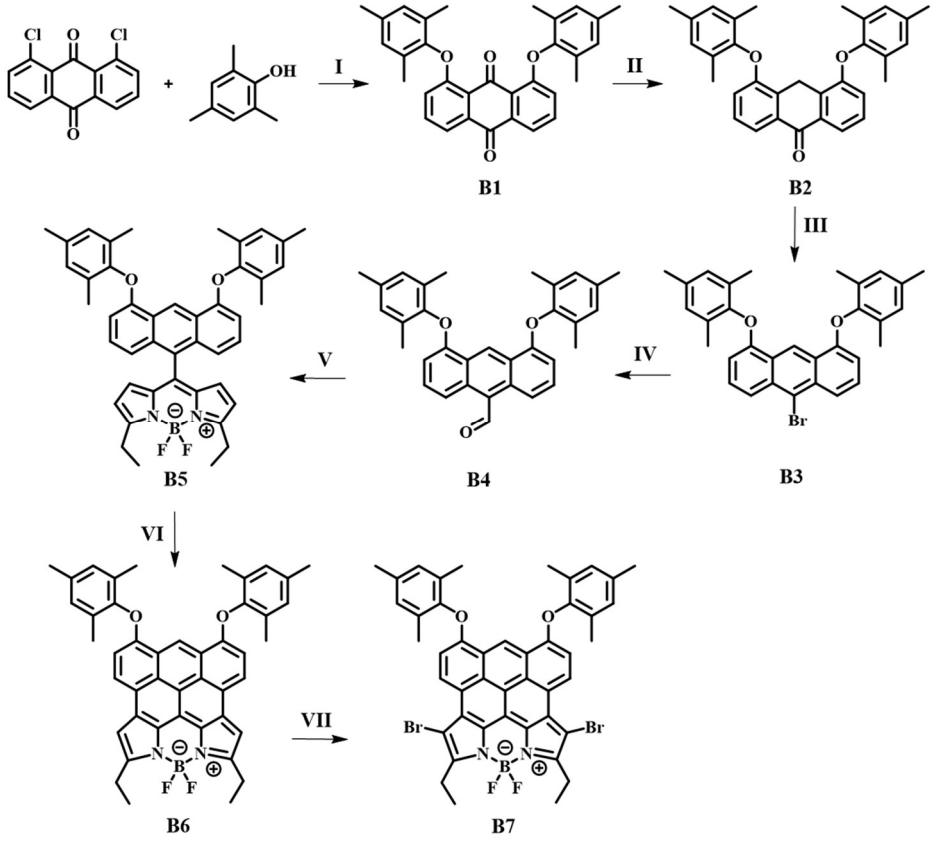

Scheme 2.6 Synthetic route for ring-fused BODIPY monomer. (I: K_2CO_3, DMF. II: $NaBH_4$, THF:MeOH (10:1). III: PBr_3. IV: *n*-BuLi, DMF, THF. V: i: 2-ethyl pyrrole, TFA, DCM, ii: DDQ, iii: Et_3N, $BF_3 \cdot OEt_2$. VI: $FeCl_3$, CH_3NO_2, DCM. VII: $CuBr_2$, THF.)

2.4.2.1.1. Synthesis of 1,8-bis(mesityloxy)anthracene-9,10-dione (B1)[62]

1,8-dichloro anthraquinone (25 g, 90 mmol), potassium carbonate (K_2CO_3) (62 g, 450 mmol) and 2,4,6-trimethylphenol (49 g, 360 mmol) were placed in two-neck, round bottom flask and dissolved in dry DMF (250 mL) under argon. The reaction mixture was refluxed at 136 °C overnight. The finalization of the reaction was checked by TLC. The reaction mixture was allowed to cool to RT, and 500 mL of water were added. The mixture

was extracted with DCM, and the organic layer was dried over magnesium sulfate (Mg_2SO_4). The solvent was removed under reduced pressure. The crude product was purified by column chromatography (silica gel, eluent hexane/diethyl ether, 9:1) and recrystallized from DCM/methanol to yield a yellow solid (36% yield).

^{1}H NMR (400 MHz, $CDCl_3$) δ/ppm: 7.91 (dd, 2H), 7.49 (dd, 2H), 6.93 (s, 4H), 6.84 (dd, 2H), 2.32 (s, 6H), 2.16 (s, 12H).

^{13}C NMR (101 MHz, $CDCl_3$) δ/ppm: 183.8, 181.8, 157.8, 148.7, 135.1, 134.7, 133.7, 130.5, 129.6, 123.4, 119.9, 119.7, 20.8, 16.1.

GC-MS (m/z): 476.30 (calc. 476.56).

2.4.2.1.2. Synthesis of 4,5-bis(mesityloxy)anthracen-9(10*H*)-one (B2)[63]

1,8-bis(mesityloxy)anthracene-9,10-dione **(B1)** (5.90 g, 12.36 mmol) was dissolved in THF (200 mL). Sodium borohydride ($NaBH_4$) (4.68 g, 124 mmol) and methanol (MeOH) (20 mL) were added in small portions (every 1h add 10 eq. $NaBH_4$ and every 2 h add 20 mL MeOH). The progress of the reaction was monitored by TLC. After 4h, the excess $NaBH_4$ was filtered off, and the solvent was removed. Meanwhile, an acetic acid/HCl (1:1) (300 mL) mixture was prepared and heated to 90 °C. This acidic mixture was poured slowly into the crude product solution and stirred for 10 min. The resulting precipitates were filtered off and washed with saturated sodium bicarbonate ($NaHCO_3$) followed by water. The product is dried under high-vacuum to yield an off-white solid (89% yield).

^{1}H NMR (400 MHz, $CDCl_3$) δ/ppm: 8.07 (d, 2H), 7.31 (t, 2H), 6.98 (s, 4H), 6.67 (d, 2H), 4.59 (s, 4H), 2.36 (s, 6H), 2.15 (s, 12H).

^{13}C NMR (101 MHz, $CDCl_3$) δ/ppm: 184.1, 155.1, 148.8, 134.7, 133.1, 130.6, 129.7, 128.9, 127.3, 120.1, 115.4, 22.8, 20.2, 16.1.

MALDI (m/z): 461.87 (calc. 462.21)

2.4.2.1.3. Synthesis of 10-bromo-1,8-bis(mesityloxy)anthracene (B3)[64]

4,5-bis(mesityloxy)anthracen-9(10*H*)-one **(B2)** (5.08 g, 11 mmol) was placed in a two-neck, round bottom flask. Phosphorus tribromide (PBr_3) (45 mL, 477 mmol) was added and the reaction mixture was heated to 110 °C under argon for 1 h. The mixture was allowed to cool down to RT and was poured into water (500 mL). The yellow precipitates were collected by filtration and washed with aq. $NaHCO_3$ solution and H_2O. The crude product

was purified by column chromatography (silica gel, toluene as solvent) to yield a yellow solid (95% yield).

^{1}H NMR (400 MHz, $CDCl_3$) δ/ppm: 9.89 (s, 1H), 8.15 (d, 2H), 7.40 (dd, 2H), 6.99 (s, 4H), 6.38 (d, 2H), 2.38 (s, 6H), 2.18 (s, 12H).

^{13}C NMR (101 MHz, $CDCl_3$) δ/ppm: 154.0, 149.1, 134.6, 132.1, 13.8, 129.6, 127.5, 124.5, 121.8, 120.5, 116.3, 104.5, 20.8, 16.0.

GC-MS (m/z): 527.14 (calc. 525.14).

2.4.2.1.4. Synthesis of 4,5-bis(mesityloxy)anthracene-9-carbaldehyde (B4)[65]

10-bromo-1,8-bis(mesityloxy)anthracene **(B3)** (5.50 g, 10.40 mmol) was placed in a Schlenk flask and dissolved in dry THF (150 mL). 1.6 M *n*-BuLi in hexane (9.81 mL, 15.70 mmol) was added dropwise at -78 °C. After 2 h dimethylformamide (DMF) (2.32 mL, 105 mmol) was added. The reaction took place another 2 h. After 2 h, the reaction was warmed up to room temperature. The finalization of the reaction was checked by TLC. After completion of the reaction, the mixture was quenched with aq. ammonium chloride (NH_4Cl). The mixture was extracted with ethyl acetate, and the organic layer was dried over sodium sulfate (Na_2SO_4). The solvent was removed under reduced pressure, and the crude product was purified by column chromatography (silica gel, toluene as the solvent) to yield a yellow solid (30% yield).

^{1}H NMR (400 MHz, $C_2D_2Cl_4$) δ/ppm: 11.46 (s,1H), 10.16 (s, 1H), 8.52 (d,2H), 7.46 (dd, 2H), 6.96 (s, 4H), 6.41 (d, 2H), 2.32 (s, 6H), 2.13 (s, 12H).

^{13}C NMR (101 MHz, $C_2D_2Cl_4$) δ/ppm: 194.0, 154.7, 148.9, 135.2, 133.7, 131.0, 130.3, 130.1, 124.6, 124.4, 123.8, 116.3, 105.1, 21.2, 16.4.

MALDI (m/z): 474.77 (calc. 474.59)

1.4.2.1.5. Synthesis of 10-(4,5-bis(mesityloxy) anthracen-9-yl)-3,7-diethyl-5,5-difluoro-5*H*-dipyrrolo[1,2-*c*:2',1'-*f*] [1,3,2] diazaborinin-4-ium-5-uide (B5)[65]

4,5-bis(mesityloxy)anthracene-9-carbaldehyde **(B4)** (1.30 g, 2.74 mmol) was dissolved in dry DCM (120 mL) under argon at RT. 2-Ethylpyrrole (0.67 mL, 6.57 mmol) and a drop of trifluoroacetic acid (TFA) was added to the reaction flask. The mixture was stirred for 3 h and the aldehyde consumption was checked by TLC. After the complete conversion of the aldehyde, 2,3-dichloro-5,6-dicyano-1,4-benzoquinone (DDQ) (0.68 g,

3.01 mmol) was added and the reaction mixture stirred for 40 min. After 40 minutes triethylamine (Et_3N) (11.08 mL, 79 mmol) and boron trifluoride diethyl etherate ($BF_3 \cdot OEt_2$) (13.88 mL, 110 mmol) were added and stirred for another 1 h. When the reaction was completed, the solvent was removed under reduced pressure. The crude product was purified by column chromatography (silica gel, eluent toluene/hexane, 3:1) to yield a red solid (50% yield).

^{1}H NMR (400 MHz, $CDCl_3$) δ/ppm: 9.99 (s, 1H), 7.46 (dd, 2H), 7.17 (t, 2H), 7.00 (s, 4H), 6.31-6.36 (m, 4H), 6.25 (d, 2H), 3.17 (q, 4H), 2.38 (s, 6H), 2.22 (s, 12H), 1.40 (t, 6H).

^{13}C NMR (101 MHz, $CDCl_3$) δ/ppm: 163.8, 153.7, 149.0, 136.1, 134.6, 132.4, 130.9, 130.2, 129.6, 129.0, 128.2, 126.7, 123.4, 119.1, 117.8, 117.4, 104.1, 22.1, 20.8, 16.1, 12.6.

APLI (m/z):692.32 (calc. 692.33)

1.4.2.1.6. Synthesis of 1,11-diethyl-12,12-difluoro-5,7-bis(mesityloxy)-12*H*-11a,12a-diaza-12boradibenzo[*cd*,*mn*]dicyclopenta[*fg*,*jk*]pyren-12a-ium-7-uide (B6)[65]

B5 (600 mg, 0.86 mmol) was dissolved in dry DCM (500 mL) under argon at RT. A solution of iron (III) chloride ($FeCl_3$) (843 mg, 5.20 mmol) in dry nitromethane (26 mL) was added dropwise to the solution. The reaction was monitored by TLC and took 20 min. The reaction mixture was quenched with saturated $NaHCO_3$ solution and extracted with DCM. The organic layer was washed with brine and water respectively and dried over Na_2SO_4. The solvent was removed under reduced pressure and the raw product purified by column chromatography (silica gel, eluent ethyl acetate (EtOAc)/hexane 1:7) to yield a blue solid (74% yield).

^{1}H NMR (400 MHz, $CDCl_3$) δ/ppm: 10.65 (s, 1H), 8.55 (d, 2H), 7.06 (s, 4H), 6.91 (s, 2H), 6.81 (d, 2H), 3.30 (q, 4H), 2.41 (s, 6H), 2.25 (s, 12H), 1.55 (t, 6H).

^{13}C NMR (101 MHz, $CDCl_3$) δ/ppm: 159.4, 157.3, 148.3, 136.1, 135.6, 131.5, 130.5, 130.0, 129.2, 128.2, 127.92, 123.72, 122.8, 121.7, 117.9, 108.2, 103.6, 99.9, 31.9, 29.6, 29.3, 22.6, 22.2, 20.8, 16.2, 14.1, 13.5.

APCI (m/z): 689.32 (calc. 689.31)

1.4.2.1.7. Synthesis of 2,10-dibromo-1,11-diethyl-12,12-difluoro-5,7-bis(mesityloxy)-12*H*-11a,12a-diaza-12-boradibenzo[*cd*,*mn*]dicyclopenta[*fg*,*jk*]pyren-12a-ium-7-uide (B7)[66]

B6 (366 mg, 0.53 mmol) and copper(II) bromide ($CuBr_2$) (297 mg, 1.33 mmol) were dissolved in dry THF (54 mL) under O_2 atmosphere for 12 h. After 12 h, the solvent was removed under reduced pressure. The residue was extracted with chloroform and the extracts were washed with water and dried over Na_2SO_4. The solvent was removed under reduced pressure again and the crude product was purified by column chromatography (silica gel, solvent as toluene) to yield a greenish-blue solid (84% yield).

^{1}H NMR (400 MHz, $CDCl_3$) δ/ppm: 10.83 (s, 1H), 9.50 (d, 2H), 7.08 (s, 4H), 6.99 (d, 2H), 3.30 (q, 4H), 2.42 (s, 6H), 2.27 (s, 12H), 1.52 (t, 6H).

^{13}C NMR (101 MHz, $CDCl_3$) δ/ppm: 159.4, 157.3, 148.3, 136.1, 135.6, 131.5, 130.5, 130.0, 129.2, 127.9, 123.7, 122.8, 121.7, 117.9, 108.2, 103.9, 99.9, 31.9, 29.6, 29.3, 22.6, 22.2, 20.8, 16.2, 14.1, 13.5.

MALDI (m/z): 846.14 (calc. 846.13)

2.4.2.2. Synthesis of donor groups

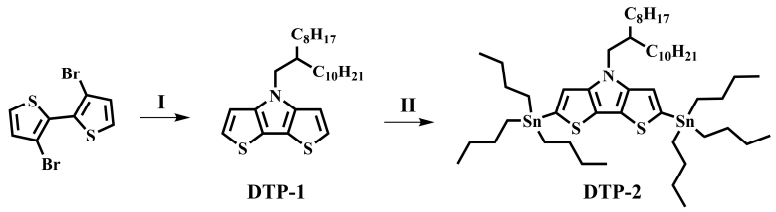

Scheme 2.7 Synthetic route for dithienopyrrole (**DTP**) compound. (I: NaOtBu, BINAP, $Pd_2(dba)_3$, 2-octyldodecane-1-amine, Toluene. II: *n*-BuLi, Bu_3SnCl, THF).

2.4.2.2.1. Synthesis of 4-(2-octyldodecyl)-4*H*-dithieno[3,2-*b*:2',3'-*d*] pyrrole (DTP-1)[67]

3,3'-dibromo-2,2'-bithiophene (6.79 g, 20.94 mmol), sodium *tert*-butoxide (3.82 g, 39.79 mmol), 2,2′-bis(diphenylphosphino)-1,1′-binaphthyl (1.56 g, 2.51 mmol), and tris(dibenzylideneacetone)dipalladium(0) (0.57 g, 0.63 mmol) were dissolved in dry toluene (70 mL) under argon. 2-Octyldodecan-1-amine (5.06 g, 17 mmol) was added to the mixture and the reaction took place at 110 °C for 12 h. The reaction mixture was poured into water and extracted with ethyl acetate. The organic layer dried over Na_2SO_4 and the solvent was removed under reduced pressure. The crude product was purified with column chromatography (silica gel, eluent hexane/DCM, 5:1) to yield a yellow oil (25% yield).

^{1}H NMR (400 MHz, $CDCl_3$) δ/ppm: 7.17 (d, 2H), 7.00 (d, 2H), 4.08 (d, 2H), 2.03 (s, 2H), 1.30 (m, 32 H), 0.92 (m, 6H).

^{13}C NMR (101 MHz, $CDCl_3$) δ/ppm: 145.3, 122.6, 114.5, 111.0, 51.7, 39.0, 31.6, 29.8, 29.5, 29.5, 26.4, 22.6, 14.1, 14.0.

2.4.2.2.2. Synthesis of 4-(2-octyldodecyl)-2,6-bis(tributylstannyl)-4*H*-dithieno[3,2-*b*:2',3'-*d*]pyrrole (DTP-2)[67]

4-(2-Octyldodecyl)-4*H*-dithieno[3,2-*b*:2',3'-*d*]pyrrole **(DTP-1)** (2.4 g, 5.22 mmol) was dissolved in dry THF (30 mL) and cooled to -78 °C under argon atmosphere. *n*-BuLi (4.66 mL, 13.05mmol) was added dropwise, and the mixture was stirred for 1 h and afterwards slowly warmed up to RT. Then, the reaction was cooled to -78 °C again and Tributyltin chloride (Bu_3SnCl) (3.54 mL, 13.05 mmol) was added in one portion. The reaction mixture was stirred overnight at RT. The reaction mixture was poured into water and extracted with $CHCl_3$. The organic layer was dried over Mg_2SO_4 and the solvent was removed under reduced pressure. The final product was obtained as a brown oil and was used without further purification (92% yield).

^{1}H NMR (400 MHz, $CDCl_3$) δ/ppm: 6.96 (s, 2H), 4.08 (d, 2H), 2.03 (s, 1H), 1.69-1.56 (m, 12H) 1.24-1.43 (m, 46 H) 1.14-1.19 (m, 10H), 0.90-0.96 (m, 24H).

^{13}C NMR (101 MHz, $CDCl_3$) δ/ppm: 148.3, 134.5, 120.1, 118.2, 51.6, 39.1, 31.9, 29.9, 29.6, 29.0, 28.2, 27.2, 16.4, 15.5, 14.0, 13.7, 13.6, 12.6, 10.9, 9.1, 8.7.

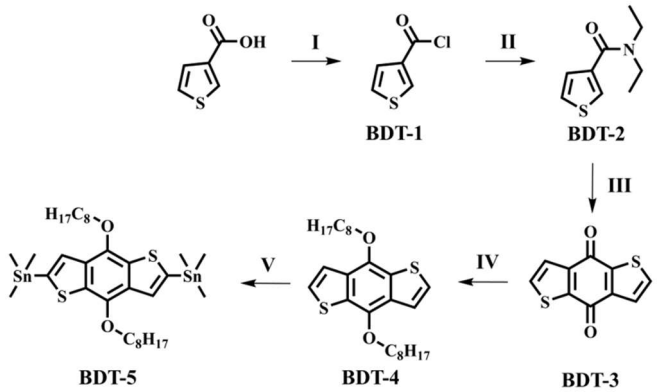

Scheme 2.8 Synthetic route for benzodithiophene (**BDT**) compound. (I: oxalyl chloride, DCM. II: $(CH_3CH_2)_2N$, DCM. III: *n*-BuLi, THF. IV: Zn, NaOH, H_2O, *n*-$C_8H_{17}Br$, TBAB. V: *n*-BuLi, Me_3SnCl, THF.)

2.4.2.2.3. Synthesis of thiophene-3-carbonyl chloride (BDT-1)[68]

Thiophene-3-carboxylic acid (28.84 g, 0.1 mol) was dissolved in DCM (25 mL) and cooled with an ice-water bath. Oxalyl chloride (25.4 g, 0.2 mol) was added to the solution and the reaction mixture stirred overnight at RT. The solvent and unreacted oxalyl chloride were removed under reduced pressure. The product was obtained as a colourless solid and was used without further purification.

2.4.2.2.4. Synthesis of N,N-Diethylthiophene-3-carboxamide (BDT-2) [68]

Diethylamine (14.6 g, 0.2 mol) was added to DCM (35 mL), and the mixture was cooled with an ice-water bath. Thiophene-3-carbonyl chloride **(BDT-1)** (14.06 g, 0.09 mol) was dissolved in DCM (25 mL) and added dropwise. After addition, the ice bath was removed and the solution was stirred at RT for 30 min. The organic phase was washed with water several times, the aqueous phase extracted with DCM. After drying the organic phase over Mg_2SO_4, the solvent was removed under reduced pressure. The crude product was purified by distillation under vacuum. N,N-Diethylthiophene-3-carboxamide **(BDT-2)** was obtained as a yellow oil (78% yield).

^{1}H NMR (400 MHz, $CDCl_3$) δ/ppm: 7.41 (s, 1H), 7.26 (d, 1H), 7.12 (d, 1H), 3.37 (m, 4H), 1.14 (t, 6H).

^{13}C NMR (101 MHz, $CDCl_3$) δ/ppm: 166.9, 136.6, 128.2, 126.4, 122.3, 42.1, 13.1.

2.4.2.2.5. Synthesis of benzo[1,2-*b*:4,5-*b′*]dithiophene-4,8-dione (BDT-3)[68]

N,N-Diethylthiophene-3-carboxamide **(BDT-2)** (9.16 g, 50 mmol) was dissolved in THF (50 mL) and cooled with an ice-bath under argon atmosphere. 2.5 M *n*-butyllithium in hexane (20 mL, 50 mmol) was added dropwise to the solution. The reaction was stirred at RT for 30 min. The reaction mixture was quenched with ice-water. The resulting suspension was filtered, and the resulting yellow precipitate was washed with water, methanol, and hexane respectively. Benzo[1,2-*b*:4,5-*b′*]dithiophene-4,8-dione **(BDT-3)** was obtained as yellow powder (60% yield).

^{1}H NMR (400 MHz, $CDCl_3$) δ/ppm: 7.68 (d, 2H), 7.65 (d, 2H).

^{13}C NMR (101 MHz, $CDCl_3$) δ/ppm: 174.7, 145.2, 142.9, 131.6, 126.4.

2.4.2.2.6. Synthesis of 4,8-bis(octyloxy)-4,8-dihydrobenzo[1,2-*b*:4,5-*b′*]dithiophene (BDT-4) [68]

Benzo[1,2-*b*:4,5-*b′*]dithiophene-4,8-dione **(BDT-3)** (2.21 g, 10 mmol), zinc powder (1.43 g, 22 mmol) and 30 mL of water were mixed in a flask. Then NaOH (6 g, 150 mmol) was added to the flask and the reaction mixture was refluxed under argon atmosphere for 1 h. After 1 h, 1-bromooctane (6.1 g, 30 mmol) and a catalytic amount of tetrabutylammonium bromide (TBAB) were added and the reaction was refluxed for 12 h. The reaction was quenched with cold water and extracted with diethyl ether. The organic phase was dried over Mg_2SO_4 and the solvent removed under reduced pressure. The crude product was recrystallized from ethanol to give 4,8-bis(octyloxy)-4,8-dihydrobenzo[1,2-*b*:4,5-*b*']dithiophene **(BDT-4)** (68% yield).

^{1}H NMR (400 MHz, $CDCl_3$) δ/ppm:7.47 (d, 2H), 7.37 (d, 2H), 4.28 (t, 4H), 1.88 (quint, 4H), 1.55 (m, 4H), 1.40-1.28 (m, 16H), 0.90 (t, 6H).

^{13}C NMR (101 MHz, $CDCl_3$) δ/ppm: 144.5, 131.6, 130.1, 125.9, 120.3, 73.9, 31.8, 30.5, 29.3, 29.2, 26.0, 22.6, 14.1.

2.4.2.2.7. Synthesis of 4,8-bis(octyloxy)-4,8-dihydrobenzo[1,2-*b*:4,5-*b′*]dithiophene-2,6diyl)bis (trimethylstannane) (BDT-5) [68]

4,8-bis(octyloxy)-4,8-dihydrobenzo[1,2-*b*:4,5-*b′*]dithiophene **(BDT-4)** (2.23 g, 5 mmol) was dissolved in THF (100 mL) under argon atmosphere. 2.5 M *n*-BuLi (11 mmol) was added dropwise at RT and stirred for 1h. When the white precipitate appeared, the flask was cooled with ice-bath and 1 M trimethyltin chloride ($SnMe_3Cl$) (12 mL, 12 mmol) was added in one portion. The cooling bath was removed and the reaction mixture was stirred at RT for 2 h. The reaction was quenched with cold water and extracted with diethyl ether. The organic layer was dried over Mg_2SO_4 and the solvent was removed under reduced pressure. The crude product was recrystallized with ethanol. **BDT-5** was obtained as colourless crystals (65% yield).

^{1}H NMR (400 MHz, $CDCl_3$) δ/ppm: 7.51 (s, 2H), 4.30 (t, 4H), 1.88 (quint., 4H), 1.58 (m, 4H), 1.43-1.31 (m, 16H), 0.90 (t, 6H), 0.45 (s, 18H).

^{13}C NMR (101 MHz, $CDCl_3$) δ/ppm: 143.6, 140.7, 135.8, 132.6, 128.2, 73.4, 31.4, 30.0, 29.0, 28.9, 26.3, 22.9, 14.0, -8.8.

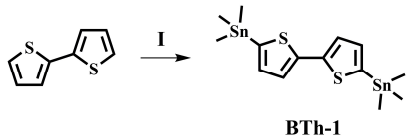

BTh-1

Scheme 2.9 Synthetic route for bithiophene (**BTh**) compound. (I: *n*-Buli, Me_3SnCl, THF)

2.4.2.2.8. Synthesis of 5,5'-bis(trimethylstannyl)-2,2'-bithiophene (BTh-1)[69]

2,2'-bithiophene (4.0 g, 24.1 mmol) was dissolved in THF (110 mL) and cooled to -78 °C under argon atmosphere. 1.6 M *n*-BuLi in hexane (35 mL, 56.0 mmol) was added dropwise at -78 °C. The mixture was stirred for 1 h at -78 °C then slowly warmed up to RT. The mixture was cooled to -78 °C again, and trimethylstannyl chloride (Me_3SnCl) (11.6 g, 58.2 mmol) in THF (10 mL) was added dropwise. The mixture was gradually warmed up to room temperature and stirred for 12 h. The mixture was extracted with DCM, and the organic phase was dried over Mg_2SO_4. The crude product was purified by column chromatography (silica gel, eluent: hexane), followed by recrystallization from MeOH, yielding white crystals (65% yield).

^{1}H NMR (400 MHz, $CDCl_3$) δ/ppm: 7.27 (d, 2H), 7.08 (d, 2H), 0.40 (s, 18H).

^{13}C NMR (101 MHz, $CDCl_3$) δ/ppm: 143.0, 138.0, 124.7, 8.3.

2.4.2.3. The general procedure of microwave-assisted Stille-type polymerization

B7 (1 eq), the corresponding distannylated comonomer (1 eq) and tetrakis(triphenylphosphine)palladium(0) ($Pd(PPh_3)_4$) (0.050 eq) were placed in a microwave vial under argon and dissolved in a dry DMF:toluene (1:3) mixture. After irradiation in the microwave reactor for 40 min at 120 °C, (400 W), the mixture was precipitated into cold methanol (MeOH), and the solid product was collected by filtration. The crude product was further purified by successive Soxhlet extractions with acetone, hexane, and ethyl acetate, respectively. The product was collected from the chloroform ($CHCl_3$) fraction. Finally, the copolymers were re-precipitated into cold methanol. The products were obtained as dark green powders.

2.4.2.3.1. P1

Dibrominated, ring-fused BODIPY **(B7)** (201 mg, 0.24 mmol), distannylated **DTP-2** (247 mg, 0.24 mmol) and $Pd(PPh_3)_4$ (13.75 mg, 0.0119 mmol) were dissolved in 20 mL of a DMF:toluene (5:15) mixture.

Yield: $CHCl_3$-fraction (180 mg, 65%) as dark green powder.

^1H NMR (600 MHz, $CDCl_3$) δ/ppm: 10.73 (s,1H), 9.44 (d, 2H), 7.46 (s, 2H), 7.29 (s, 4H), 7.19 (d,2H), 3.92-3.85 (m, 2H), 3.74 (q, 4H), 2.34 (s, 6H), 2.21 (s, 12H),2.04 (m, 1H), 1.58-1.30 (m, 36H), 0.90 (s, 6H).

^{13}C NMR (151 MHz, $CDCl_3$) δ/ppm: 192.6, 186.3, 173.3, 145.6, 136.5, 135.9, 130.4, 130.1, 129.0, 123.7, 123.7, 122.7, 120.9, 114.6, 108.6, 66.7, 51.9, 49.1, 47.5, 38.6, 33.9, 31.8, 30.3, 29.5, 28.8, 24.4, 23.7, 22.8, 14.0.

GPC (THF, PS standard): M_n= 7.1 kg/mol, M_w= 22.0 kg/mol.

TGA: 160 °C (5 % weight loss) (argon).

2.4.2.3.2. P2

Dibrominated, ring-fused BODIPY **(B7)** (190 mg, 0.22 mmol), distannylated **BDT-5** (173 mg, 0.22 mmol) and $Pd(PPh_3)_4$ (13 mg, 0.01112mmol) were dissolved in 12 mL of a DMF:toluene (3:9) mixture.

Yield: $CHCl_3$-fraction (160 mg, 61%) as dark green powder.

^1H NMR (600 MHz, $CDCl_3$) δ/ppm: 10.74 (s, 1H), 8.67 (d, 2H), 7.72 (d, 2H), 7.06-6.97 (m, 6H), 6.69 (d, 2H), 4.40 (m, 4H), 3.76 (m, 4H), 2.40 (s, 6H), 2.25 (s, 12H), 1.63-1.13 (m, 30H), 0.88 (s, 6H).

^{13}C NMR (151 MHz, $CDCl_3$) δ/ppm: 192.7, 186.9, 186.4, 159.9, 148.1, 144.3, 135.7, 132.2, 132.1, 130.8, 130.6, 130.3, 130.0, 128.5, 128.4, 126.2, 122.6, 121.4, 74.0, 51.9, 50.6, 49.3, 48.9, 47.5, 44.0, 42.2, 42.2, 31.7, 31.7, 30.5, 29.3, 29.1, 26.0, 22.5, 22.5, 16.2, 14.0.

GPC (THF, PS standard): M_n= 19.6 kg/mol, M_w= 91.1 kg/mol.

TGA: 150 °C (5 % weight loss) (argon).

2.4.2.3.3. P3

Dibrominated, ring-fused BODIPY **(B7)** (180 mg, 0.21 mmol), distannylated **BTh-1** (105 mg, 0.21 mmol) and $Pd(PPh_3)_4$ (12.31 mg, 0.01065 mmol) were dissolved in 12 mL of a DMF:toluene (3:9) mixture.

Yield: $CHCl_3$-fraction (120 mg, 64%) as dark green powder.

^1H NMR (600 MHz, $CDCl_3$) δ/ppm: 9.24 (s, 1H), 8.54-8.70 (d, 2H), 7.35 (d, 2H), 7.12-7.25 (s, 4H), 7.08 (d, 2H), 6.77 (d, 2H), 3.56 (q, 4H), 2.40 (s, 6H), 2.26 (s, 12H), 1.45-1.65 (m, 6H).

^{13}C NMR (151 MHz, $CDCl_3$) δ/ppm: 192.1, 186.4, 159.6, 148.1, 135.7, 130.4, 130.0, 128.4, 124.0, 122.7, 117.6, 29.2, 21.0, 20.8, 16.2, 13.5.

GPC (THF, PS standard): M_n= 5.1 kg/mol, M_w= 6.3 kg/mol.

TGA: 149 °C (5 % weight loss) (argon).

2.5. References

1. V. Yakubovskyi, M. Shandura, P. Mykola, Y. Kovtun, *Eur. J. Org. Chem.*, **2009**, *19*, 3237.
2. M. Matsuoka, *J. Soc. Dyers Colourists*, **1989**, *105*, 167.
3. A. Loudet, K. Burgess, *Chem. Rev.* **2007**, *107*, 4891.
4. T. Rousseau, A. Cravino, T. Bura, G. Ulrich, Z. Ziessel, J. Roncali, *Chem. Commun.* **2009**, *19*, 2298.
5. J. Karolin, L. B.-A. Johansson, L. Strandberg, T. Ny, *J. Am. Chem. Soc.* **1994**, *116*, 7801.
6. G. Ulrich, R. Ziessel, A. Harriman *Angew. Chem. Int. Ed.* **2008**, *47*, 1184.
7. A. Schmitt, B. Hinkeldey, M. Wild, G. Jung, *J. Fluor.* **2009**, *4*, 755.
8. T. Rousseau, A. Cravino, T. Bura, G. Ulrich, R. Ziessel, J. Roncali, *J. Mater. Chem.* **2009**, *19*, 2298.
9. T. Rousseau, A. Cravino, T. Bura, G. Ulrich, R. Ziessel, J. Roncali, *Chem. Commun*. **2009**, *0*, 1673.
10. S. Erten-Ela, M. D. Yilmaz, B. Icli, Y. Dede, S. Icli, E. U. Akkaya, *Org. Lett.* **2008**, *10*, 3299.
11. S. Koleman, Y. Cakmak, S. Erten-Ela, Y. Altay, J. Brendel, M. Thelakkat, E. U. Akkaya, *Org. Lett.* **2010**, *12*, 3812.
12. X. Peng, J. Du, J. Fan, J. Wang, Y. Wu, J. Zhao, S. Sun, T. Xu, *J. Am. Chem. Soc.* **2007**, *129*, 1500.
13. L. Zeng, E. Miller, A. Pralle, E. Y. Isacoff, C. J. Chang, *J.Am. Chem. Soc*. **2005**, *128*, 10.
14. O. A. Bozdemir, R. Guliyev, O. Buyukcakir, S. Selcuk, S. Koleman, G. Gulseren, T. Nalbantoglu, H. Boyaci, E. U. Akkaya, *J. Am. Chem. Soc*. **2010**, *132*, 8029.
15. T. L. Arbeloa, F. L. Arbeloa, I. L. Arbeloa, I. Garcia-Moreno, A. Costela, R. Sastre, F. Amat-Guerri, *Chem. Phys. Lett.* **1999,** *299,* 315.
16. T. A. Golovkova, D. V. Kozlov, D. C. Neckers, *J. Org. Chem.* **2005,** *70*, 5545.
17. C. Trieflinger, K. Rurack, J. Daub, *Angew. Chem. Int. Ed.* **2005,** *44*, 2288.
18. A. Kamkaew, S. H. Lim, H. B. Lee, L. V. Kiew, L. Y. Chung, K. Burgess, *Chem.Soc. Rev*. **2012**, *42*, 77.
19. A. Treibs, F. H. Kreuzer, *Justus Liebigs Ann. Chem*. **1968**, *718*, 208.

20. T. Wood, A. Thompson, *Chem. Rev.*, **2007**, 107, 1831
21. A. Entwistle, M. Noble, *J. Microsc.* **1992**, *168*, 219.
22. N. Boens, V. Leen, W. Dehaen, *Chem. Soc. Rev*. **2012**, *41*, 1130.
23. M. Shah, K. Thangaraj, M. Soong, M. Wolford, J. Boyer, I. Politzer, T. Pavlopoulos, *Heteroat. Chem.* **1990**, *1*, 389.
24. Z. Li, E. Mintzer, R. Bittman, *J. Org. Chem*. **2006**, *71*, 1718.
25. V. Yakubovskyi, M. Shandura, P. Mykola, Y. Kovtun, *Eur. J. Org. Chem.* **2009**, *19*, 3237.
26. Z. Shen, H. Rohr, K. Rurack, H. Uno, M. Spieles, B. Schulz, G. Reck, N. Ono, *Chem. Eur. J.* **2004**, *10*, 4853.
27. H. Xiang, J. Cheng, X. Ma, X. Zhou, J. J. Chruma, *Chem. Soc. Rev.* **2013**, *42*, 6128.
28. S.-i. Todoroki, S. Sakaguchi, K. Sugii, *Jpn. J. Appl. Phys., Part 1*. **1995**, *34*, 3128.
29. A. Burghart, H. Kim, M. B. Welch, L. H. Thoresen, J. Reibenspies, K. Burgess, F. Bergström, L. B. -A. Johansson, *J. Org. Chem.* **1999,** *64*, 7813.
30. Y.-H. Yu, Ana B. Descalzo, Z. Shen, H. Röhr, Q. Liu, Y.-W. Wang, M. Spieles, Y.-Z. Li, K. Rurack, X.-Z. You, *Chem. Asian. J.* **2006**, *1*, 176.
31. G. Ulrich, S. Goeb, A. De Nicola, P. Retailleau, R. Ziessel, *Synlett* **2007**, *10*, 1517.
32. K. Umezawa, A. Matsui, Y. Nakamura, D. Citterio, K. Suzuki, *J. Am. Chem. Soc*. **2008**, *130*, 1550.
33. K. Umezawa, A. Matsui, Y. Nakamura, D. Citterio, K. Suzuki, *Chem. Eur. J*. **2009**, *15*, 1096.
34. C. Jiao, K. Huang, J. Wu, *Org. Lett*. **2011**, *13*, 632.
35. C. Jiao, L. Zhu, J. Wu, *Chem. Eur. J*. **2011**, *17*, 6610.
36. L. Zeng, C. Jiao, X. Huang, K. Huang, W. Chin and J. Wu, *Org. Lett.* **2011**, *13*, 6026.
37. M. A. T. Rogers, *J. Chem. Soc.* **1943**, 590.
38. J. Killoran, L. Allen, J. F. Gallagher, W. M. Gallagher, D. F. O'Shea, *Chem.Commun.* **2002**, 1862.
39. A. Gorman, J. Killoran, C. O'Shea, T. Kenna, W. M. Gallagher, D. F. O'Shea, *J. Am. Chem. Soc.* **2004**, *126*, 10619.
40. X. Zhang, H. Yu, Y. Xiao, *J. Org. Chem.* **2012**, *77*, 669.

41. Q. Bellier, F. Dalier, E. Jeanneau, O. Maury, C. Andraud, *New J. Chem.* **2012**, *36*, 768.
42. H. Lu, S. Shimizu, J. Mack, Z. Shen, N. Kobayashi, *Chem. Asian J.* **2011**, *6*, 1026.
43. W. Zhao, E. M. Carreira, *Angew. Chem. Int. Ed.* **2005**, *44*, 1677.
44. W. Zhao, E. M. Carreira, *Chem.Eur. J.* **2006**, *12*, 7254.
45. J. Li, Y. Zhao, H. S. Tan, Y. Guo, C.-A. Di, G. Yu, Y. Liu, M. Lin, S. H. Lim, Y. Zhou, H. Su, B. S. Ong, *Sci. Rep.* **2012**, *2*, 754.
46. H. E. Katz, Z. Bao, S. L. Gilat, *Acc. Chem. Res.* **2001**, *34*, 359.
47. L. Chua, J. Zaumseil, J. Chang, E. C.-W. Ou, P. K.-H. Ho, H. Sirringhaus, R. H. Friend, *Nature* **2005**, *434*, 194.
48. M.-C. Chen, S. Vegiraju, C.-M. Huang, P.-Y. Huang, K. Prabakaran, S. L. Yau, W.-C.Chen, W.-T. Peng, I. Chao, C. Kim, Y.-T. Tao, *J. Mater. Chem. C* **2014**, *2*, 8892.
49. D. Cortizo-Lacalle, C. T. Howells, S. Gambino, F. Vilela, Z. Vobecka, N. J. Findlay, A. R. Inigo, S. A. J. Thomson, P. J. Skabara, I. D. W. Samuel, *J. Mater. Chem.* **2012**, *22*, 14119.
50. H.-Y. Lin, W.-C. Huang, Y.-C. Chen, H.-H Chou, C.-Y. Hsu, J. T. Lin, H.-W. Lin, *Chem. Commun.* **2012**, *48*, 8913.
51. B. C. Popere, A. M. D. Pelle, S. Thayumanavan, *Macromolecules* **2011**, *44*, 4767.
52. T. Bura, N. Leclerc, S. Fall, P. Lévêque, T. Heiser, P. Retailleau, S. Rihn, A. Mirloup, R. Ziessel, *J. Am. Chem. Soc.* **2012**, *134*, 17404.
53. H. Usta, M. D. Yilmaz, A. J. Avestro, D. Boudinet, M. Denti, W. Zhao, J. F. Stoddart, A. Facchetti, *Adv. Mater.* **2013**, *25*, 4327.
54. A. M. Poe, A. M. Della Pelle, A. V. Subrahmanyam, W. White, G. Wantz, S. Thayumanavan, *Chem. Commun.* **2014**, *50*, 2913.
55. S. Singh, V. Venugopalanac, K. Krishnamoorthy, *Phys. Chem. Chem. Phys*. **2014**, *16*, 13376.
56. M. Ozdemir, D. Choi, G. Kwon, Y. Zorlu, B. Cosut, H. K. Kim, A. Facchetti, C. Kim, H. Usta, *ACS Appl. Mater. Interfaces* **2016**, *8*, 14077.
57. M. Ozdemir, D. Choi, G. Kwon, Y. Zorlu, B. Cosut, H. K. Kim, C. Kim, H. Usta, *New J. Chem.* **2017**, *41*, 6232.
58. S. Wanwong, P. Khomein, S. Thayumanavan, *Chem. Cent. J.* **2018**, *12,* 60.

59. B. M. Squeo, V. G. Gregoriou, Y. Han, A. Palma-Cando, S. Allard, E. Serpetzoglou, I. Konidakis, E. Stratakis, A. Avgeropoulos, T. D. Anthopoulos, M. Heeney, U. Scherf, C. L. Chochos, *J. Mater. Chem. C* **2018**, 6, 4030.
60. A. Mirloup, N. Leclerc, S. Rihn, T. Bura, R. Bechara, A. Hebraud, P. Leveque, T. Heiser, R. Ziessel, *New J. Chem*. **2014**, *38*, 3644.
61. Q. Huaulmé, A. Sutter, S. Fall, D. Jacquemin, P. Lévêque, P. Retailleau, G. Ulrich, N. Leclerc, *J. Mater. Chem. C* **2018**, *6*, 9925.
62. N. K. S. Davis, A. L. Thompson, H. L. Anderson, *Org. Lett*. **2010**, *12*, 2124.
63. K. Naoda, H. Mori, N. Aratani, B. S. Lee, D. Kim, A. Osuka, *Angew. Chem. Int. Ed.* **2012**, *51*, 9856.
64. N. K.S. Davis, A. L. Thompson, H. L. Anderson, *J. Am. Chem. Soc*. **2011**, *133,* 30.
65. L. Zeng, C. Jiao, X. Huang, K.-W. Huang, W.-S. Chin, J. Wu, *Org. Lett*. **2011**, *13*, 6026.
66. J. -H. Ye, G. Wang, C. Huang, Z. Hu, W. Zhang, Y. Zhang, *Synhtesis* **2012**, *44*, 104.
67. X. Zhang, T. T. Steckler, R. R. Dasari, S. Ohira, W. J. Postcavage Jr, S. P. Tiwari, S. Coppee, S. Ellinger, S. Barlow, J.-L. Bredas, B. Kippelen, J. R. Reynolds, S. R. Marder, *J. Mater. Chem.* **2010**, *20*, 123.
68. H. -Y. Chuang, S. L. -C. Hsu, P. -I. Lee, J. -F. Lee, S. -Y. Huang, S. -W. Lin, P. -Y. Lin, *Polym. Bull.* **2014**, *71*, 1117.
69. S. Kotani, K. Shiina, K. Sonogashira, *J. Organomet. Chem*. **1992**, *429*, 403.
70. C. M. Cardona, W. Li, A. E. Kaifer, D. Stockdale, G. C. Bazan, *Adv. Mater*. **2011**, *23*, 2367.

CHAPTER 3

POLY(TETRAPHENYLETHYLENE) DERIVATIVES FOR NITROAROMATIC COMPOUND DETECTION[1]

3.1. Introduction[1]

Aggregation-induced emission (AIE) has attracted much attention since it was first reported in 2001.[2] This young field of current materials research is developing fastly and recent reviews have summarized the state-of-the-art developments of AIE-type macromolecules, including their design, syntheses, structures, π-electron-topologies, substitution patterns, and applications.[3-5] The number of publications is growing exponentially, and great progress has been made so far.

In this study, five different AIE active linear poly(TPE)s were synthesized in a reductive polyolefination starting from bis (*α*,*α*-dichlorobenzyl)arene monomers. These polymers were first described by Hörhold et al., about 40 years ago, but without a clear description of AIE properties.[6-10] In contrast to Hörhold and coworkers, dicobalt octacarbonyl was used in this work as the condensing agent, a method that has been developed by Scherf and coworkers in 1990's.[11] Modification of the electronic nature of the polymer backbone delivers a versatile tool for fine-tuning of the optical properties of the resulting polymers regarding the degree of electronic configuration and the nature of the aryl rotors. In this line, the substitution of the main chain phenylene units and the aryl rotors were varied. Moreover, the main chain phenylene was also replaced by diphenylether units. In addition to the AIE properties, the promising applications of these materials in OLED and fluorometric detection of nitroaromatic compounds have been investigated in this chapter.

In the following sections of the introduction, basic principles about AIE phenomena and recent progresses in literature about syntheses, characterizations and applications are explained briefly.

3.1.1. Aggregation-caused quenching (ACQ)

The process named as "concentration quenching" was first reported in Förster and Kasper's study with pyrene in 1954.[12] In this study it was observed that the major factor responsible for fluorescence quenching is the formation of aggregates in solution or solid-state. Most common organic luminophores such as naphthalene, anthracene, perylene, carbazole, fluorene, triphenylamine, diketopyrrolopyrrole, perylene diimide, naphthalene diimide, porphyrins, etc. display the aggregation-caused quenching effect in aggregated form. As these and many other luminophores possess π-conjugation and a rigid planar structure; they are subjected to strong intermolecular π-π stacking interactions which lead to aggregates in the solid-state. The excited states of these aggregates often decay non-radiatively and result in reduced or complete loss of emission.[13-20]

The ACQ effect limits the usage and implementation of these luminogens in real-life practical applications such as OLEDs, OFETs, chemical, and bio-sensors. Many studies have been done to overcome this problem such as attachment of bulk branched groups, blending with transparent polymers or encapsulation by surfactants, etc. to prevent aggregation.[21-25] However, these solutions reached a limited success since the loss of other important properties stays an issue.

To overcome the ACQ effect, developing of a system is required in which aggregation affects positively the enhancement of luminescence.

3.1.2. Aggregation-induced emission (AIE)

The unusual effect, aggregation-induced emission (AIE) was pioneered by Tang and coworkers in 2001.[2] In their first study; it was observed that the 1,1,2,3,4,5-hexaphenyl-1*H*-silole (HPS) molecule is intensely emissive in the aggregated state while non-emissive in dilute solution. The restriction of intramolecular motions, including rotations and vibrations, were rationalized as the origin of this effect by experimental and theoretical analyses.[26-29] As the light emission is enhanced due to the aggregation, this phenomenon represents an "anti-ACQ" effect. Starting from the HPS molecule, the findings induced the development of numerous AIE luminogens such as tetraphenylethylene (TPE), distyreneanthracene (DSA), tetraphenylpyrazine (TPP), etc. as shown in Figure 3.1.

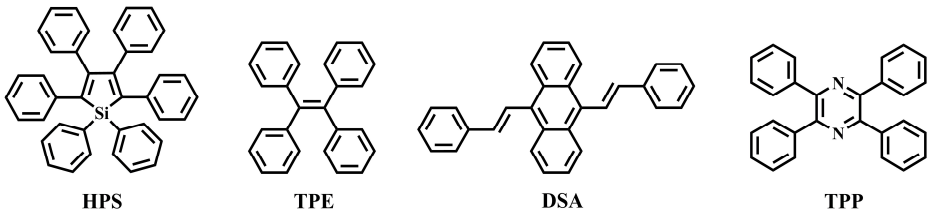

Figure 3.1 Chemical structures of different AIE luminogens.

The discovery of this unique characteristic led to the development of potential applications of AIE luminogens as solid-state emitters in devices, chemosensors, bioprobes, and so on.

3.1.3. AIE working principle

For the structural design and technological applications, it is crucial to understand the photophysics behind the AIE phenomenon. In the last years, several hypotheses have been reported to explain the AIE behaviour such as J-aggregate formation, twisted intramolecular charge transfer (TICT), conformational planarization, cis-trans isomerization, but none of them can be generalized for every AIE molecule.[30-33] According to the systematic studies, the restriction of intramolecular motions (RIM), including rotations (RIR) and vibrations (RIV), were rationalized as the mechanism of this phenomena as indicated in previous section.[26-29]

The non-radiative relaxation process of an excited state molecule can occur via molecular movements such as rotations or vibrations. RIR mechanism (Figure 3.2 (a)) mainly is seen in non-planar propeller-shaped molecules with rotatable groups (rotors).[34-36] Due to the high freedom of space in dilute solution of these molecules, the rotors consume the photon energy with rotational movements and relax non-radiatively to the ground state without light emission. However, in the aggregated state, the intramolecular rotation of these rotors is blocked, and the radiative relaxation becomes favourable which resulted in luminescence. HPS and TPE are the most well-known examples that follow RIR mechanism. The other non-planar AIE active molecules which do not bear rotors obey the RIV mechanism.[37-39] The excited state of these molecules in solution allows for vibrational motions (such as conformational changes) resulting in non-radiative excited state decay. Upon aggregation, existent molecular vibrations are significantly blocked, and radiative relaxation occurs in the excited state. 10,10′,11,11′-tetrahydro-5,5′-bidibenzo[*a*,*d*]

[7]annulenylidene (THBA) (Figure 3.2 (b)) which was reported by Tang and coworkers[37] is an example which shows luminescence in the solid-state due to the RIV mechanism. The RIM mechanism is mainly seen in molecules as in Figure 3.3 which exhibit a vibrative core and rotors at the periphery. The luminescence is observed due to the restriction of both rotation and vibration in the same system.

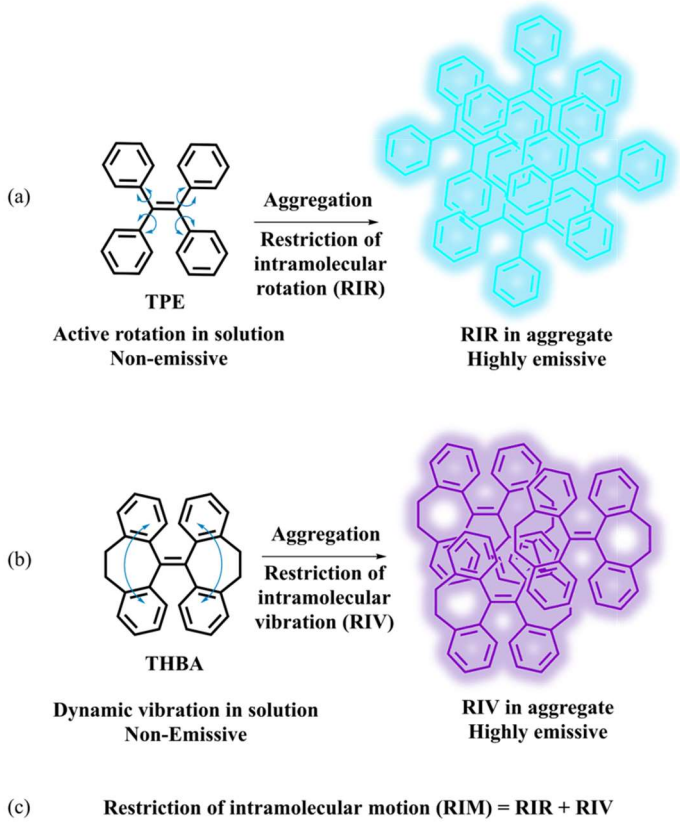

Figure 3.2 The AIE working principle of (a) propeller-shaped luminogen showing RIR, (b) mussel shell-like luminogen showing RIV, and (c) RIM. (Resketched image.[34])

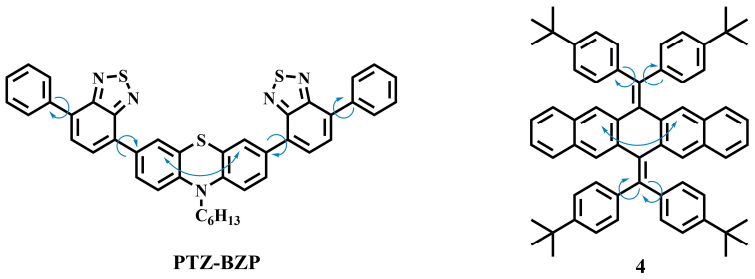

Figure 3.3 AIE luminogens[40,41] showing RIM mechanism.

3.1.4. TPE-based AIE-active polymers

Since the first synthesis reported in 1888 by De Boissieu and coworkers[42], the monomer TPE has been extensively studied due to its high emission efficiency in the solid-state, easy preparation, and various possibilities for post-functionalization. Recently, some interest is shifted to AIE-active polymers as some superior properties (high solid-state emission, easy processability, good thermal stability, photo-, thermo-, and chemosensitivity) have been found as compared to the monomeric AIEgens. Thus, synthesis and research on novel TPE-based, AIE-active polymers have been inevitable. The typical direct polymerization methods for the design of these polymeric materials can be the direct linking of monomeric AIEgens (Scheme 3.1 (a)) or copolymerization with another monomer (Scheme 3.1 (b)), moreover forming AIE active polymers from AIE inactive precursors by generating AIEgen core structures (Scheme 3.1 (c)), homo- and copolymerization of AIEgens which are attached to the polymer as side chain (Scheme 3.1 (d) and (e)) or using initiators containing AIEgens to form linear polymers (Scheme 3.1 (f)) as illustrated in Scheme 3.1. Examples (reactions and polymers) from the literature are explained briefly in the following.

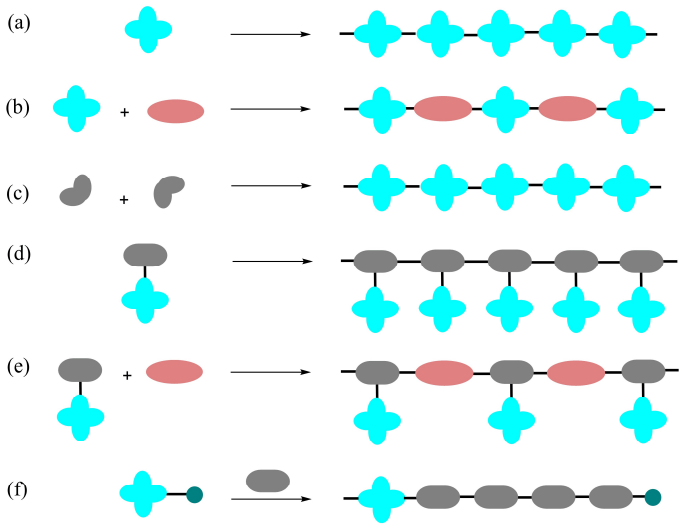

Scheme 3.1 Design strategies for TPE-based, AIE-active polymers. (Resketched scheme.[4])

In 2012, Tang and coworkers[43] published research about TPE-based homopolymers (Figure 3.4) which were synthesized via Suzuki, Wittig, and Sonogashira coupling reactions. The polymers **P1**, **P2** and **P3** showed AIE properties with photoluminescence

quantum yield (PLQY) in the aggregated state (Φ_{aggr}) of 28%, 64%, and 18% respectively. Apart from the optical and electronic characterizations, the effect of picric acid on the light emission intensity of these polymers were observed, resulting in large fluorescence quenching constants. These results suggested that polymers can be used as efficient chemosensors for explosive detection.

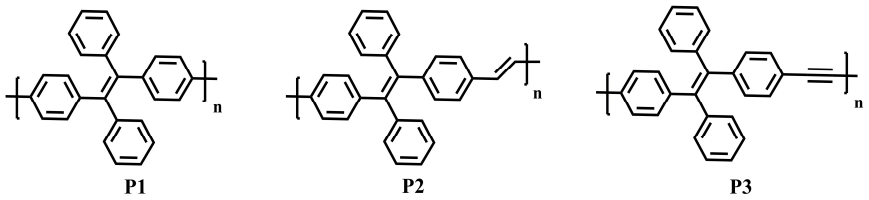

Figure 3.4 The structures of TPE-containing homopolymers.

An example where TPE was used as a side chain in homopolymers was reported by Scherf and coworkers in 2015.[44] Two AIE-active polytriphenylamines with TPE as side group (Figure 3.5) were synthesized via Yamamoto-type coupling. The solid-state PLQYs of **P1** and **P2** are 16.9% and 34.3%, respectively. The interaction of these polymers with trinitrobenzene (TNB) vapor resulted in fluorescence quenching of 50% for **P1** and 63% for **P2** in 1min. These results demonstrated a very competitive performance among materials in the literature which were synthesized for the detection of nitroaromatic explosives.

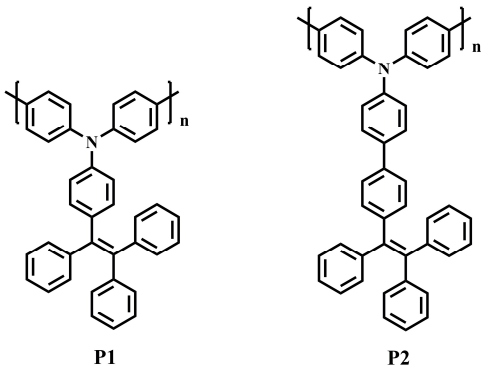

Figure 3.5 The structures of polytriphenylamines with TPE as side groups.

In another work of Tang and coworkers[45], the triphenylamine-containing bis-ketone monomer (as non-AIEgen) was polymerized via a McMurry coupling, and the AIE-active polymer **PTAE** was obtained. The PLQY of the polymer reached 57% in the solid film. The polymer was used to fabricate two-dimensional photoresist patterns which can be used

in the construction of electronic devices and biological probing systems as shown in Figure 3.6.

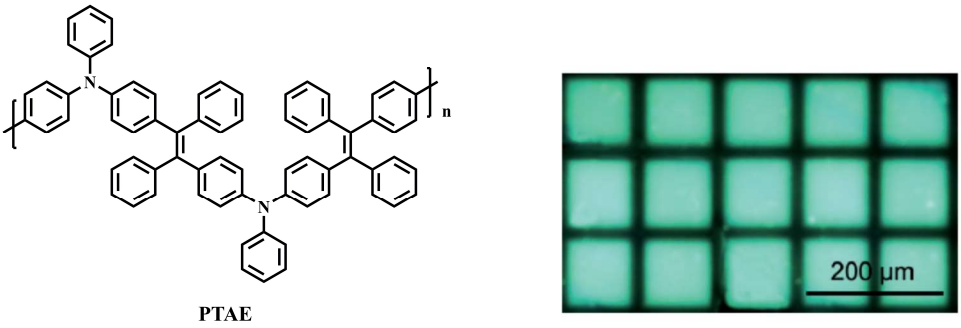

Figure 3.6 The structure of AIE-active polymer **PTAE** which was synthesized from a non-AIEgen ketone monomer and its fluorescent photopattern. (The picture is taken with permission.[45])

The copolymerization of AIEgen-containing monomers with other comonomers is another way to form AIE-active polymers via direct polymerization as indicated at the beginning of this section. One example with an AIEgen embedded in the main chain was reported by Li and coworkers in 2012.[46] The polymer **P3** (Figure 3.7) was synthesized via Suzuki polycondensation. The aggregation-induced emission enhancement (AIEE) active polymer showed 28% PLQY in the aggregated state thanks to the TPE moiety. Applications as an explosive chemosensor, as well as use as active layer in polymer light emitting diode (PLED) were also investigated by the researchers. Compared with other analogues of this study, **P3** showed better EL performance with a maximum brightness of 3609 cd/m^2 and a luminescence efficiency of 1.17 cd/A.

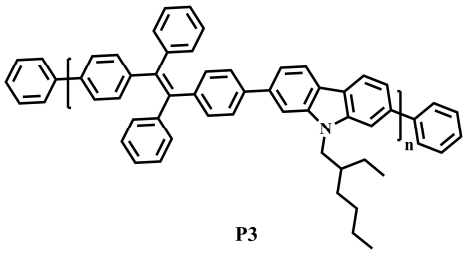

Figure 3.7 The structure of main-chain TPE-containing copolymers.[46]

An example for copolymers with an AIEgen at the side chain was described in the recent work of Scherf and coworkers[47]. The polytriphenylamine derivative polymers **PTPA1-TPE** and **PTPA2-TPE** (Figure 3.8) were synthesized via Yamamoto-type

coupling. These polymers showed AIE properties with PLQY of 20% and 37% respectively in powder form. The explosive detection properties were investigated with different analytes. The paper strip test demonstrated an amplified PL quenching with the TNT analyte. The results suggested that both polymers are promising materials for sensory applications.

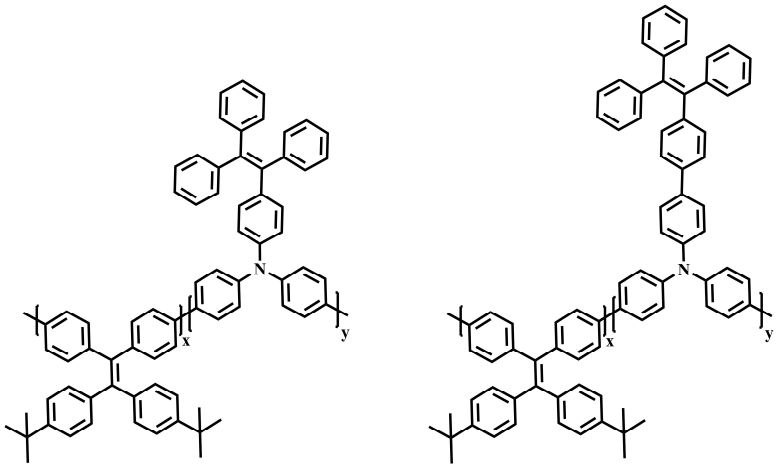

Figure 3.8 The structure of polytriphenylamine copolymers with TPE side chain unit.[47]

In a recent work of Tang and coworkers[48], a group of TPE-containing dithiocarbamate initiators was used for reversible addition fragmentation chain transfer (RAFT) polymerization to prepare AIE-active non-conjugated polymers. The versatility of the polymerization process in situ was monitored in 12 different polymerization systems. One of the polymer structures in which methyl methacrylate (MMA) was used as a monomer with TPE-containing initiator is shown in Figure 3.9.

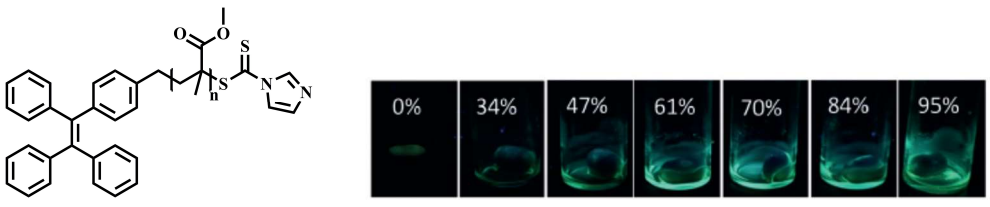

Figure 3.9 The structure of the polymer that is formed in the presence of AIEgen-containing initiator and an MMA monomer. The image shows fluorescent photos of the polymer solution at different conversion under 365 nm UV irradiation. (The image is taken with permission.[48])

Last but not the least, apart from the linear polymer structures, the TPE unit has also been incorporated into hyperbranched polymers[49-51] or conjugated, microporous polymers[52-55]. For example, Tang and coworkers[49] synthesized AIE-active hyperbranched polytriazoles via a Cu(I)-catalyzed click polymerization (Figure 3.10). The polymers **hb-P1a** and **hb-P1b** showed an aggregated state PLQY of 38.3% and 32.2% with a fluorescence enhancement by a factor of 347 and 229 respectively, if compared to the PLQY in solution. Thanks to the AIE effect, the polymers were used to detect explosives with a so-called "super-amplification effect".

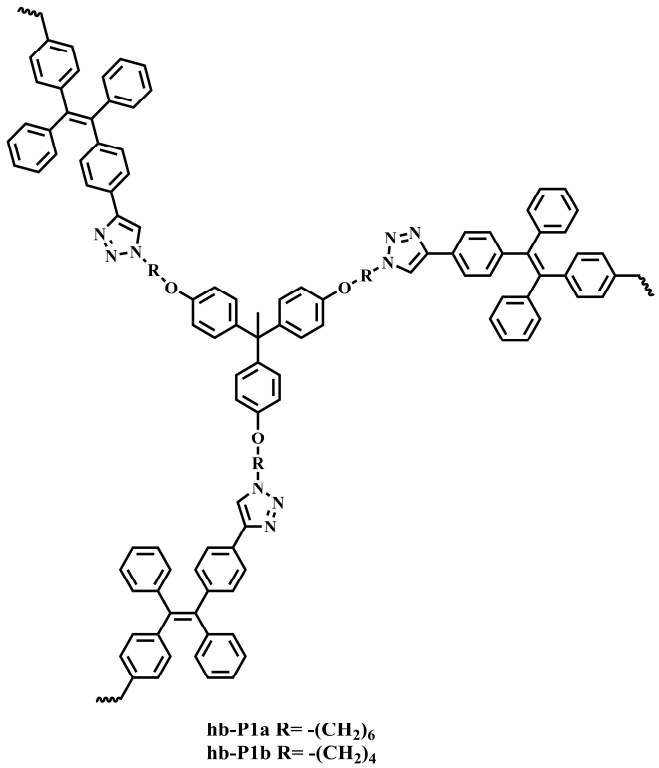

Figure 3.10 The structure of TPE-containing hyperbranched polytriazoles.

A study of Scherf and coworkers[55] presents an example of AIE-active microporous polymer networks. The tetraarylethylene-based microporous polymer networks (Figure 3.11) were synthesized via reductive polyolefination. Among the polymers, **P4** has shown the best solid-state PLQY with 25.3%. Moreover, **P4** showed a moderately high BET surface area of 475 m^2/g. The results of vapor exposure tests with amine analytes suggested that **P4** is a promising material for optical solid-state sensors.

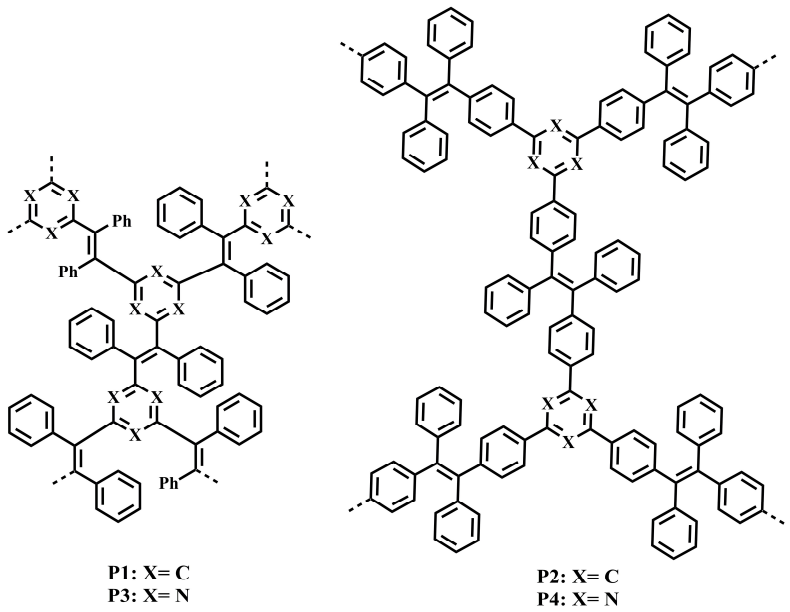

Figure 3.11 The structure of tetraarylethylene-based, microporous polymer networks.

3.1.5. Applications

Easy processability, structural diversity, good thermal stability, photo-, thermo-, and chemosensitivity, and the main property "high solid-state emission" made the AIE-active polymers applicable in diverse areas including optoelectronic applications[43,46,56-58], fluorescent chemo-sensors[44,59-62], biological applications[63,64] and some other special fields like microporous materials[54], stimuli-responsive materials[61,] and photopatternable materials[45,65].

Among these various application areas, the materials that were synthesized and explained in the following Section 3.2 were used in the applications of OLED and explosive detection as indicated before. The theoretical explanations and working principles of these applications were explained in Chapter 1 (Section 1.5.2 and 1.5.3). In this section, some recent progress on AIE-active polymers and small molecules in the related applications will be discussed briefly.

3.1.5.1. Nitroaromatic compound detection

The detection of nitroaromatic compounds is a demanding topic in today's world because it is serving for security purposes. AIE-active polymers have been investigated extensively for sensor applications due to their quick and reliable responses upon interaction with nitroaromatic compounds. This response occurs as a strong fluorescence

quenching with a so-called "superamplification-effect" (in many cases) due to the energy transfer from electron-donor type AIE polymers to the electron-deficient nitroaromatic analytes during an interaction following a static quenching mechanism.[66] The quenching constant which is calculated from Stern-Volmer plot indicates the sensitivity of the AIE material to the analyte. State of the art for the values of these quenching constants reach up to 1.09×10^6 M^{-1} for picric acid (PA) (**P5**), 1.26×10^6 M^{-1} for trinitrobenzene (TNB) (**PCzTPE0.5**) and 1.33×10^6 M^{-1} for trinitrotoluene (TNT) detection (**3**) with the materials are shown in Figure 3.12.[60,67,68]

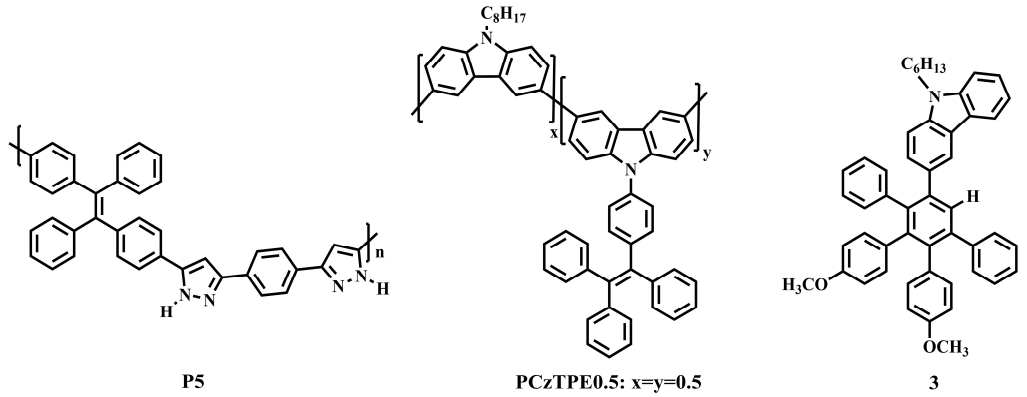

Figure 3.12 The chemical structures of AIE luminogens used for explosive detection.

Besides, explosive vapors can be detected by thin films of AIE-active polymers as in the case of polytriphenylamine derivatives with TPE side groups (Figure 3.5). The trinitrobenzene (TNB) vapors quench the fluorescence intensity of AIE polymers[44] by more than half in short time periods as 1 min. Another extraordinary result was achieved for the detection of dinitrotoluene (DNT) by the AIE polymer **P1** with a 70% fluorescence quenching in 30 s.[61]

3.1.5.2. Organic light emitting diode

Another widely researched application area of AIE-active polymers and small molecules is the field of OLEDs and PLEDs due to their strong solid-state emission. According to the functional units that AIE materials contain, they can be used in the device structure as a light-emitting layer, electron-transporting, and hole transporting layer.

A TPE-based AIE materials, **TPVAn** ($PLQY_{film}$: 89%, λ_{em}: 456 nm), was synthesized by Shu and coworkers[69] and was used as an emitting layer in non-doped

OLEDs. The bright saturated-blue emissive device achieved a maximum external quantum efficiency (EQE) of 5.3% a value that is near the achievable performance limit for a conventional fluorescence material[70] with 4.9 V turn-on voltage (V_{on}) and 5.3 cd/A of maximum luminous efficiency.

In addition to polymer **P3** which was indicated in the previous section and Figure 3.7, polymer **P4** is another example used in PLED applications. The presence of carbazole groups in **P3** and oxadiazole unit in **P4** provides good hole- and electron-transporting properties, respectively. **P3** showed a slightly better performance if compared to **P4** with a maximum brightness of 3109 cd/m^2 and 1.14 cd/A maximum luminescence efficiency.[46]

A hyperbranched AIE polymers, **HP-TPE-Cz**, was used as an emitting layer in PLEDs. The PLED showed a remarkable EL performance with 5914 cd/m^2 maximum brightness and 2.13 cd/A maximum luminescence efficiency due to the hole-transporting properties of the incorporated carbazole units.[71]

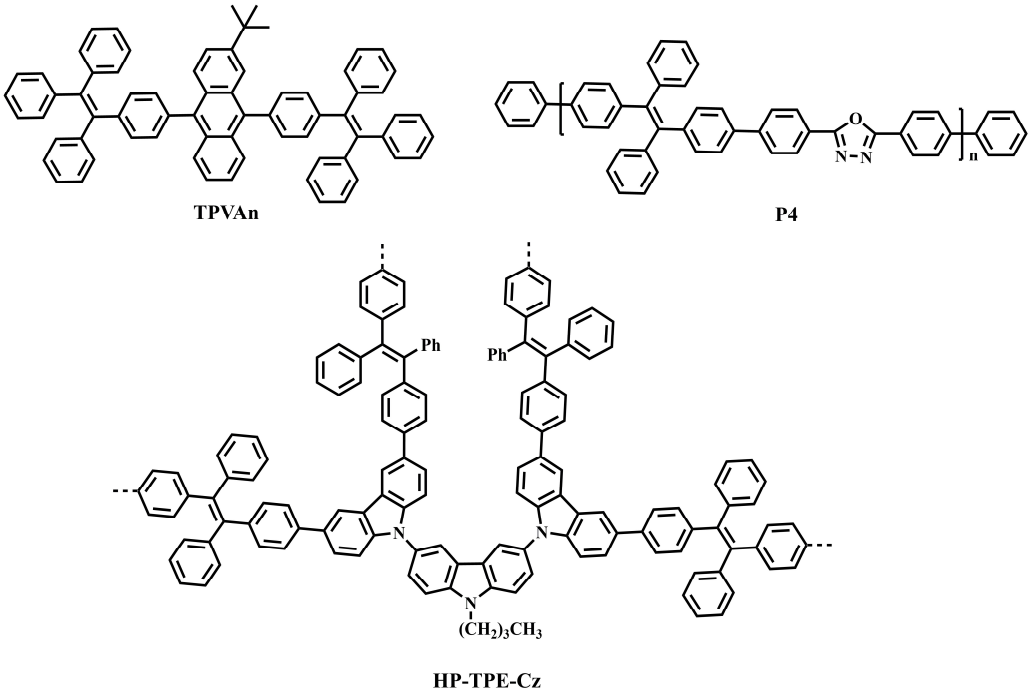

Figure 3.13 The chemical structures of AIE luminogens used for OLEDs and PLEDs.

The combination of the most recently discovered breakthrough phenomenon of "thermally activated delayed fluorescence" (TADF) and the AIE phenomenon resulted in OLEDs with very high EQEs up to 11% for non-doped OLEDs, and EQEs up to 23.2% for doped OLEDs.[72,73]

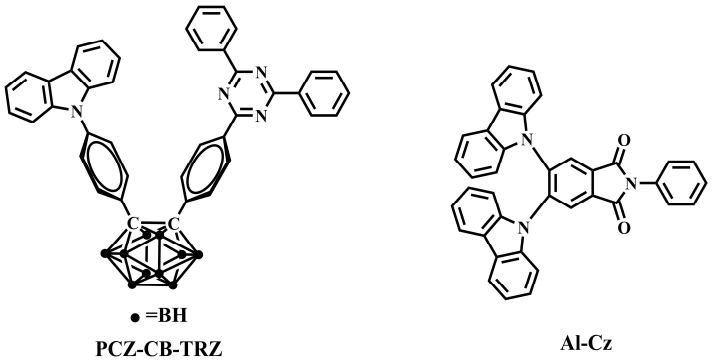

Figure 3.14 The materials showed both AIE and TADF phenomenon.

3.2. Results and Discussions

3.2.1. Synthesis of poly(tetraphenylethylene) derivatives

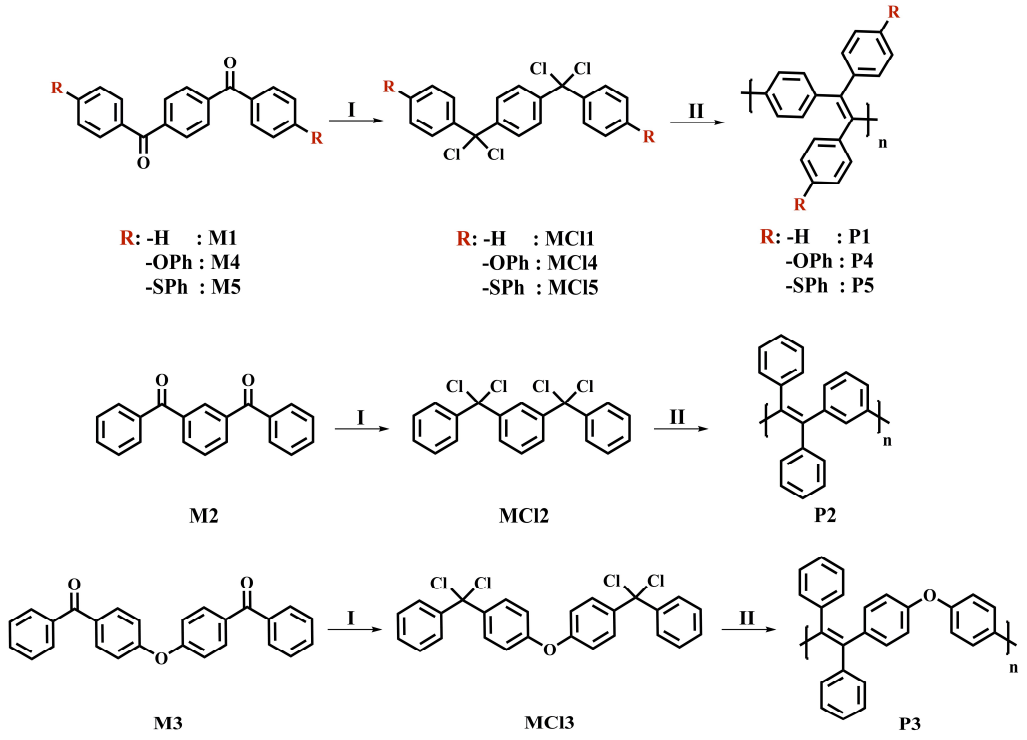

Scheme 3.2 Synthesis route for poly-TPEs. (I: PCl_5, II: $Co_2(CO)_8$)

The starting materials 1,4-dibenzoylbenzene (**M1**) and 1,3-dibenzoylbenzene (**M2**) were obtained from commercial suppliers and were used without further purification. 4,4′-dibenzoyldiphenylether (**M3**), 1,4-bis(4-phenoxybenzoyl)benzene (**M4**) and 1,4-bis(4-thiophenoxybenzoyl)benzene (**M5**) were synthesized according to a modified Friedel-Crafts protocol.[8,74,75] The detailed procedures are explained in the experimental section. The general synthesis route to the polymers **P1**-**P5** is outlined in Scheme 3.2. Tetrachloro-substituted monomers (**MCl1**-**MCl5**) were generated from the corresponding diketones by reaction with phosphorus pentachloride (PCl_5) in chlorobenzene as the solvent. After removal of both phosphorus oxychloride ($POCl_3$) by distillation and excess PCl_5 by sublimation, respectively, the resulting oily product was used without further purification. The reductive polyolefination into the linear polyarylenevinylenes **P1**-**P5** was accomplished by using dicobaltoctacarbonyl $Co_2(CO)_8$ as reducing/condensing agent.[11,76] The coupling products were precipitated into cold methanol and the crude polymers were purified by Soxhlet extraction. The final products are obtained as yellow powders. After Soxhlet extraction yields of 61%, 74%, 60%, 92%, and 86% for **P1**, **P2** **P3**, **P4**, **P5**, respectively, are isolated (1,4-dioxane fraction for **P1**, **P2**, **P4**, and **P5** and $CHCl_3$ fraction for **P3**). The chemical structures of the monomers were confirmed by nuclear magnetic resonance (NMR) spectroscopy and mass spectrometry (detailed information at experimental section). The chemical structures of obtained polymers were confirmed by NMR spectroscopy (detailed information at experimental section), and besides, the average molecular weights and polydispersity indexes were estimated by gel permeation chromatography with THF as solvent and polystyrene calibration (GPC). (Table 3.1).

Table 3.1 Polymerization results for **P1-P5**.

	Yield [%]	M_n [kg/mol]	M_w [kg/mol]	PDI
P1	61	8.3	14.0	1.7
P2	74	12.1	67.9	5.6
P3	60	11.3	24.7	2.2
P4	92	18.6	36.7	1.9
P5	86	9.4	16.4	1.7

3.2.2. Photophysical properties

Next, the effect of different substituents at the main chain and as aryl rotors was investigated photophysically. The absorption and PL spectra of the polymers recorded in $CHCl_3$ and as spin-coated film are shown in Figure 3.15.

The absorption spectra of all polymers in the film showed no change or a slight blue-shift compared to the solution. In contrast to this, the PL spectra of all polymers in film showed ~10-20 nm red-shifts compared to the solutions. Additionally, remarkable Stokes shifts of ~150-180 nm stand out for both solutions and films. Looking at the results in detail, meta-positioned phenylene units in the main chain of the polymer **P2** ($\lambda_{UV\text{-}sol}$: 250, 315nm, $\lambda_{PL\text{-}sol}$: 485nm, $\lambda_{UV\text{-}f}$: 250, 315nm, $\lambda_{PL\text{-}f}$: 498nm) and replacement of the main chain para-phenylene by a diphenylether unit in **P3** ($\lambda_{UV\text{-}sol}$: 250, 325nm, $\lambda_{PL\text{-}sol}$: 477nm, $\lambda_{UV\text{-}f}$: 250, 320nm, $\lambda_{PL\text{-}f}$: 496 nm) resulted in absorption and emission features at shorter wavelengths, if compared to **P1** ($\lambda_{UV\text{-}sol}$: 250, 302sh, 360nm, $\lambda_{PL\text{-}sol}$: 515nm, $\lambda_{UV\text{-}f}$: 250, 352nm, $\lambda_{PL\text{-}f}$: 532nm). On the other hand, substitution of the phenyl aryl rotors with diphenylether groups (**P4**, $\lambda_{UV\text{-}sol}$: 266, 304sh, 371nm, $\lambda_{PL\text{-}sol}$: 526nm, $\lambda_{UV\text{-}f}$: 266, 303sh, 364nm $\lambda_{PL\text{-}f}$: 534nm) or diphenylsulfide groups (**P5**, $\lambda_{UV\text{-}sol}$: 256, 310, 376sh nm, $\lambda_{PL\text{-}sol}$: 539nm, $\lambda_{UV\text{-}f}$: 256, 310, 373sh nm, $\lambda_{PL\text{-}f}$: 551nm) led to bathochromic shifts, especially in the PL spectra if compared to **P1**.

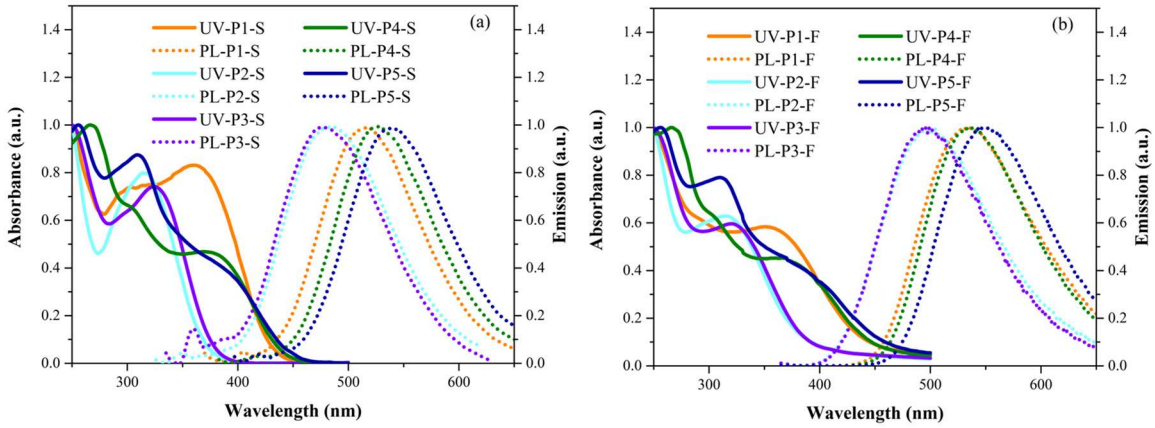

Figure 3.15 Absorption and PL spectra of **P1-P5** (a) in $CHCl_3$ solution (10^{-5} M), (b) in spin-coated films.

The photoluminescence quantum yields (PLQYs) of polymers **P1-P5** in thin films and solution (solvent: $CHCl_3$) were also investigated. The polymers **P1-P5** in solution displayed PLQYs between 0.5-2.0%. On the other hand, polymer films of **P1-P5** showed

intense photoluminescence with PLQYs of 37% for **P1** (greenish-yellow), 32% for **P2** (sky blue), 44% for **P3** (sky blue), 73% for **P4** (greenish-yellow), and 63% for **P5** (yellow) for excitation at 350 nm. The fluorescence images of polymer films **P1**-**P5** are depicted in Figure 3.17 (f).

Table 3.2 Summary of the photophysical properties of **P1**-**P5**. ([a]Excitation wavelength 350 nm; solution $CHCl_3$, thin films on quartz plates, [b]Measured by atmospheric pressure photoelectron spectroscopy (AC-2 method), [c]LUMO=HOMO(AC-2)+$E_{g(opt)}$, [d]Calculated from low energy onset of thin film absorption band)

	UV		PL						
	λ_{max}^{sol} [nm]	λ_{max}^{film} [nm]	λ_{max}^{sol} [nm]	λ_{max}^{film} [nm]	$\Phi_F^{sol\ a}$ [%]	$\Phi_F^{film\ a}$ [%]	HOMO[b] [eV]	LUMO[c] [eV]	$E_g^{opt\ d}$ [eV]
P1	360	352	515	532	0.8	37	-5.71	-2.96	2.75
P2	315	315	485	498	1.3	32	-5.90	-2.70	3.20
P3	325	320	477	496	0.5	44	-5.83	-2.68	3.15
P4	371	364	526	534	2.0	73	-5.64	-2.94	2.70
P5	376sh	373sh	539	551	1.6	63	-5.68	-3.06	2.62

The optical band gaps of **P1**-**P5** were estimated according to the correlation of energy and wavelength by using the low energy onset of the thin film absorption band. Regarding the energy levels, the highest occupied molecular orbital (HOMO) energy was measured by atmospheric pressure photoelectron spectroscopy (AC-2 method), and the lowest unoccupied molecular orbital (LUMO) energy calculated by subtraction of HOMO from the band gap. The optical data are summarized in Table 3.2. According to the estimated energy levels, all polymers have a deep-lying HOMO energy level. Among the polymers, **P5** has the lowest band gap (2.62 eV).

3.2.3. PLQYs as a function of storage time of the films

The PLQYs of polymer films which were prepared from different solutions (chloroform and toluene) are reported in Table 3.3. The photoluminescence of the resulted polymer films was collected from an Andor Shamrock 163 spectograph coupled with an Andor Newton EMCCD. The PLQY experiments were carried out using an integrating sphere setup. For all PL experiments, samples were excited by using 375 nm laser diodes (average power below 1mW).

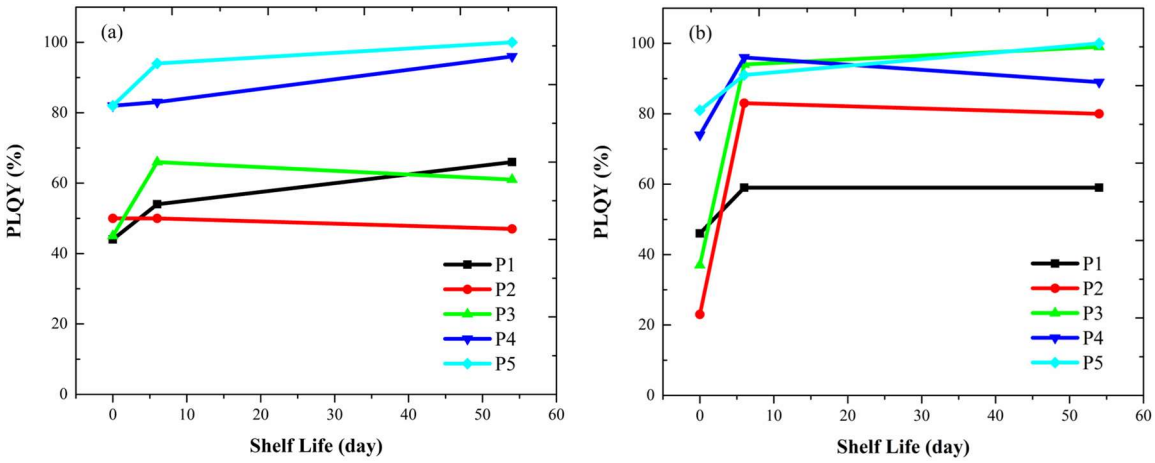

Figure 3.16 PLQYs of films deposited from (a) chloroform and (b) toluene as a function of the storage time.

The highest PLQY were achieved for **P4** and **P5** which confirms the results in the previous section. The films deposited from $CHCl_3$ solution achieved higher PLQY (at 0 days) than those prepared from toluene solutions. The possible explanation could be the fast evaporation rate of $CHCl_3$ compared to toluene, leading to a faster formation of denser packed aggregates which enhances emission. The PLQY measurements were repeated in the time period of 2 months with the same samples. The results have shown that PLQYs are increasing with increasing storage time, achieving efficiencies of almost 100% for **P3**, **P4** and **P5**, for films prepared both from chloroform or toluene solution. Figure 3.16 shows the PLQYs as a function of storage time. The storage leads to a removal of leftover solvent traces and to a denser packing with enhanced PLQYs.

Table 3.3 PLQYs of films deposited by chloroform and toluene as a function of the storage time.

	$CHCl_3$			Toluene		
	Φ_F^{film} day 0 [%]	Φ_F^{film} day 6 [%]	Φ_F^{film} day 54 [%]	Φ_F^{film} day 0 [%]	Φ_F^{film} day 6 [%]	Φ_F^{film} day 54 [%]
P1	44	54	66	46	59	59
P2	50	50	47	23	83	80
P3	45	66	61	37	94	99
P4	82	83	96	74	96	89
P5	82	94	100	81	91	100

3.2.4. Aggregation-induced emission (AIE) characterization

To investigate the AIE properties of the polymers, their PL properties in solvent/non-solvent mixtures were investigated. In this study chloroform was selected as good solvent for **P1**-**P5** and ethanol as aggregation-inducing non-solvent. By increasing the non-solvent fraction (in vol. %), the solvent polarity and in turn, the degree of aggregation was gradually increased.

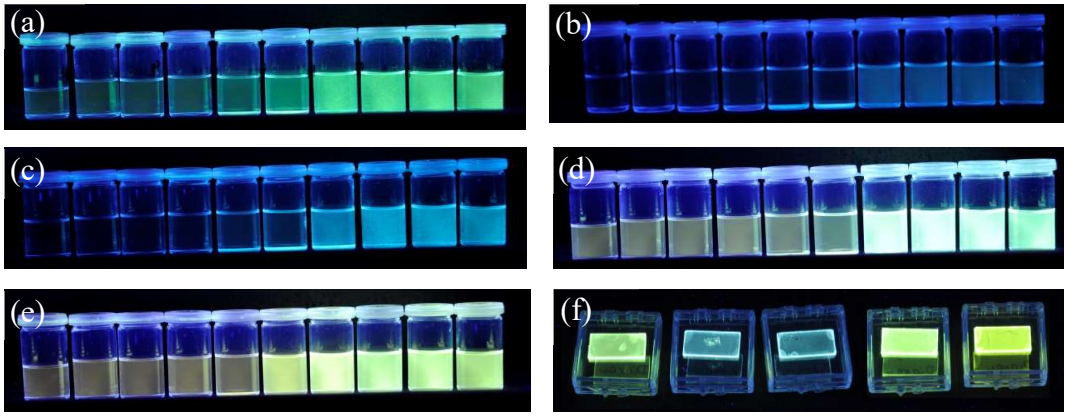

Figure 3.17 Fluorescence images of (a) **P1**, (b) **P2**, (c) **P3**, (d) **P4**, and (e) **P5** in $CHCl_3$/ethanol mixtures of different ethanol content (0-90%) (polymer concentration: 10^{-5} M); (f) Fluorescence images of **P1**-**P5** respectively in films.

The PL intensity of polymers **P1**-**P5** in chloroform/ethanol solvent mixtures are shown in Figure 3.18. The PL emission of **P1**-**P5** is slightly blue-shifted with the gradual increase of polarity. All polymers (**P1**-**P5**) are weakly emissive in dilute chloroform solution, but starting from ethanol contents of 30-40% their PL progressively increases before reaching a saturation value at ethanol contents of >70 % (Figure 3.17 and Figure 3.18 (f)). The PL intensity of the aggregated samples (90% ethanol) is ca. 33 times higher for **P1** compared to pure chloroform, 16 times higher for **P2**, 115 times higher for **P3**, 20 times higher for **P4**, and 16 times higher for **P5**. The emission increase for all polymers should be induced by aggregation; in other words, all polymers are AIE-active. This is connected to the presence of the AIE-active TPE unit: In pure chloroform solution, the relatively weak emission is mainly caused by rotations of main and side chain phenyl rings; in the aggregates, however, these rotations are strongly suppressed, thus increasing the PL intensity due to the basic principles of the AIE effect.[4]

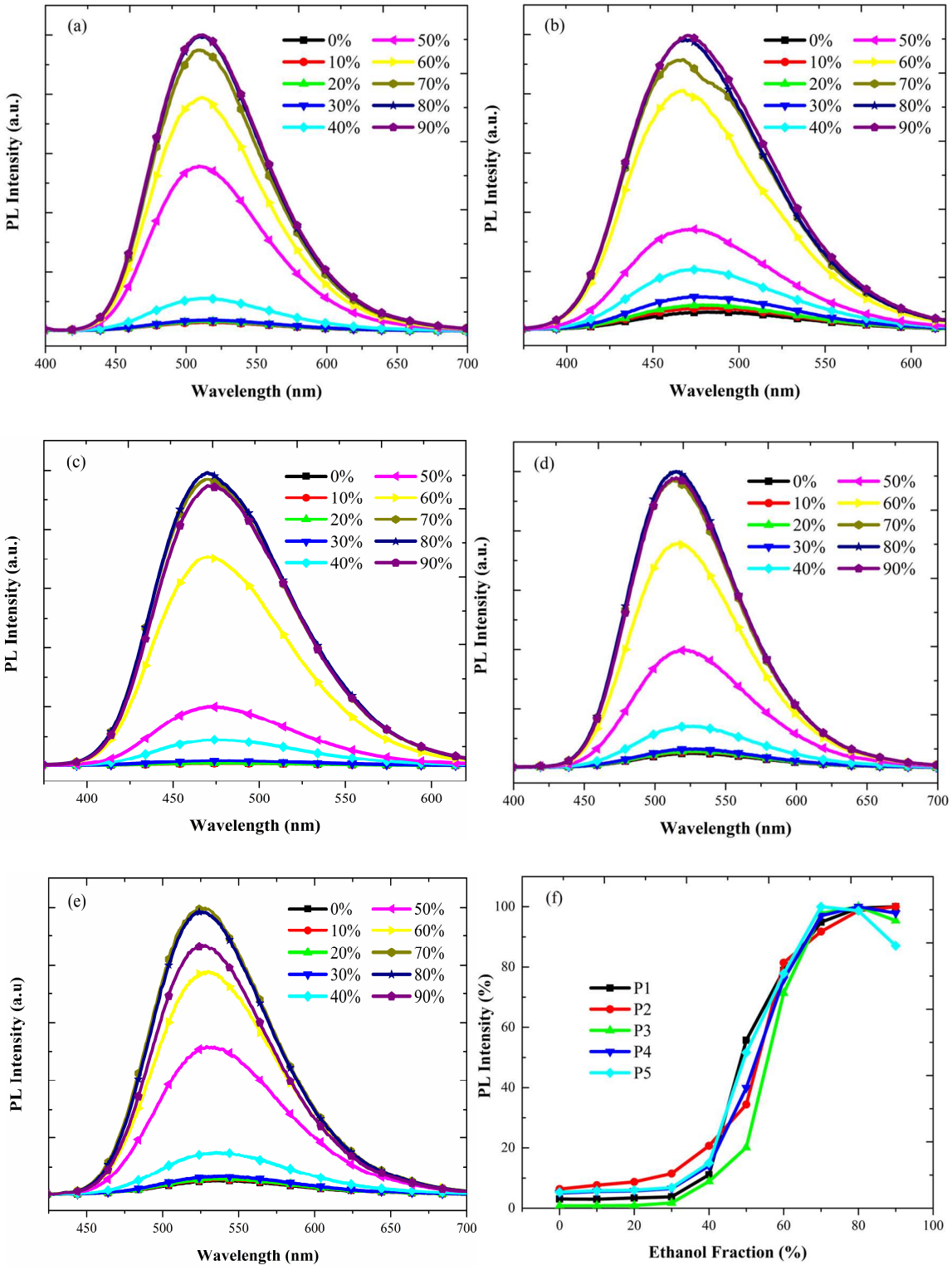

Figure 3.18 PL spectra of (a) **P1**, (b) **P2**, (c) **P3**, (d) **P4**, and (e) **P5** in $CHCl_3$/ethanol mixtures at different ethanol contents. (f) The change of PL intensity with increasing ethanol fraction.

3.2.5. Explosive detection

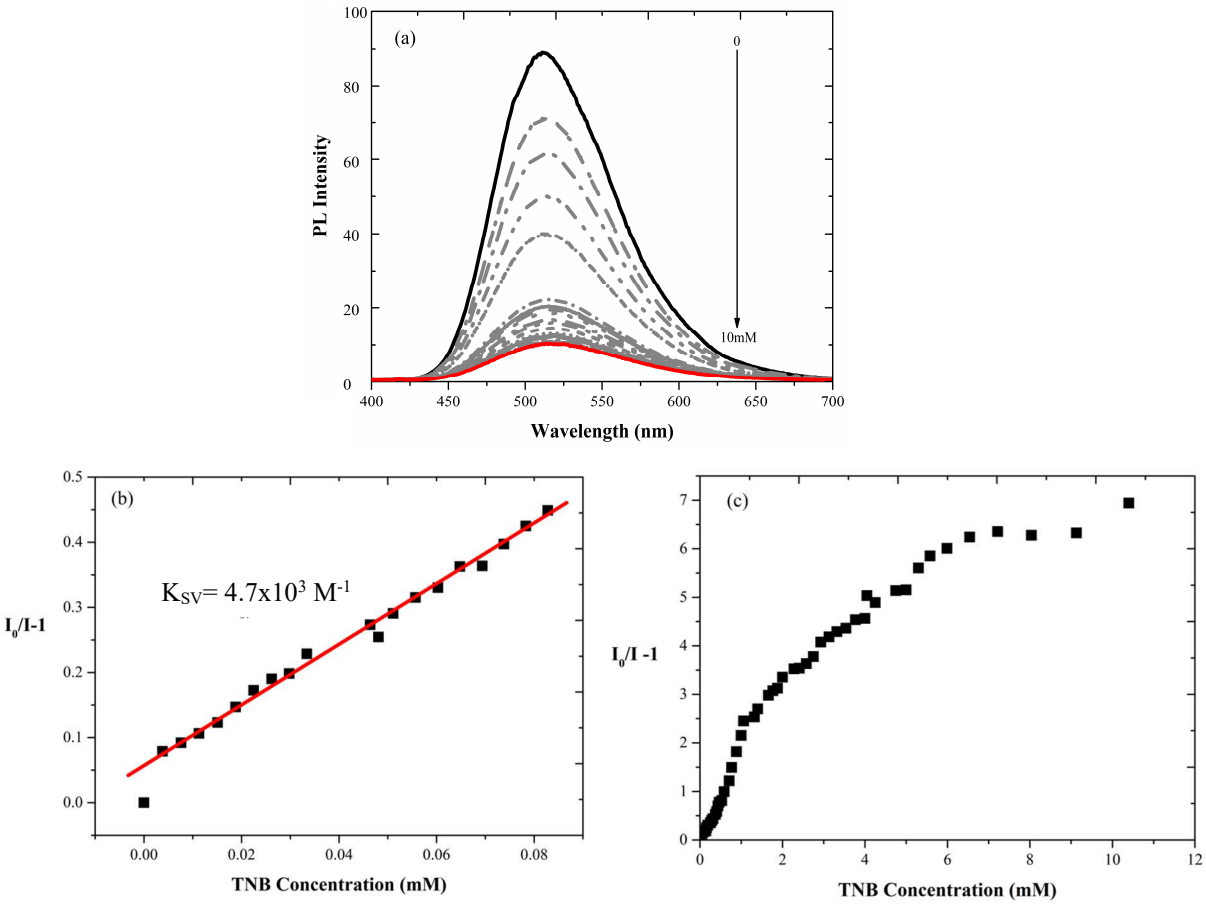

Figure 3.19 (a) PL spectra of **P4** in $CHCl_3$/ethanol (1:9) containing different amounts of 1,3,5-trinitrobenzene (polymer concentration: 10^{-5} M; λ_{ex}: 373 nm) (b) linear and, (c) non-linear part of the Stern-Volmer plot (PL intensity I_0/I-1 *vs.* TNB concentration (I = PL intensity, I_0 = PL intensity without TNB).

Based on the AIE-related high solid-state PLQYs of the polymers (according to Table 3.2) the possible use of **P4** for the detection of nitroaromatic compounds by PL quenching was explored. The investigations were performed with aggregated **P4** in chloroform/ethanol 1:9 (polymer concentration: 10^{-5} µM) and 1,3,5-trinitrobenzene (TNB) as prototypical nitroaromatic analyte. As shown in Figure 3.19 (a), significant photoluminescence quenching was already observed upon addition of micromolar amounts of TNB. The main mechanism of fluorescence quenching should be an excited state electron transfer from the excited, electron-rich polymer to the electron-deficient, nitroaromatic analyte.[77] The quenching response was analyzed by fitting the data with the Stern-Volmer equation. Due to lack of complete photoluminescence quenching, two

different scenarios are considered: Firstly, Figure 3.19 (b) depicts the linear part of the Stern-Volmer plot indicating dynamic PL quenching, leading to a PL quenching constant (K_{sv}) of $4.7x10^3$ M^{-1} for low TNB concentrations. Secondly, Figure 3.19 (c) depicts the non-linear part of the Stern-Volmer plot for higher TNB concentrations indicating collisional quenching.[78]

3.2.6. OLEDs

Due to the promising high PLQYs of polymers **P1**, **P4** and **P5**, OLED devices were fabricated in cooperation with the group of Professor Franco Cacialli from the London Centre for Nanotechnology.

OLEDs were fabricated by sandwiching the AIE active polymers (**P1**, **P4** and **P5**) between indium-tin oxide (ITO)/PEDOT:PSS anodes and Ca/Al cathodes as shown in Figure 3.20. The electroluminescence (EL) spectra of polymer films, the density-voltage-radiance (JVR) plot and the external quantum efficiency (EQE) versus current density plots are depicted in Figure 3.21. The OLEDs data are summarized in Table 3.4.

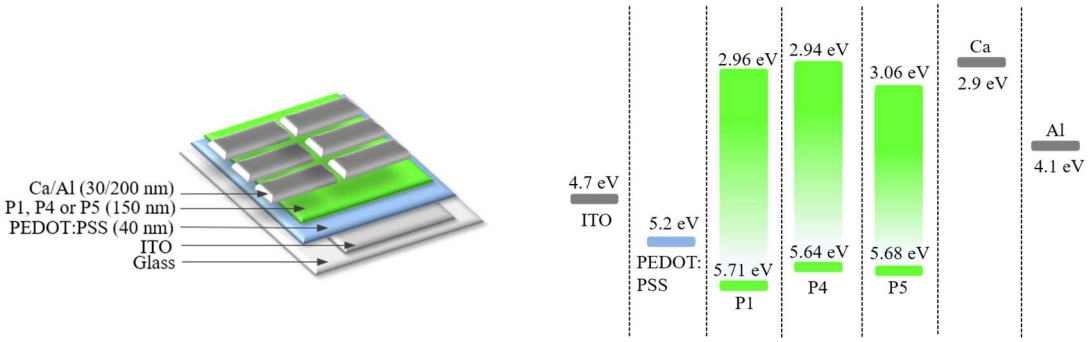

Figure 3.20 The device structure of the prepared OLEDs and the energy diagrams of the used components.

Considering the energy level alignment of the devices, it is seen that the electron energy barrier for injection of the devices **P1**, **P4** and **P5** are 0.06 eV, 0.04 eV and 0.16 eV while barriers for hole injection are 0.51 eV, 0.44 eV, and 0.48 eV respectively.

As seen in Figures 3.21 (a) and (d), the EL of both polymers **P1** and **P4** are green and the EL of **P5** is yellowish-green in colour with EL bands peaking at around 550-560 nm, with a 12-13 nm red-shift if compared to the PL spectra. In terms of device performance, the polymers **P1**, **P4** and **P5** showed 0.01%, 0.05% and 0.02% EQE with the radiance of 0.035, 0.74 and 0.24 mW/cm^2 at 12V, 19V and 12V respectively. Among the

investigated OLEDs, the EL of **P5** showed the lowest turn-on voltage with 6.13 V. The reduced turn-on voltage may attribute to its improved charge transport properties due to the thiophenoxide side group of **P5**, if compared to unsubstituted **P1**.

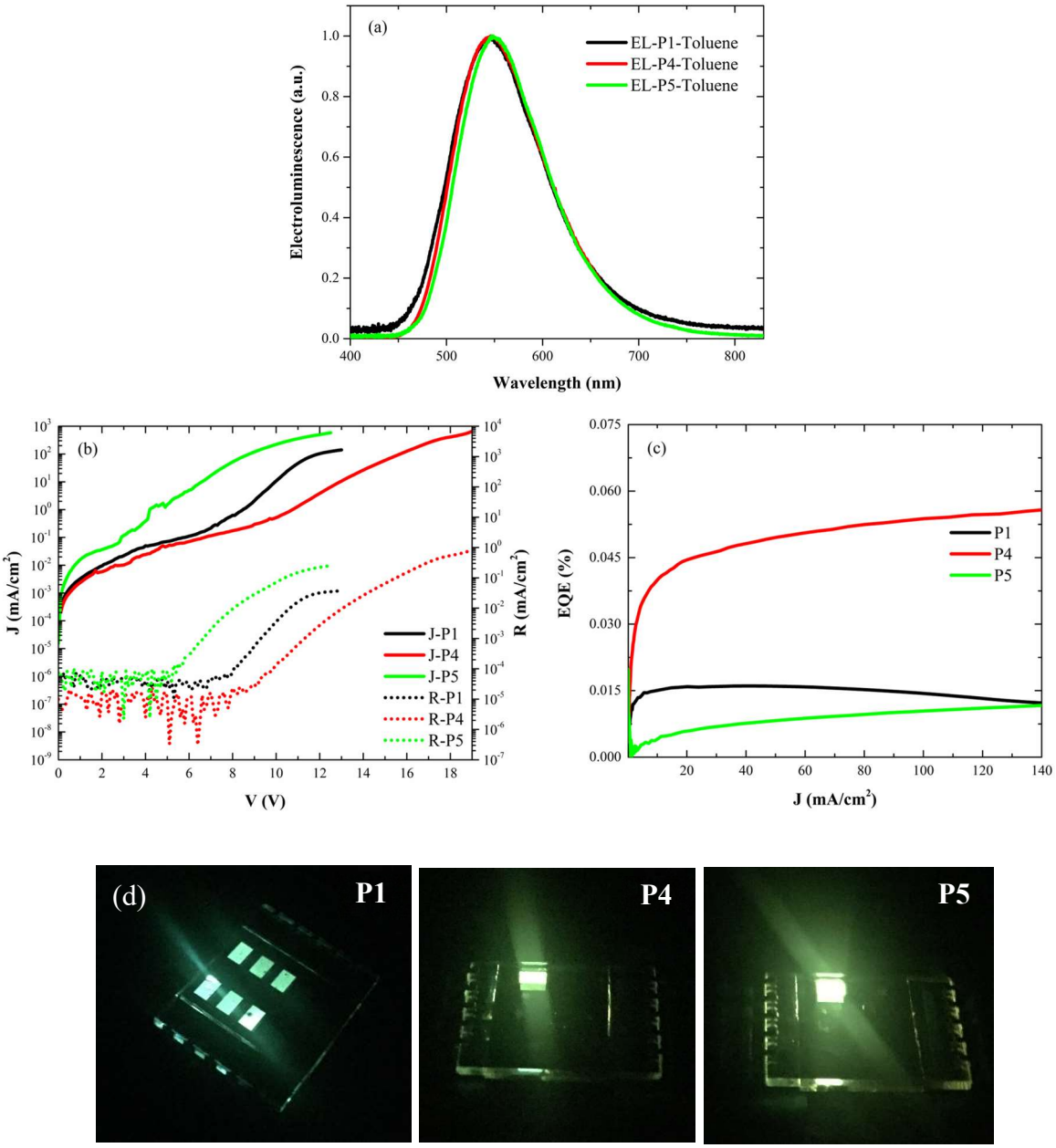

Figure 3.21 (a) EL spectra, (b) JVR curves, (c) EQE versus current density plots, and (d) photos of OLEDs incorporating **P1**, **P4** and **P5** as emitting layer.

Table 3.4 OLEDs data of the devices with **P1**, **P4** and **P5** as emissive layer. ([a] Voltage at which the emission is ~10 times the noise level, [b] Measured at 12V for **P1** and **P5**, 19V for **P4**)

	λ_{EL} [nm]	V_{ON} [a] [V]	Radiance [mW/cm^2]	EQE_{max} [b] [%]
P1	545	8.25±0.27	0.036±0.009	0.01±0.00
P4	546	8.06±0.59	0.74±0.11	0.05±0.00
P5	563	6.13±0.01	0.24±0.02	0.02±0.01

3.3. Conclusion

In conclusion, five poly(arylene-diarylvinylene)s **P1**-**P5** have been synthesized by reductive polyolefination starting from bis(α,α-dichlorobenzyl)-substituted aromatic monomers and dicobalt octacarbonyl as condensing agent. All polymers have shown high solid-state photoluminescence quantum yields of 32-73% based on the presence of aggregation-induced-emission (AIE)-active main-chain tetraphenylethylene units. Hereby, **P4** with diphenyl ether side groups (rotors) displays the most intense photoluminescence peaking at 534 nm, and with a remarkably high solid-state PLQY of 73%. Aggregated **P4** shows amplified PL quenching behaviour during the addition of trinitrobenzene (TNB) as a prototypical nitroaromatic analyte towards a $CHCl_3$/ethanol (1/9, v/v) dispersion of polymer aggregates. The Stern-Volmer quenching constant was calculated as 4.7×10^3 M^{-1} for the linear part of the plot for TNB concentrations up to 80 µM. **P4** is a promising candidate for an application as solid-state PL sensors for nitroaromatic analytes. Additionally, PLED devices were fabricated from the polymers **P1**, **P4**, and **P5**, with an EQE of 0.05% for **P4** and a low turn-on voltage of 6.13 V for P5.

3.4. Experimental

3.4.1. Materials and Instrumentation

1,4-Dibenzoylbenzene (**M1**) and 1,3-dibenzoylbenzene (**M2**) were obtained from commercial suppliers and were used without further purification. All reactions were carried out under argon atmosphere by standard and Schlenk techniques, if not specified otherwise. The solvents were used as commercial p.a. quality. Dry solvents were bought from Acros. 1,4-bis(4-phenoxybenzoyl)benzene, 1,4-bis(4-thiophenoxybenzoyl)benzene and 4,4′-dibenzoyldiphenylether were synthesized in a modified Fridel-Crafts protocol.[8,74,75]

NMR spectra were recorded on a Bruker AVANCE 400 or AVANCE III 600. Gel permeation chromatography (GPC) measurements were carried out on a PSS/Agilent SECurity GPC System equipped with polystyrene gel columns using chloroform as the eluent. APLI (Atmospheric Pressure Laser Ionization) measurements were carried out on Bruker Daltronik Bremen with micrOTOF. UV-visible absorption spectra were recorded on a Jasco V-670 spectrometer and PL spectra on a Horiba Fluoromax-4. Elemental analyses were performed on a Vario EL II (CHNS) instrument. The PL quantum efficiencies of the solid polymers were measured with an integrating sphere. The HOMO (highest occupied molecular orbital) levels were estimated on a Surface Analyzer MODEL AC-2 from RIKEN, given as the threshold where photoelectron emission first occurs. The TGA was recorded with TGA/DSC1 STAR^e System, Mettler Toledo. **AIE Characterization:** To understand the AIE features of the materials, their luminescence behaviour upon aggregation in aqueous media was investigated by photoluminescence (PL) spectroscopy. Photoluminescence was collected from a Horiba Fluoromax-4 spectrofluorometer and excitation wavelength for each sample are indicated in Section 3.2.2. For the preparation of samples, dry chloroform ($CHCl_3$) was selected as good solvent while ethanol was selected as aggregation-inducing non-solvent. Stock solutions were prepared. Aliquots of the stock solution were transferred to 10 mL vials and appropriate amounts of THF were added with a micropipette. Then, water was added dropwise to each vial with increasing fraction (between 0–90 vol% water). The final mixture concentrations were fixed to 10^{-6} M. PL measurements of 10 samples for each compound were performed immediately. **OLED Fabrication and Characterization:** OLEDs were fabricated by sandwiching the polymer films between ITO/PEDOT:PSS anodes and Ca/Al cathodes. ITO substrates were cleaned with acetone and isopropanol in an ultrasonic bath and treated in an O_2 plasma chamber for 10 min. A 40 nm layer of PEDOT:PSS (Sigma Aldrich) was spin-coated at 5000 rpm from a 2.8 wt.% dispersion in water and annealed at 150 ºC for 10 min. The active layer was spin-coated on top of the annealed PEDOT:PSS in N_2 environment from the same 10 mg/mL toluene solutions used for the optical characterization in the solid-state. A Ca/Al (30/200 nm) cathode was thermally evaporated on top. The samples were then encapsulated with a UV-curable epoxy resin (OSSILA E132) and measured in air using a Keithley 2400 source meter for both the current measurement and the voltage supply. The optical output of the PLEDs were measured with a calibrated silicon photodiode, and the EL spectra were collected with an Andor Shamrock

163 spectrograph coupled with an Andor Newton EMCCD.

3.4.2. Synthesis of poly-TPEs

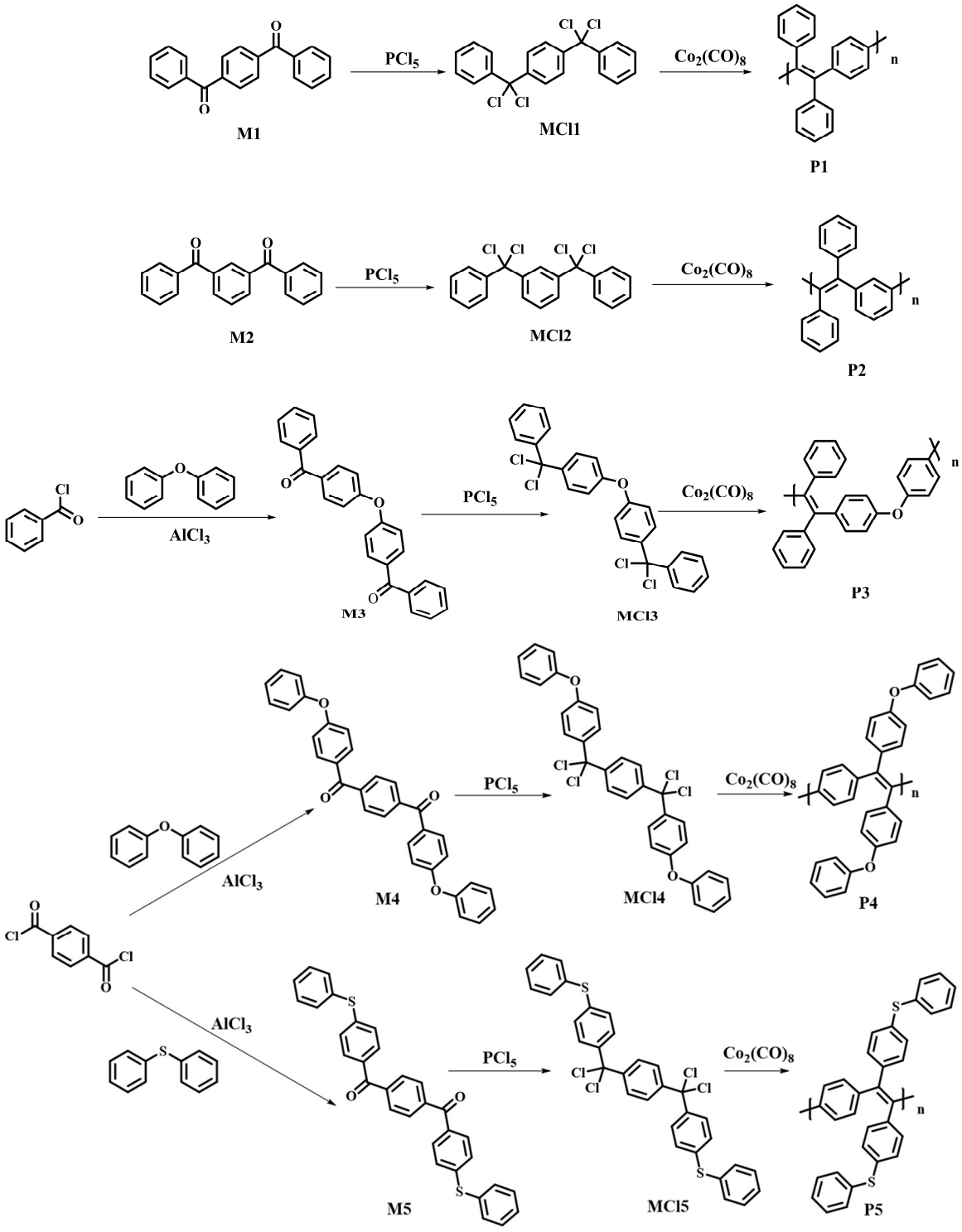

Scheme 3.3 Detailed synthesis route for poly-TPEs.

3.4.2.1. Synthesis of 4,4´-dibenzoyldiphenylether (M3)

Benzoyl chloride (18.17 g, 129 mmol), aluminium chloride (17.2 g, 129 mmol) and diphenylether (10 g, 58.8 mmol) were dissolved in 1,2-dichloroethane (40 mL). The reaction mixture was heated under reflux for 24 h. (Attention: HCl evolution!) A large amount of cold water was added to stop the reaction, and the reaction mixture was then extracted with DCM. The organic layer was washed with water and dried over magnesium sulfate. After filtration and solvent evaporation, the crude product was washed three times with ca. 100 mL hot ethanol. The product was obtained as a white solid (21.1 g; 95 % yield)
^{1}H NMR (400 MHz, $C_2D_2Cl_4$) δ/ppm: 7.89 (d, J = 8.7 Hz, 4H), 7.81(d, J= 7.0 Hz, 4H), 7.67 - 7.59 (m, 2H), 7.57-7.48 (m, 4H), 7.18 (d, J = 8.7 Hz, 4H).
^{13}C NMR (101 MHz, $C_2D_2Cl_4$) δ/ppm: 195.6, 160.0, 137.7, 133.3, 132.8, 132.8, 130.1, 128.7, 118.9.
APLI (m/z): 379.1213 (calc. 379.1329).

3.4.2.2. Synthesis of 1,4-bis(4-phenoxybenzoyl)benzene (M4)

Terephthaloyl dichloride (5 g, 24.6 mmol), aluminium chloride (7.2 g, 54.2 mmol) and diphenylether (25 mL, 157 mmol) were heated under reflux for 2 h. (Attention: HCl evolution!) If needed, an excess of diphenylether could be used to improve the stirring. A large amount of cold water was added to stop the reaction, and the reaction mixture was then extracted with DCM. The organic layer was washed with water and dried over magnesium sulfate. After filtration and solvent evaporation, the crude product was washed three times with ca. 100 mL of hot ethanol. The product was obtained as a white solid (9.8 g; 85 % yield).
^{1}H NMR (400 MHz, $C_2D_2Cl_4$) δ/ppm: 7.87 (s, 4H), 7.86 (d, *J* = 8.9 Hz, 4H), 7.48 - 7.40 (m, 4H), 7.28 - 7.21 (m, 2H), 7.13 (dd, *J* = 8.6, 1.0 Hz, 4H), 7.08 (d, *J* = 8.8 Hz, 4H).
^{13}C NMR (101 MHz, $C_2D_2Cl_4$) δ/ppm: 194.9, 162.3, 155.4, 141.0, 132.8, 131.4, 130.4, 129.8, 125.1, 120.5, 117.5.
APLI (m/z): 471.1466 (calc. 471.1591).

3.4.2.3. Synthesis of 1,4-bis(4-thiophenoxybenzoyl)benzene (M5)

Terephthaloyl dichloride (5 g, 24.6 mmol), aluminium chloride (7.2 g, 54.2 mmol) and diphenylsulfide (25 mL, 149 mmol) were dissolved in 1,2-dichloroethane (40 mL). The reaction mixture was heated under reflux for 3 h. (Attention: HCl evolution!) A large amount of cold water was added to stop the reaction, and the reaction mixture was then extracted with DCM. The organic layer was washed with water and dried over magnesium sulfate. After filtration and solvent evaporation, the crude product was washed three times with ca. 100 mL hot ethanol. The product was obtained as a white solid (10.0 g; 81 % yield).

^{1}H NMR (400 MHz, $C_2D_2Cl_4$) δ/ppm: 7.86 (s, 4H), 7.74 (d, *J* = 8.5 Hz, 4H), 7.60 - 7.54 (m, 4H), 7.47 - 7.41 (m, 6H), 7.33 (d, *J* = 8.4 Hz, 4H).

^{13}C NMR (101 MHz, $C_2D_2Cl_4$) δ/ppm: 194.8, 145.0, 141.0, 134.6, 133.9, 132.5, 130.8, 129.9, 129.6, 129.0, 127.9.

APLI (m/z): 502.0908 (calc. 502.1056).

3.4.2.4. General procedure for bis(*α*,*α*-dichlorobenzyl)-substituted compounds (MCl1-MCl5)

Diketon (**M1-M5**) (1 eq) and phosphorus pentachloride (2.2 eq) were dissolved in 20 mL of chlorobenzene under argon. The reaction mixture was heated at 120 °C for 1 d. The mixture was cooled down to 80 °C, chlorobenzene and $POCl_3$ were removed by distillation under reduced pressure. Finally, unreacted phosphorus pentachloride was removed by sublimation. The remaining yellow oils (quant. yield) were used for the reductive polycondensation experiments without further purification.

3.4.2.4.1. 1,4-Bis(*α*,*α*-dichlorobenzyl)benzene (MCl1)[7,8]

^{1}H NMR (400 MHz, $C_2D_2Cl_4$) δ/ppm: 7.68 - 7.63 (m, 4H), 7.61 (s, 4H), 7.45 - 7.38 (m, 6H).

^{13}C NMR (101 MHz, $C_2D_2Cl_4$) δ/ppm: 144.9, 143.3, 129.6, 128.6, 127.6, 127.4, 91.5.

3.4.2.4.2. 1,3-bis(*α*,*α*-dichlorobenzyl)benzene (MCl2)[8]

^{1}H NMR (400 MHz, $C_2D_2Cl_4$) δ/ppm: 7.93 (t, *J* = 1.9 Hz, 1H), 7.65 - 7.55 (m, 6H), 7.44 - 7.34 (m, 7H).

^{13}C NMR (101 MHz, $C_2D_2Cl_4$) δ/ppm: 144.2, 143.5, 129.5, 128.5, 128.4, 128.3, 127.5, 126.8, 91.7.

3.4.2.4.3. 4,4´-bis(α,α-dichlorobenzyl)diphenylether (MCl3)[8]

^{1}H NMR (400 MHz, $C_2D_2Cl_4$) δ/ppm: 7.72 - 7.64 (m, 2H), 7.60 (d, J = 8.9 Hz, 2H), 7.46 - 7.37 (m, 3H), 7.03 (d, J = 8.9 Hz, 2H).
^{13}C NMR (101 MHz, $C_2D_2Cl_4$) δ/ppm: 157.1, 143.9, 139.6, 129.5, 129.5, 128.5, 127.6, 118.5, 92.0.

3.4.2.4.4. 1,4-bis(4-phenoxy-α,α-dichlorobenzyl)benzene (MCl4)[10]

^{1}H NMR (400 MHz, $C_2D_2Cl_4$) δ/ppm: 7.65 (s, 4H), 7.57 (d, J = 9.0 Hz, 4H), 7.40 (dd, J = 8.5, 7.5 Hz, 4H), 7.22 - 7.16 (m, 2H), 7.09 (dd, J = 8.6, 1.1 Hz, 4H), 6.98 (d, J = 9.0 Hz, 4H).
^{13}C NMR (101 MHz, $C_2D_2Cl_4$) δ/ppm: 158.5, 156.0, 144.9, 137.8, 130.3, 129.3, 127.5, 124.6, 120.1, 117.6, 91.3.

3.4.2.4.5. 1,4-bis(4-thiophenoxy-α,α-dichlorobenzyl)benzene (MCl5)[9]

^{1}H NMR (400 MHz, $C_2D_2Cl_4$) δ/ppm: 7.60 (s, 4H), 7.52 - 7.47 (m, 8H), 7.39 (dd, J = 7.2, 0.6 Hz, 4H), 7.20 (d, J = 8.8 Hz, 4H).
^{13}C NMR (101 MHz, $C_2D_2Cl_4$) δ/ppm: 144.6, 141.2, 139.6, 133.4, 132.9, 129.9, 128.7, 128.3, 128.2, 127.5, 91.1.

3.4.2.5. General procedure for reductive polyolefination towards polymers P1-P5

The bis(α,α-dichlorobenzyl)-substituted monomers **MCl1**-**MCl5** (2.27 mmol), and dicobalt octacarbonyl (2.7 g, 7.83 mmol) were dissolved in 20 mL of chlorobenzene under argon. The reaction mixture was heated up to 100 °C for 50 min (gas formation starts at around 80 °C). For stopping the reaction, 10 mL of 1,2-dibromoethane were added, and the mixture was stirred for another 10 min. Next, the reaction mixture was purged into methanol and the solid product was collected by filtration. After washing with methanol, the crude product was further purified by successive Soxhlet extractions with methanol and ethyl acetate. The product was collected by extraction with 1,4-dioxane (chloroform for

P3). The final polymers were precipitated into cold methanol. The products were obtained as yellow powders.

3.4.2.5.1. Poly(1,4-phenylene-1,2-diphenylvinylene)-P1

MCl1 (1.20 g, 3.03 mmol), dicobalt octacarbonyl (2.28 g, 6.66 mmol).

Yield: dioxane fraction (525 mg, 61 %) as yellow powder.

^{1}H NMR (400 MHz, $C_2D_2Cl_4$) δ/ppm: 7.20-6.86 (m, 10H), 6.85-6.55 (m, 4H).

^{13}C NMR (101 MHz, $C_2D_2Cl_4$) δ/ppm: 143.7, 142.1, 140.9, 131.6, 130.9, 127.8, 126.7.

GPC (THF, PS standard): M_n = 8.3 kg/mol, M_w = 14.0 kg/mol.

TGA: 534°C (5 % weight loss) (argon); 0.45 % residue left at 800°C (air).

3.4.2.5.2. Poly(1,3- phenylene-1,2-diphenylvinylene)-P2

MCl2 (1.04 g, 2.63 mmol), dicobalt octacarbonyl (1.98 g, 5.78 mmol).

Yield: dioxane fraction (550 mg, 74 %) as yellow powder.

^{1}H NMR (600 MHz, $C_2D_2Cl_4$) δ/ppm: 7.12 – 6.58 (m, 14H).

^{13}C NMR (151 MHz, $C_2D_2Cl_4$) δ/ppm: 143.3, 140.8, 131.3, 129.6, 127.7, 127.5, 126.3.

GPC (THF, PS standard): M_n = 12.1 kg/mol, M_w = 67.9 kg/mol.

TGA: 540 °C (5 % weight loss) (argon); 0.33 % residue left at 800°C (air).

3.4.2.5.3. Poly(4,4´-diphenyloxy-1,2-diphenylvinylene)-P3

MCl3 (1.30 g, 2.66 mmol), dicobalt octacarbonyl (2.00 g, 5.86 mmol).

Yield: dioxane fraction (200 mg, 20 %) as yellow powder; chloroform fraction (600 mg, 60 %) as yellow powder.

^{1}H NMR (400 MHz, $C_2D_2Cl_4$) δ/ppm: 7.22 – 7.01 (m, 10H), 7.02 - 6.89 (m, 4H), 6.71 (bs, 4H).

^{13}C NMR (101 MHz, $C_2D_2Cl_4$) δ/ppm: 155.4, 143.8, 140.3, 138.9, 132.9, 131.5, 128.0, 126.7, 118.1.

GPC (THF, PS standard): M_n = 11.3 kg/mol, M_w = 24.7 kg/mol.

TGA: 544 °C (5 % weight loss) (argon); 0.44 % residue left at 800°C (air).

3.4.2.5.4. Poly(1,4-phenylene-1,2-(4-phenoxyphenyl)vinylene)-P4

MCl4 (1.30 g, 2.24 mmol), dicobalt octacarbonyl (1.68 g, 4.93 mmol).

Yield: dioxane fraction (960 mg, 92 %) as yellow powder.

^{1}H NMR (600 MHz, $C_2D_2Cl_4$) δ/ppm: 7.38 – 6.46 (m, 22H).

^{13}C NMR (151 MHz, $C_2D_2Cl_4$) δ/ppm: 157.3, 155.7, 142.3, 140.1, 138.9, 133.0, 131.1, 130.0, 123.5, 119.0, 118.2.

GPC (THF, PS standard): M_n = 18.6 kg/mol, M_w = 36.7 kg/mol.

TGA: 540 °C (5 % weight loss) (argon); 1.90 % residue left at 800°C (air).

3.4.2.5.5. Poly(1,4-phenylene-1,2-(4-thiophenoxyphenyl)vinylene-P5

MCl5 (1.40 g, 2.29 mmol), dicobalt octacarbonyl (1.72 g, 5.03 mmol).

Yield: dioxane fraction (980 mg, 86 %) as yellow powder.

^{1}H NMR (600 MHz, $C_2D_2Cl_4$) δ/ppm: 7.34 – 6.57 (m, 1H).

^{13}C NMR (151 MHz, $C_2D_2Cl_4$) δ/ppm: 142.2, 140.6, 135.8, 134.0, 132.4, 130.8, 129.5, 127.3.

GPC (THF, PS standard): M_n = 9.4 kg/mol, M_w = 16.4 kg/mol.

TGA: 470 °C (5 % weight loss) (argon); 0.14 % residue left at 800°C (air).

3.5. References

1. S. Baysec, E. Preis, S. Allard, U. Scherf, *Macromol. Rapid Commun*. **2016**, *37*, 1802.
2. J. Luo, Z. Xie, J. W. Y. Lam, L. Cheng, H. Chen, C. Qiu, H. S. Kwok, X. Zhan, Y. Liu, D. Zhu, B. Z. Tang, *Chem. Commun*. **2001**, *18*, 1740.
3. A. Qin, J. W. Y. Lam, B. Z. Tang, *Prog. Polym. Sci.* **2012**, *37*, 182.
4. R. Hu, N. L. C. Leung, B. Z. Tang, *Chem. Soc. Rev*. **2014**, *43*, 4494.
5. R. Hu, Y. Kang, B. Z. Tang, *Polym. J.* **2016**, *48*, 359.
6. H.-H. Hörhold, M. Helbig, D. Raabe, J. Opfermann, U. Scherf, R. Stockmann, D. Weiß, *Z. Chem*. **1987**, *27*, 126.
7. H.-H. Hörhold, J. Gottschalk, J. Opfermann, *J. Prakt. Chem*. **1977**, *319*, 611.
8. H.-H. Hörhold, D. Raabe, *Acta Polym*. **1979**, *30*, 86.
9. W. Holzer, A. Penzkofer, R. Stockmann, H. Mysel, H. Liebegott, H.-H. Hörhold, *Polymer* **2001**, *42*, 3183.
10. H.-H. Hörhold, M. Helbig, *Macromol. Chem., Macromol. Symp*. **1987**, *12*, 229.
11. H. Reisch, U. Wiesler, U. Scherf, N. Tuytuylkov, *Macromolecules* **1996**, *29,* 8204.
12. T. Forster, K. Z. Kasper, *Phys. Chem*. **1954**, *1,* 275.
13. J. B. Birks, Photophysics of Aromatic Molecules; *John Wiley & Sons Ltd*: London, **1970**.
14. J. Slavik, Fluorescence Microscopy and Fluorescent Probes; *Plenum Press*: New York, **1996**.
15. B. Valeur, Molecular Fluorescence: Principle and Applications; *Wiley-VCH Verlag GmbH*, Weinheim, **2002**.
16. S. M. Borisov, O. S. Wolfbeis, *Chem. Rev*. **2008**, *108*, 423.
17. M. Belletete, J. Bouchard, M. Leclerc, G. Durocher, *Macromolecules*, **2005**, *38*, 880.
18. A. Menon, M. Galvin, K. A. Walz, L. Rothberg, *Synth. Met*. **2004**, *141*, 197.
19. R. Jakubiak, C. J. Collison, W. C. Wan, L. Rothberg, *J. Phys. Chem. A* **1999**, *103*, 2394.
20. U. Lemmer, S. Heun, R. F. Mahrt, U. Scherf, M. Hopmeier, U. Siegner, E. O. Gobel, K. Müllen, H. Bassler, *Chem. Phys. Lett*. **1995**, *240*, 373.

21. C. L. Chiang, S. M. Tseng, C. T. Chen, C. P. Hsu, C. F. Shu, *Adv. Funct. Mater*. **2008**, *18*, 248.
22. J.-S. Yang, J.-L. Yan, *Chem. Commun*. **2008**, 1501.
23. B. S. Gaylord, S. Wang, A. J. Heeger, G. C. Bazan, *J. Am. Chem. Soc*. **2001**, *123*, 6417.
24. V. Bulović, A. Shoustikov, M. A. Baldo, E. Bose, V. G. Kozlov, M. E. Thompson, S. R. Forrest, *Chem. Phys. Lett*. **1998**, *287*, 455.
25. J. N. Moorthy, P. Natarajan, P. Venkatakrishnan, D.-F. Huang, T. J. Chow, *Org. Lett*. **2007**, *9*, 5215.
26. J. Chen, C. C. W. Law, J. W. Y. Lam, Y. Dong, S. M. F. Lo, I. D. Williams, D. Zhu, B. Z. Tang, *Chem. Mater.* **2003**, *15*, 1535.
27. Z. Li, Y. Dong, B. Mi, Y. Tang, M. Häussler, H. Tong, Y. Dong, J. W. Y. Lam, Y. Ren, H. H. Y. Sung, K. S. Wong, P. Gao, I. D. Williams, H. S. Kwok, B. Z. Tang, *J. Phys. Chem. B* **2005**, *109*, 10061.
28. C. Fang, Y. Xie, M. R. Johnston, Y. Ruan, B. Z. Tang, Q. Peng, Y. Tang, *J. Phys. Chem. A* **2015**, *119*, 8049.
29. T. Zhang, Y. Jiang, Y. Niu, D. Wang, Q. Peng, Z. Shuai, *J. Phys. Chem. A* **2014**, *118*, 9094.
30. S. Choi, J. Bouffard, Y. Kim, *Chem. Sci.* **2014**, *5*, 751.
31. R. Hu, E. Lager, A. Aguilar-Aguilar, J. Liu, J. W. Y. Lam, H. H. Y. Sung, I. D. Williams, Y. Zhong, K. S. Wong, E. Peña-Cabrera, B. Z. Tang, *J. Phys. Chem. C* **2009**, *113*(36), 15845.
32. X. Yuan, W. Zhang, L.-H. Xie, J. Ma, W. Huang, W. Liu, *J. Phys. Chem. B* **2015**, *119*, 10316.
33. C. J. Zhang, G. Feng, S. Xu, Z. Zhu, X. Lu, J. Wu, B. Liu, *Angew. Chem. Int. Ed.* **2016**, *55*, 6192.
34. J. Mei, Y. Hong, J. W. Y. Lam, A. Qin, Y. Tang, B. Z. Tang, *Adv. Mater*. **2014**, *26*, 5429.
35. J. Mei, N. C. L. Leung, R. T. K. Kwok, J. W. Y. Lam, B. Z. Tang, *Chem. Rev*. **2015**, *115*, 11718.
36. J. Chen, C. C. W. Law, J. W. Y. Lam, Y. Dong, S. M. F. Lo, I. D. Williams, D. Zhu, B. Z. Tang, *Chem. Mater*. **2003**, *15*, 1535.

37. N. L. Leung, N. Xie, W. Yuan, Y. Liu, Q. Wu, Q. Peng, Q. Miao, J. W. Lam, B. Z. Tang, *Chem. Eur. J*. **2014**, *20*, 15349.
38. T. Nishiuchi, K. Tanaka, Y. Kuwatani, J. Sung, T. Nishinaga, D. Kim, M. Iyoda, *Chem. Eur. J.* **2013**, *19*, 4110.
39. C. Yuan, S. Saito, C. Camacho, T. Kowalczyk, S. Irle, S. Yamaguchi, *Chem. Eur. J.* **2014**, *20*, 2193.
40. L. Yao, S. Zhang, R. Wang, W. Li, F. Shen, B. Yang, Y. Ma, *Angew. Chem. Int. Ed*. **2014**, *53*, 2119.
41. J. L. Banal, J. M. White, K. P. Ghiggino, W. W. H. Wong, *Sci Rep*, **2014**, *4*, 4635.
42. P. D. Boissieu, *J. Chem. Soc*. **1888**, *54*, 928.
43. R. Hu, J. L. Maldonado, M. Rodriguez, C. Deng, C. K. W. Jim, J. W. Y. Lam, M. M. F. Yuen, G. Ramos-Ortiz, B. Z. Tang, *J. Mater. Chem*. **2012**, 22, 232.
44. W. Dong, Y. Pan, M. Fritsch, U. Scherf, *J. Polym. Sci. Part A: Polym. Chem.* **2015**, *53*, 1753.
45. Y. Liu, X. Chen, Y. Lv, S. Chen, J. W. Y. Lam, F. Mahtab, H. S. Kwok, X. Tao, B. Z. Tang, *Chem. Eur. J.* **2012**, *18*, 9929.
46. W. Wu, S. Ye, R. Tang, L. Huang, Q. Li, G. Yu, Y. Liu, J. Qin, Z. Li, *Polymer* **2012**, *53*, 3163.
47. W. Dong, T. Fei, U. Scherf, *RSC Adv*. **2018**, *8*, 5760.
48. S. Liu, Y. Cheng, H. Zhang, Z. Qiu, R. T. K. Kwok, J. W. Y. Lam, B. Z. Tang, *Angew. Chem. Int. Ed*. **2018**, *57*, 6274.
49. J. Wang, J. Mei, W. Yuan, P. Lu, A. Qin, J. Sun, Y. Ma, B. Z. Tang, *J. Mater. Chem.* **2011**, *21*, 4056.
50. J. Wang, J. Mei, E. Zhao, Z. Song, A. Qin, J. Z. Sun, B. Z. Tang, *Macromolecules* **2012**, *45*, 7692.
51. W. Wu, S. Ye, G. Yu, Y. Liu, J. Qin, Z. Li, *Macromol. Rapid Commun.* **2012**, *33*, 164.
52. V. M. Suresh, S. Bonakala, S. Roy, S. Balasubramanian, T. K. Maji, *J. Phys. Chem. C* **2014**, *118*, 24369.
53. P. Zhang, K. Wu, J. Guo, C. Wang, *ACS Macro. Lett.* **2014**, *3*, 1139.
54. C. Gu, N. Huang, Y. Wu, H. Xu, D. Jiang, *Angew. Chem. Int. Ed.* **2015**, *54*, 11540.
55. E. Preis, W. Dong, G. Brunklaus, U. Scherf, *J. Mater. Chem. C* **2015***, 3,* 1582.

56. W. Wu, S. Ye, L. Huang, L. Xiao, Y. Fu, Q. Huang, G. Yu, Y. Liu, J. Qin, Q. Li, Z. Li, *J. Mater. Chem.* **2012**, *22*, 6374.
57. X. Liu, J. Jiao, X. Jiang, J. Li, Y. Cheng, C. Zhu, *J. Mater. Chem. C* **2013**, *1*, 4713.
58. S. Zhang, Y. Sheng, G. Wei, Y. Quan, Y. Chen, C. Zhu, *Poly. Chem.* **2015**, *6*, 2416.
59. H. Zhou, J. Li, M. H. Chua, H. Yan, B. Z. Tang, J. Xu, *Polym. Chem*. **2014**, *5*, 5628.
60. W. Dong, T. Fei, A. Palma-Cando, U. Scherf, *Polym. Chem*. **2014**, *5*, 4048.
61. K. R. Ghosh, S. K. Saha, Z. Y. Wang, *Polym. Chem.* **2014**, *5*, 5638.
62. S. K. Saha, K. R. Ghosh, J. P. Gao, Z. Y. Wang, *Macromol. Rapid Commun*. **2014**, *35*, 1592.
63. Z. Wang, T-Y. Yong, J. Wan, Z-H. Li, H. Zhao, Y. Zhao, L. Gan, X-L. Yang, H-B. Xu, C. Zhang, *ACS Appl. Mater. Interfaces* **2015**, *7*, 3420.
64. H. Wang, G. Liu, S. Dong, J. Xiong, Z. Du, X. Cheng, *J. Mater. Chem. B* **2015**, *3*, 7401.
65. R. Hu, J. W. Y. Lam, J. Liu, H. H. Y. Sung, I. D. Williams, Z. Yue, K. S. Wong, M. M. F. Yuen, B. Z. Tang, *Polym. Chem.* **2012**, *3*, 1481.
66. J. Liu, Y. Zhong, P. Lu, Y. Hong, J. W. Y. Lam, M. Faisal, Y. Yu, K.S. Wong, B. Z. Tang, *Polym. Chem*. **2010***, 1*, 426.
67. J. Li, J. Liu, J. W. Y. Lam, B. Z. Tang, *RSC Adv.* **2013***, 3*, 8193.
68. M. Kumar, V. Vij, V. Bhalla, *Langmuir,* **2012**, *28*, 12417.
69. P.-I Shih, C.-Y. Chuang, C.-H. Chien, E. W.-G. Diau, C.-F. Shu, *Adv. Funct. Mater.* **2007**, *17*, 3136.
70. T. Yu, L. Liu, Z. Xie, Y. Ma, *Sci. China Chem*. **2015**, *58*, 907.
71. W. Wu, S. Ye, L. Huang, L. Xiao, Y. Fu, Q. Huang, G. Yu, Y. Liu, J. Quin, Q. Li, Z. Li, *J. Mater. Chem*. **2012**, *22*, 6374.
72. R. Furue, T. Nishimoto, I. S. Park, J. Lee, T. Yasuda, *Angew. Chem. Int. Ed.* **2016**, *55*, 7171.
73. M. Li, Y. Liu, R. Duan, X. Wei, Y. Yi, Y. Wang, C.-F. Chen, *Angew. Chem. Int. Ed.* **2017**, *56*, 8818.
74. R. W. Murray, A. M. Trozzolo, *J. Org. Chem*. **1960**, *26*, 3109.
75. W. Dilthey, E. Bach, H. Grütering, E. Hausdörfer, *J. Prakt. Chem*. **1927**, *117*, 337.
76. E. Preis, U. Scherf, *Macromol. Rapid Commun*. **2006**, *27*, 1105.
77. X.-M. Hu, Q. Chen, D. Zhou, J. Cao, Y.-J. He, B.-H. Han, *Polym. Chem*. **2011**, *2*, 1124.

78. D. M. Jameson, Introduction to Fluorescence; *Taylor&Francis Group LLC*: Abingdon UK, **2014**.

CHAPTER 4

TETRAPHENYLETHYLENE-BODIPY DERIVATIVES FOR NEAR-INFRARED POLYMER-LIGHT EMITTING DIODES[1]

4.1. Introduction[1]

Recent developments in many fields of modern science and medicine show that oligomeric and polymeric dyes absorbing or emitting in the red/near-infrared (NIR) region (650-900 nm) have great importance.[2-4] NIR dye unit can be either attached as a side chain or incorporated into the oligomer or polymer backbone. The main advantages of such oligomeric or polymeric dyes are a high homogeneity of the resulting active layer (thin films), an enhanced processability and high stability.[5]

As stated in Chapter 2 (Section 2.1.3.), among several organic fluorescent dyes, BODIPY (4,4'-difluoro-4-bora-3a,4a-diaza-s-indacene) still retains high popularity due to its excellent spectroscopic features such as a high absorption coefficient, narrow absorption and emission bands, high fluorescence quantum yields in solution (Φ_F >0.5), and excellent chemical and photostability.[6-8] Furthermore, the emission band can be spectrally tuned from the green to the NIR spectral range by chemical modifications at the BODIPY molecular core. However, as most other organic dyes, BODIPY and its derivatives suffer from aggregation-caused quenching and small Stokes shifts which limits their applications in organic electronics, for instance in organic light-emitting diodes (OLEDs).

A promising approach to improve the photophysical properties of BODIPY dyes is to promote Aggregation-Induced Emission (AIE) behaviour, e.g. by incorporating one of the most prominent member of the AIE organic luminogen family: TPE (tetraphenylethylene). The AIE-active luminogen shall improve the solid-state emission properties of BODIPY by overcoming the Aggregation-Caused Quenching (ACQ) problem while maintaining the already mentioned advantages of the BODIPY chromophore.[9-14] As indicated in Chapter 3 (Section 3.1.2.), design and application of AIE luminogens are a hot research topic since the AIE phenomenon was first reported in 2001 by Tang and co-

workers.[15] AIE luminogens are poorly emissive in dilute solutions but form highly emissive aggregates in the condensed state, i.e. either by the addition of a non-solvent or in the solid-state. The AIE effect is mainly due to the propeller-shape structure of the luminogens, which cause restriction of intramolecular rotations upon aggregation.[16]

In this context, 6 different small molecules and 4 different polymers were synthesized. This study provides a systematic investigation of substitution effects (alkyl substituents, number of TPE groups) in both small molecules and polymers, and the consequences on the OLED performance of the most promising candidates with high-solid-costate emission intensity.

To the best of our knowledge, only few articles[17-25] have investigated the substituted of BODIPY with varying numbers of AIE active aryl substituents in different positions, with substitution in 8-position of BODIPY allowing for the most distinct variation of the aggregated state emission. In the following section (4.1.1), the transformation of the BODIPY chromophore from ACQ to AIE will be explained briefly by examples from the literature.

4.1.1. Transformation of BODIPY from ACQ to AIE: Red to N-IR solid-state emission

The most convenient way to synthesize non-aggregating chromophores with high intensity solid-state emission is a chemical modification of the chromophores. Here, the AIE phenomenon steps in and provides new design strategies to develop novel materials with superior properties. Not only the famous TPE moiety, but also other propeller-like structures which function as rotor groups enable the transformation of ACQ chromophores into AIE-active materials. In the studies of Tang et al.[18], Qian et al.[20], and Ma et al.[24], triphenylamine (TPA) was used as AIEgen (AIE-active group) at the BODIPY core. TPA and TPA derivatives substituting BODIPY (in 2-, 6- or 8-positions) functioned as rotor groups, and promote twisted intramolecular charge transfer (TICT) from TPA to BODIPY unit, resulting in red emissive AIE luminogens.

Through synthetic design, the TPE-substitution positions on BODIPYs include the 2-, 6-, and 8-positions, and can contain spacers between TPE and BODIPY, e.g. vinyl bridges, etc.[17,19,21-23,25] In one example, Tang and coworkers[22] in 2012 designed and synthesized TPE-containing BODIPYs with different functional bridge groups between BODIPY and TPE unit, (Figure 4.1) and investigated their bioimaging applications. While

the absorption maxima of the materials were located between 498 and 508 nm, their emission maxima were tunable from the visible to the near-IR region depending on the polarity of the solvents used. All molecules showed AIE properties in the solid-state and resulted in higher solid-state emission intensities if compared to the solutions.

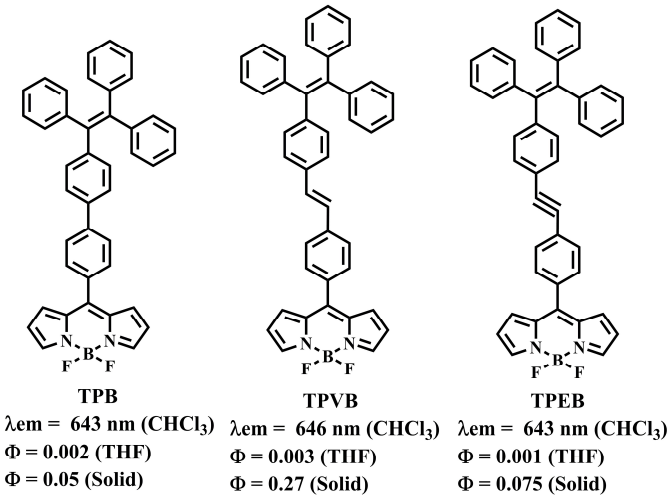

Figure 4.1 The chemical structure and optical properties of TPE-substituted BODIPY derivatives (8-positioned) with different functional bridges.

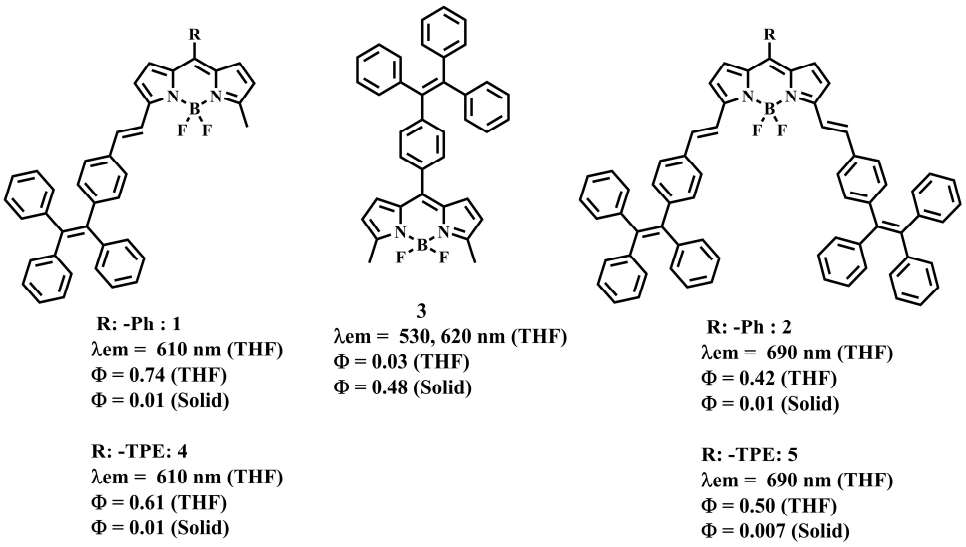

Figure 4.2 The chemical structure and optical properties of BODIPY derivatives substituted by TPE on different positions (3-, 5-, and 8-positions) and with different bridging units.

In 2015, Tang and coworkers[17] have designed and synthesized five different TPE-substituted BODIPY derivatives with direct links in 8-position or links through vinyl bridges in 3- and 5-positions of the BODIPY core (Figure 4.2). As also indicated in Chapter

2, the functionalization of BODIPY in 3- and 5-positions results in absorption and emission bands at longer wavelengths due to an increased conjugation length, but in poor solid-state emission. On the other hand, 8-positioned TPE unit at BODIPY cores contributes less to the conjugation but extraordinarily increased the solid-state emission through a TICT-induced AIE effect. The high solid-state emissive compound **3** was investigated for the intracellular imaging applications.

Based on the results of Tang and coworkers[17] several related TPE-BODIPY hybrids are described in this chapter.

4.2. Results and Discussions

4.2.1. Synthesis of TPE-substituted BODIPY small molecules and polymers

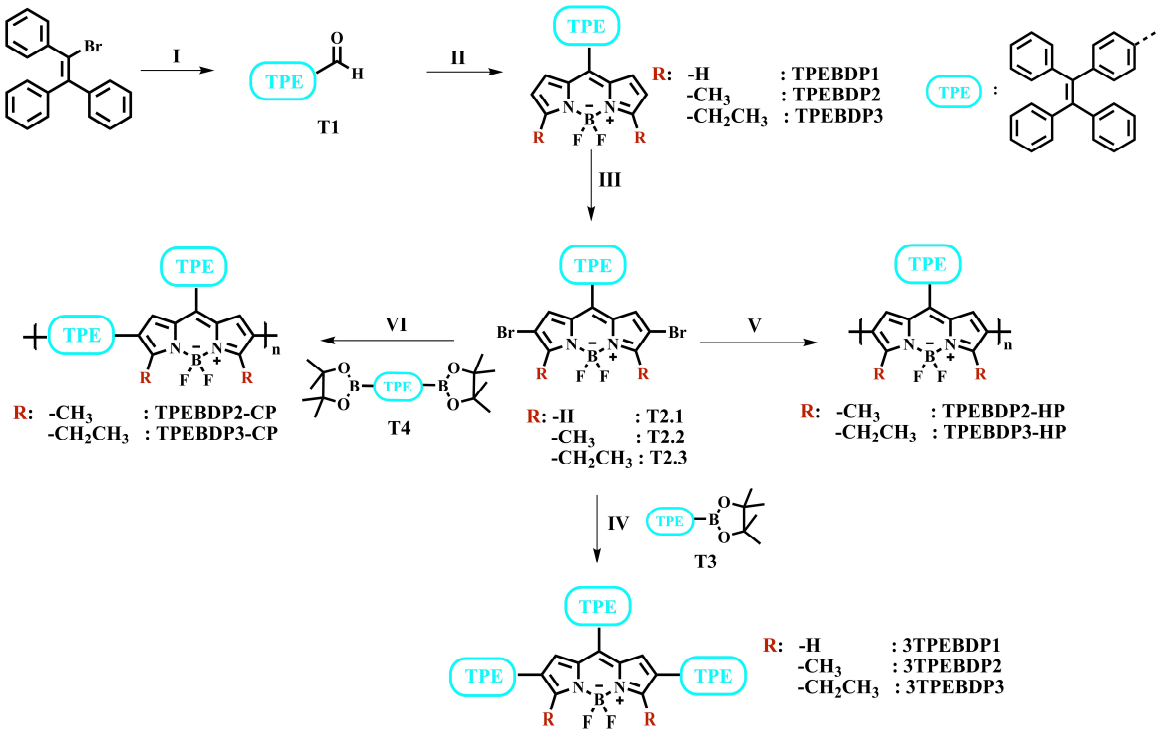

Scheme 4.1 Synthesis route for TPE-substituted BODIPY-based small molecules and polymers (I: (4-formylphenyl) boronic acid, TBAB, $Pd(PPh_3)_4$, toluene. II: corresponding pyrrole, TFA, DDQ, Et_3N, $BF_3{\cdot}OEt_2$, DCM. III: NBS, DCM:DMF(50:50). IV: K_2CO_3, $Pd(PPh_3)_4$, THF:water(80:20). V: $Ni(COD)_2$, COD, bpy, THF. VI: K_2CO_3, $Pd(PPh_3)_4$, THF:water(80:20)).

The general synthesis route to the TPE-substituted BODIPY small molecules and polymers is outlined in Scheme 4.1. The starting materials (2-bromo-1,2-diphenylvinyl)

benzene and 4-formylphenylboronic acid were obtained from commercial suppliers and used without further purification. The obtained triphenylvinylbenzaldehyde (**T1**) was condensed with the corresponding pyrrole in the presence of trifluoroacetic acid (TFA), followed by oxidative dehydrogenation with 2,3-dichloro-5,6-dicyano-1,4-benzoquinone (DDQ) and complexation with boron trifluoride diethyl etherate ($BF_3 \cdot OEt_2$) to give the corresponding mono-TPE-substituted BODIPYs (**TPEBDP1/2/3**). To obtain triple-TPE-substituted BODIPYs, mono-substituted-BODIPYs were brominated with NBS to the corresponding 2,6-dibromo derivatives. In a microwave-assisted Suzuki coupling, the 2,6-dibromo-substituted BODIPY derivatives (**T2.X**) were coupled with a boronic ester-substituted TPE (**T3**) to yield 2,6,8-tri-TPE-substituted BODIPYs (**3TPEBDP1/2/3**). The detailed procedures are explained in the experimental section.

Homopolymer **TPEBDP2-HP** and **TPEBDP3-HP** were synthesized from the corresponding 2,6-dibromo derivatives (**T2.X**) by microwave-assisted Yamamoto-type coupling. Copolymers **TPEBDP2-CP** and **TPEBDP3-CP** were synthesized from corresponding 2,6-dibromo derivatives (**T2.X**) and diboronic ester-substituted TPE (**T4**) in microwave-assisted Suzuki-cross couplings. The homo- and copolymers were precipitated into cold methanol, and the crude polymers were purified by Soxhlet extraction. The final products were received as dark green powders for homopolymers and purple powders for copolymers with yields (of the $CHCl_3$ fraction) of 66%, 54%, 58%, and 50% for **TPEBDP2-HP**, **TPEBDP3-HP**, **TPEBDP2-CP**, and **TPEBDP3-CP**, respectively.

The chemical structures of all monomers were confirmed by nuclear magnetic resonance (NMR) spectroscopy and mass spectrometry (detailed information at experimental section). The chemical structures of the obtained polymers were also confirmed by NMR spectroscopy (detailed information at experimental section). The average molecular weights and polydispersity indexes were estimated by gel permeation chromatography (GPC). (Table 4.1).

Table 4.1 Polymerization results for polymers.

	Yield [%]	M_n [kg/mol]	M_w [kg/mol]	PDI
TPEBDP2-HP	66	29.0	53.1	1.8
TPEBDP3-HP	54	21.4	63.7	2.9
TPEBDP2-CP	58	5.2	40.0	7.7
TPEBDP3-CP	50	4.5	5.6	1.2

4.2.2. Photophysical properties

4.2.2.1. Photophysical properties of TPE-substituted BODIPY small molecules

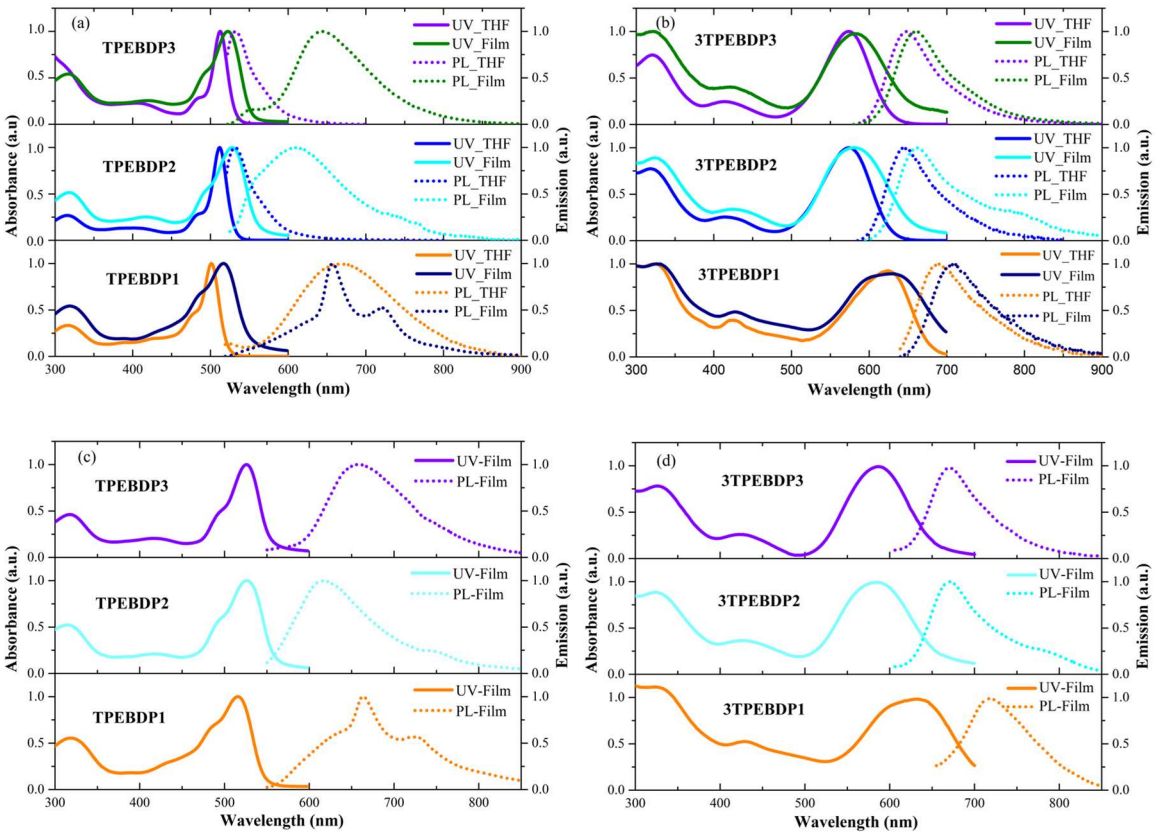

Figure 4.3 Absorption and PL spectra of (a) **TPEBDPx**, (b) **3TPEBDPx** in THF solution (10^{-5} M) and as spin-coated film from THF solution, (c) **TPEBDPx** and (d) **3TPEBDPx** spin-coated films from toluene solution.

The effect of different substituents (alkyl substituents and number of TPE groups) on the BODIPY core was investigated photophysically. The absorption and photoluminescence properties of solutions (THF) and spin-coated films (from THF solution) of the **TPEBDPx** and **3TPEBDPx** series are shown in Figures 4.3 (a) and (b). Moreover, the absorption and photoluminescence properties of the **TPEBDPx** and **3TPEBDPx** series were also studied for spin-coated films from toluene solution (Figures 4.3 (c) and (d)) since toluene as the solvent allowed to obtain more uniform films. The homogeneity of the emitting layer is an important prerequisite to fabricate efficient light-emitting devices.

For a proper comparison, the absorption and PL spectra of solution and films from THF solution are discussed first.

The absorption spectra of the mono-TPE substituted molecules (**TPEBDPx**) are dominated by the absorption of the BODIPY moiety peaking at ~ 510 nm. Most likely due to aggregation, a broadening and ~15 nm red-shift were observed when going from solution to film. Whereas in solution **TPEBDP2** and **TPEBDP3** exhibit a PL emission peaking at 532 nm with full width at half maximum (FWHM) of only 30 nm, which is typical of 2,6-unsubstituted BODIPYs[26], the PL spectra of the corresponding spin-coated films exhibit broad PL spectra with maxima at 609 nm for **TPEBDP2** and 640 nm for **TPEBDP3**. Such a substantial (80-120 nm) Stokes shift is most likely the result of aggregation in the solid-state. Regarding the α-unsubstituted **TPEBDP1**, it is noted that both solution and film present a PL peak at ~660 nm.

Table 4.2 Summary of optical data of **TPEBDPx** and **3TPEBDPx** ([a] Samples are excited at their absorption maxima. [b] Samples are excited with 520 nm laser diode with the average power < 1mW.).

	Solution		Film			
	THF		THF		Toluene	
	λ_{max}^{UV} [nm]	$\lambda_{max}^{PL\ a}$ [nm]	λ_{max}^{UV} [nm]	$\lambda_{max}^{PL\ a}$ [nm]	λ_{max}^{UV} [nm]	$\lambda_{max}^{PL\ b}$ [nm]
TPEBDP1	501	666	516	660-723	515	670-729
TPEBDP2	512	532	528	609	525	615
TPEBDP3	512	532	523	640	525	650
3TPEBDP1	623	689	628	709	635	720
3TPEBDP2	574	646	580	663	580	670
3TPEBDP3	575	648	583	662	580	670

Looking at the tri-TPE substituted molecules (**3TPEBDPx**), a substantial red-shift of the absorption and emission spectra was observed as compared to the **TPEBDPx** series, reaching up to ~110 nm for **3TPEBDP1** due to the increased conjugation length. This effect is also confirmed by the band gap values in Table 4.3. Furthermore, in contrast to what is observed with **TPEBDP1/2/3**, both absorption and emission spectra of the **3TPEBDP1/2/3** molecules in the solid-state (Figure 4.3 (b)) are only slightly red-shifted (10-20 nm) and somewhat broader, compared to those measured in solution. Namely, the absorption spectra of films (from THF solution) are dominated by a broad band in the 500-650 nm spectral region and maximum ~580 nm for **3TPEBDP2** and **3TPEBDP3**, and in the 550-700 nm range with maximum at 628 nm for **3TPEBDP1**. The PL, spectra measured from **3TPEBDP2** and **3TPEBDP3** films peak at ~660 nm, whereas the PL of **3TPEBDP1** shows a maximum in the NIR at 709 nm. The results are summarized in Table 4.2.

Table 4.3 PL quantum efficiency (Φ_F), highest occupied molecular orbital (HOMO) and lowest occupied molecular orbital level (LUMO) energy levels of **TPEBDPx** and **3TPEBDPx**. (PL efficiency values are to be considered with a 10 % uncertainty on the absolute values. [a] For the PL efficiency measurements, samples were excited with a 520 nm laser diode (average power below 1 mW). [b] Measured by atmospheric pressure photoelectron spectroscopy (AC-2 method). [c]LUMO=HOMO(AC-2)+$E_{g(opt)}$. [d] calculated from low energy onset of thin film absorption band.)

	THF		Toluene			
	Φ_F sol[a] [%]	Φ_F film[a] [%]	Φ_F film[a] [%]	HOMO[b] [eV]	LUMO[c] [eV]	E_g^{opt} [d] [eV]
TPEBDP1	8	8	10	-5.63	-3.39	2.24
TPEBDP2	4	6	4	-5.84	-3.64	2.20
TPEBDP3	4	8	5	-5.82	-3.59	2.23
3TPEBDP1	47	6	10	-5.69	-3.96	1.73
3TPEBDP2	29	68	39	-5.69	-3.82	1.87
3TPEBDP3	44	98	48	-5.65	-3.78	1.87

The PLQY measurements show that with the exception of **3TPEBDP1**, all oligomers show similar or slightly higher Φ_F for the solid-state films compared to the solution values (Table 4.3). **3TPEBDP2** and **3TPEBDP3** films from THF solution show in the solid-state Φ_F values of 68% and 98%, respectively, which are notably high and not easily attainable with conventional molecular chromophores when spin-coated from solution as neat films. For completeness, the PL spectra and corresponding Φ_F values obtained for films deposited from toluene solution were also measured. By comparing the spectra of the films obtained from toluene (Figure 4.3 (c), (d)) and those obtained from THF (Figure 4.3 (a), (b)) no major variations can be detected. Furthermore, for the **TPEBDPx** series, the Φ_F values, reported in Table 4.3, for films spin-coated from THF are quite similar to those obtained from toluene. On the contrary, due to the additional TPE units in the **3TPEBDPx** dyes, a remarkable variation between film processed from THF or toluene is observed, especially for **3TPEBDP2** and **3TPEBDP3**. Namely, for the films obtained from toluene solution, the Φ_F values are lower with 39% for **3TPEBDP2** and 48% for **3TPEBDP3**. However, the films from toluene appeared much more homogeneous when exciting different areas of the THF-processed films, a significant scattering of the PLQY values is observed (values of < 40% up to > 90%).

4.2.2.2. Photophysical properties of TPE-substituted BODIPY homo- and copolymers

The absorption and PL spectra of homo- and copolymers were recorded in $CHCl_3$ solution and as spin-coated thin films, and are shown in Figure 4.4.

At first sight, it is easily seen that the absorption of homopolymers **TPEBDP2-HP** and **TPEBDP3-HP** showed a large bathochromic shift compared to their small molecule analogs due to the extended π-conjugation through the polymer chains. The decrease of the HOMO/LUMO gap values confirms this fact (Table 4.4 and Table 4.3) The absorption spectra of both polymers present a spectral broadening with a ~10 nm red-shift when moving from solution to film. Both polymers emit in the NIR region in solution and film. A remarkable solid-state Stokes shift up to 155 nm may be attributed to aggregation in the solid-state as observed in thin film measurements. The PLQYs of the homopolymers in $CHCl_3$ were determined as 9.8% for **TPEBDP2-HP** and 34.1% for **TPEBDP3-HP**, while the PLQYs of films are low (0.2% and 0.4%, respectively). These results show that both homopolymers do not exhibit AIE properties.

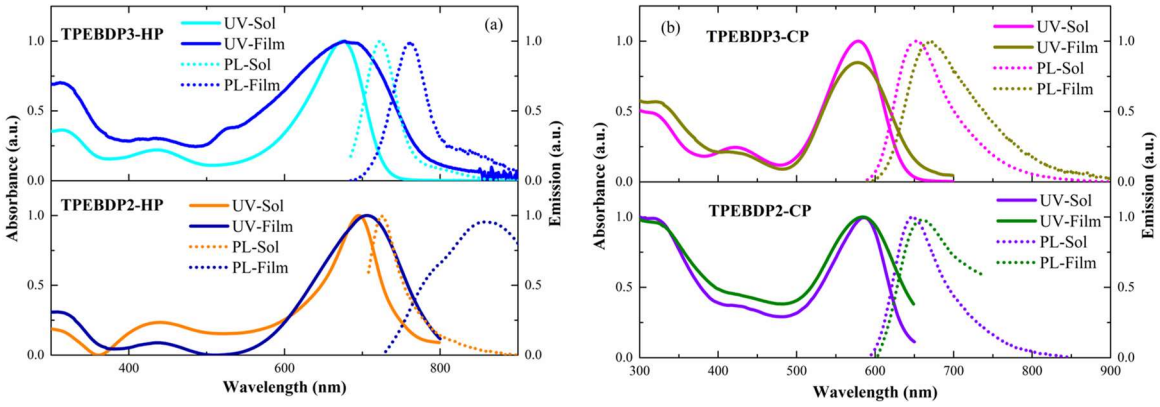

Figure 4.4 Absorption and PL spectra of (a) homo- and (b) copolymers in $CHCl_3$ solution (10^{-5} M) and as spin-coated film from $CHCl_3$ solution.

The absorption spectra of the copolymers **TPEBDP2-CP** and **TPEBDP3-CP** show a spectral broadening in the solid-state without any shift when comparing solution and film. On the other hand, the PL spectra of both copolymer films show a slight red-shift of 10-15 nm if compared to the solutions, probably due to aggregation. Both copolymers show hypsochromically shifted absorption maxima if compared to the homopolymers, most probably due to the low degree of polymerization and due to the incorporation of TPE unit into the main chains, as listed in Table 4.1, associated with larger band gaps. The PLQYs

of the **TPEBDP3-CP** in dilute $CHCl_3$ solution and film were determined as 32.9% and 2.9% respectively. On the other hand, in **TPEBDP2-CP** no emission was observed. In conclusion, both copolymers do not exhibit any AIE properties.

Compared to the small molecules (**TPEBDPx** and **3TPEBDPx**), both homo- and copolymers show much lowered solid-state PLQY values, possibly due to quenching processes of defects in the polymer chains.

Table 4.4 Summary of the optical data of **TPEBDPx-HP** and **TPEBDPx-CP** ([a]Samples are excited at their absorption maxima. [b] Measured by atmospheric pressure photoelectron spectroscopy (AC-2 method). [c] LUMO=HOMO(AC-2)+$E_{g(opt)}$. [d] calculated from low energy onset of thin film absorption band.)

	Solution (s)		Film (f)						
TPEBDP	λ_{max}^{UV} [nm]	λ_{max}^{PL} [nm]	λ_{max}^{UV} [nm]	λ_{max}^{PL} [nm]	$\Phi_F^{s\,a}$ [%]	$\Phi_F^{f\,a}$ [%]	HOMO[b] [eV]	LUMO[c] [eV]	$E_g^{opt\,d}$ [eV]
2-HP	695	726	706	861	9.8	0.4	-5.59	-4.04	1.55
3-HP	675	723	685	762	34.1	0.2	-5.50	-3.92	1.58
2-CP	586	649	585	659	N.A.	N.A.	-5.47	-3.64	1.83
3-CP	578	653	578	669	32.9	2.9	-5.63	-3.75	1.88

4.2.3. Aggregation-induced emission (AIE) characterization

The solid-state photoluminescence quantum yield of **TPEBDPx** and **3TPEBDPx** series demonstrated promising results which initiated further investigations of the AIE features of the materials. With this aim, their photoluminescence spectra were investigated in THF/water mixtures with increasing water fraction (in vol.%). By this method, the solvent polarity and thus, the amount of aggregation, can be fine-tuned.

The PL spectra of mono-TPE-substituted BODIPYs (**TPEBDPx**) are shown in Figure 4.6. **TPEBDP2** and **TPEBDP3** in THF solutions show an emission around 530 nm (excitation wavelength: 511 nm) due to the BODIPY core. With gradual addition of water into THF the emission was reduced, and bathochromically shifted to 609 nm for **TPEBDP2** and 640 nm for **TPEBDP3**. Such a large bathochromic shift of PL can also be visually perceived by colour change of the solutions, both under daylight and UV illumination (Figure 4.5). **TPEBDP2** has already been reported by Tang et al., who also investigated the effects of solvent polarity and temperature on the emission.[17] Namely, they demonstrated that the spectral changes associated with the increase of solvent polarity can be explained by the AIE effect and the concomitant formation of a twisted intramolecular charge-transfer

(TICT) state. Furthermore, for both **TPEBDP2** and **TPEBDP3**, the molecules start to show AIE effects at ca. 80 vol.% water (Figure 4.6 (d)). However, the starting emission intensity is not fully recovered to its highest value.

In the case of **TPEBDP1** (Figure 4.6 (a)), the emission in THF is peaking at ~ 670 nm (excitation wavelength: 501 nm). As the water content is increased, the intensity of emission first decreases. Starting from 80 vol.% water **TPEBDP1** shows an obvious AIE effect with a weak blue-shift of the emission ($\lambda_{max\ em}$: 658 nm). It is likely that the lack of alkyl substituents promotes the formation of aggregates at higher water contents. The maximum of fluorescence was achieved for 90 vol.% water.

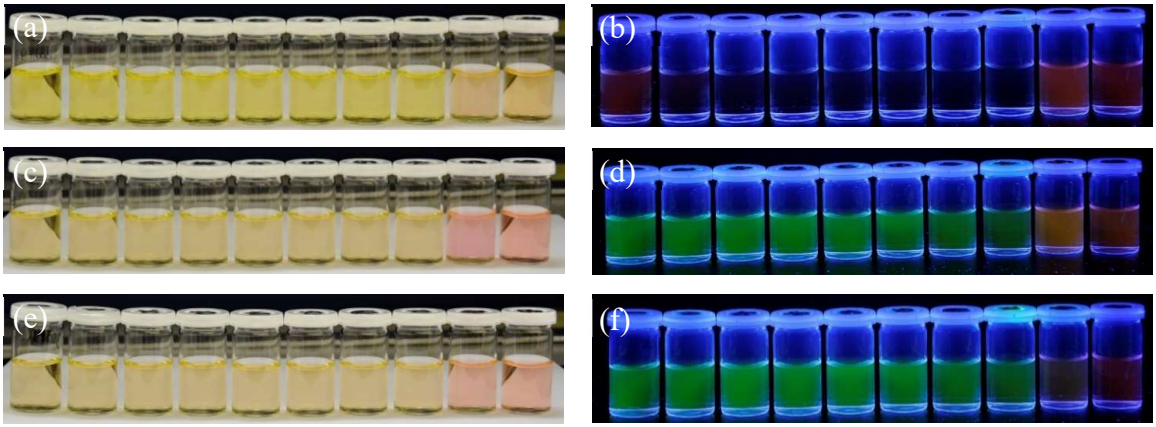

Figure 4.5 Colour images under daylight (a) **TPEBDP1**, (c) **TPEBDP2**, (e) **TPEBDP3**, and fluorescence images under UV excitation (365 nm) (b) **TPEBDP1**, (d) **TPEBDP2**, (f) **TPEBDP3**.

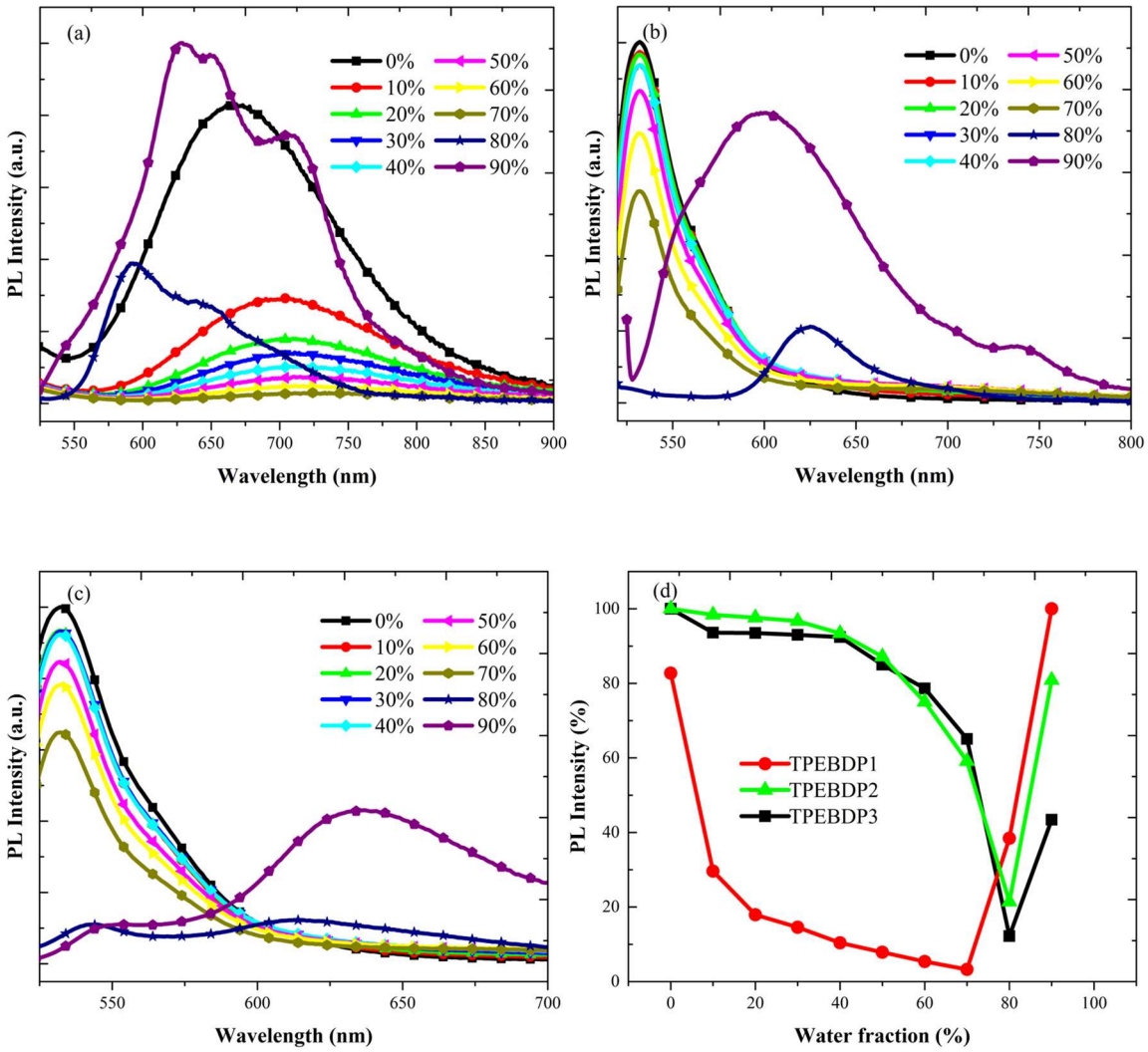

Figure 4.6 PL spectra of (a) **TPEBDP1**, (b) **TPEBDP2**, (c) **TPEBDP3** in THF/water mixtures at different water contents; (d) The change of PL intensity with increasing water fraction.

The PL spectra of the three tri-TPE-substituted BODIPYs (**3TPEBDPx**) are shown in Figure 4.7. The emission maxima in THF were observed at 689, 646, and 648 nm respectively. With the gradual increase of the water content in the THF/water mixture, the PL intensities decreased up to 60 vol.%, 40 vol.%, and 50 vol.% water fraction, respectively, for **3TPEBDP1/2/3**. Continued water addition causes aggregate formation which results in increased PL intensities by reaching the highest value at 90 vol.% water. The PL intensity of the aggregated samples (90% water) compared to pure THF solution is ca. 1.53 times higher for **3TPEBDP1**, 1.5 times higher for **3TPEBDP2**, and 1.40 times higher for **3TPEBDP3**, thus showing a clear, but moderate AIE effect. (see Figure 4.7 (d))

The addition of two extra TPE units to the **TPEBDPx** series induces a more pronounced AIE effect, as expected, due to the increased number of rotor units if compared to the mono-TPE-substituted analogues.

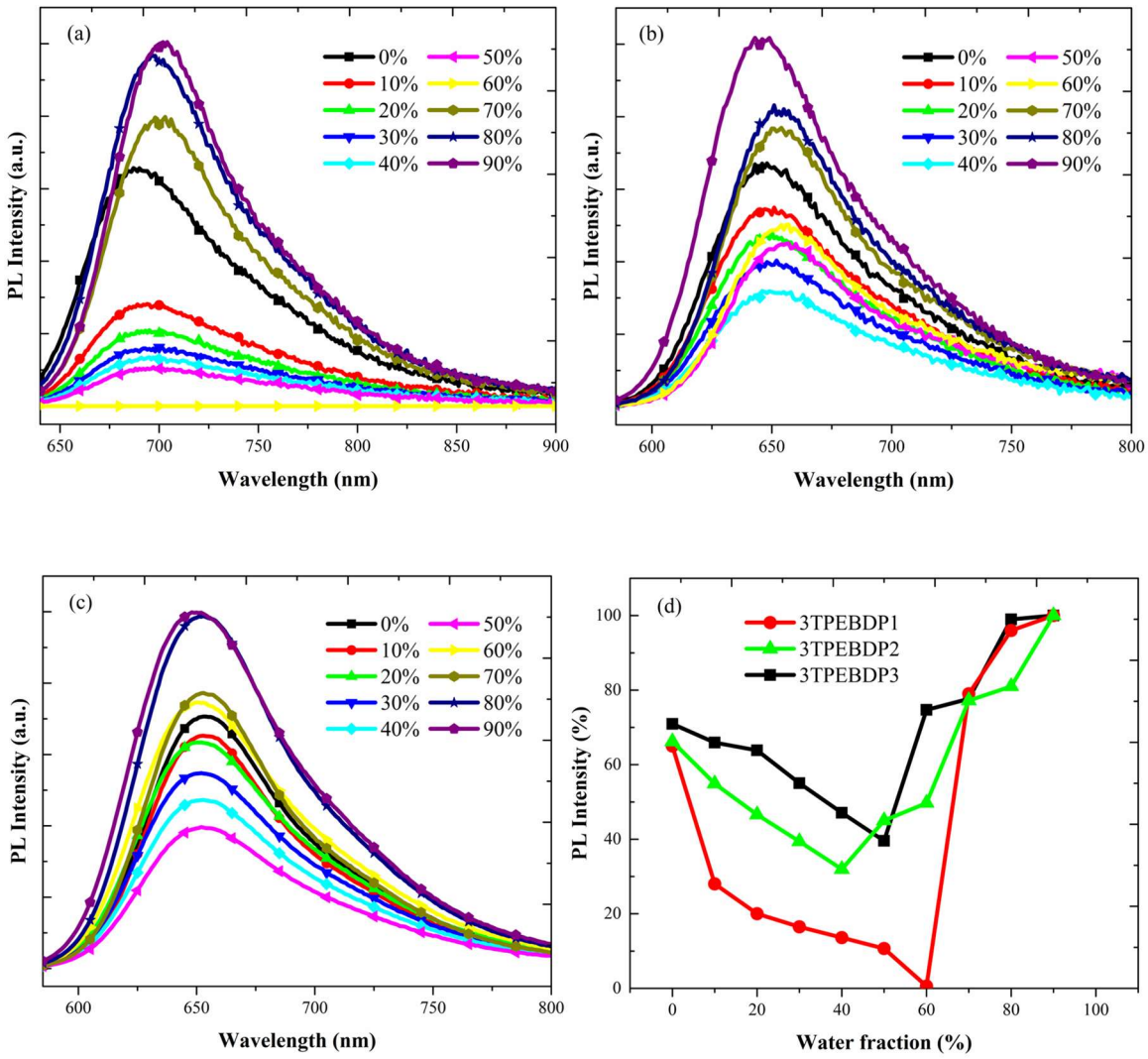

Figure 4.7 PL spectra of (a) **3TPEBDP1**, (b) **3TPEBDP2**, (c) **3TPEBDP3** in THF/water mixtures of different water contents; (d) The change of PL intensity with increasing water fraction.

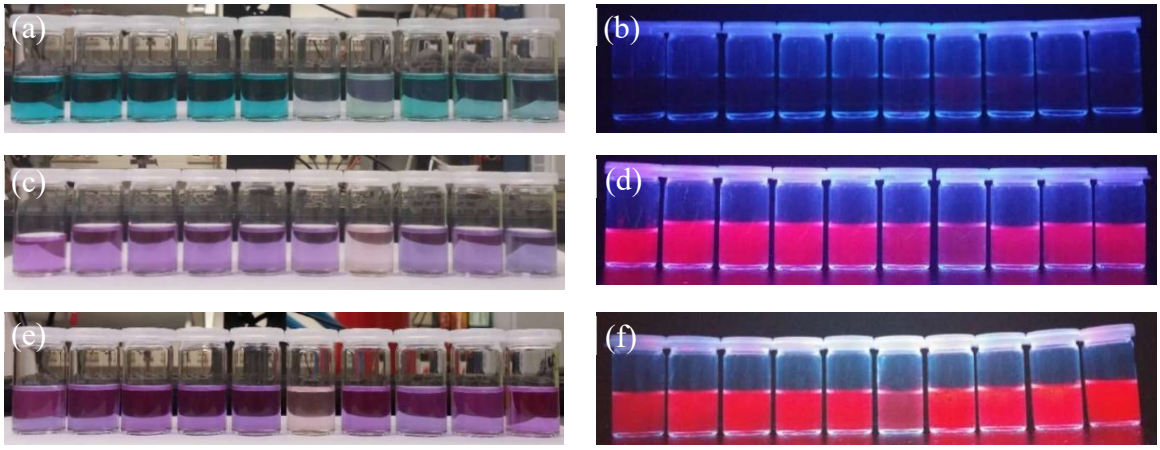

Figure 4.8 Colour images under daylight (a) **3TPEBDP1**, (c) **3TPEBDP2**, (e) **3TPEBDP3**, and fluorescence images under UV excitation (365 nm) (b) **3TPEBDP1**, (d) **3TPEBDP2**, (f) **3TPEBDP3**.

4.2.4. Temperature-dependent photoluminescence properties

Experiments done by Tang and coworkers[27] have shown that cooling reduces the thermally induced (or activated) molecular rotations thus causing an enhancement of the photoluminescence intensity. Therefore, the temperature-dependent fluorescence intensity of the small molecules **TPEBDPx** and **3TPEBDPx** in thin films was studied, as depicted in Figure 4.9.

For the **TPEBDPx** series, the PL intensities are enhanced by a factor of 1.7, 10.2 and 2.6, respectively, as the temperature is dropped from 300 K to 7 K. In the PL spectra of **TPEBDP1** the two emission peaks at 670 nm and 729 nm were hypsochromically shifted to 639 nm with a shoulder at 655 nm after cooling. The spectral profile of **TPEBDP2** and **TPEBDP3** were virtually unaffected by lowering the temperature. However, **TPEBDP3** showed a hypsochromic shift of ~ 20 nm while no shift was observed for **TPEBDP2**.

For the **3TPEBDPx** series, the PL intensities are enhanced by a factor of 3.0, 2.1 and 2.4, respectively, as the temperature is dropped from 300 K to 7 K. As effect of cooling on the PL spectra of **3TPEBDP1** an 8 nm bathochromic shift is observed accompanied by the occurrence of an additional, pronounced shoulder at 805 nm. In the case of **3TPEBDP2** and **3TPEBDP3**, no spectral shifts are observed. However, shoulders for **3TPEBDP2** at 750 nm, and for **3TPEBDP3** at 715 nm are more pronounced at 7 K. The shoulders for all **3TPEBDPx** derivatives can be interpreted as vibrational sidebands (0-1 transition).

In conclusion, cooling-enhanced emission was observed for all mono- and tri-TPE-substituted BODIPY small molecules due to a reduced amount of molecular rotations.

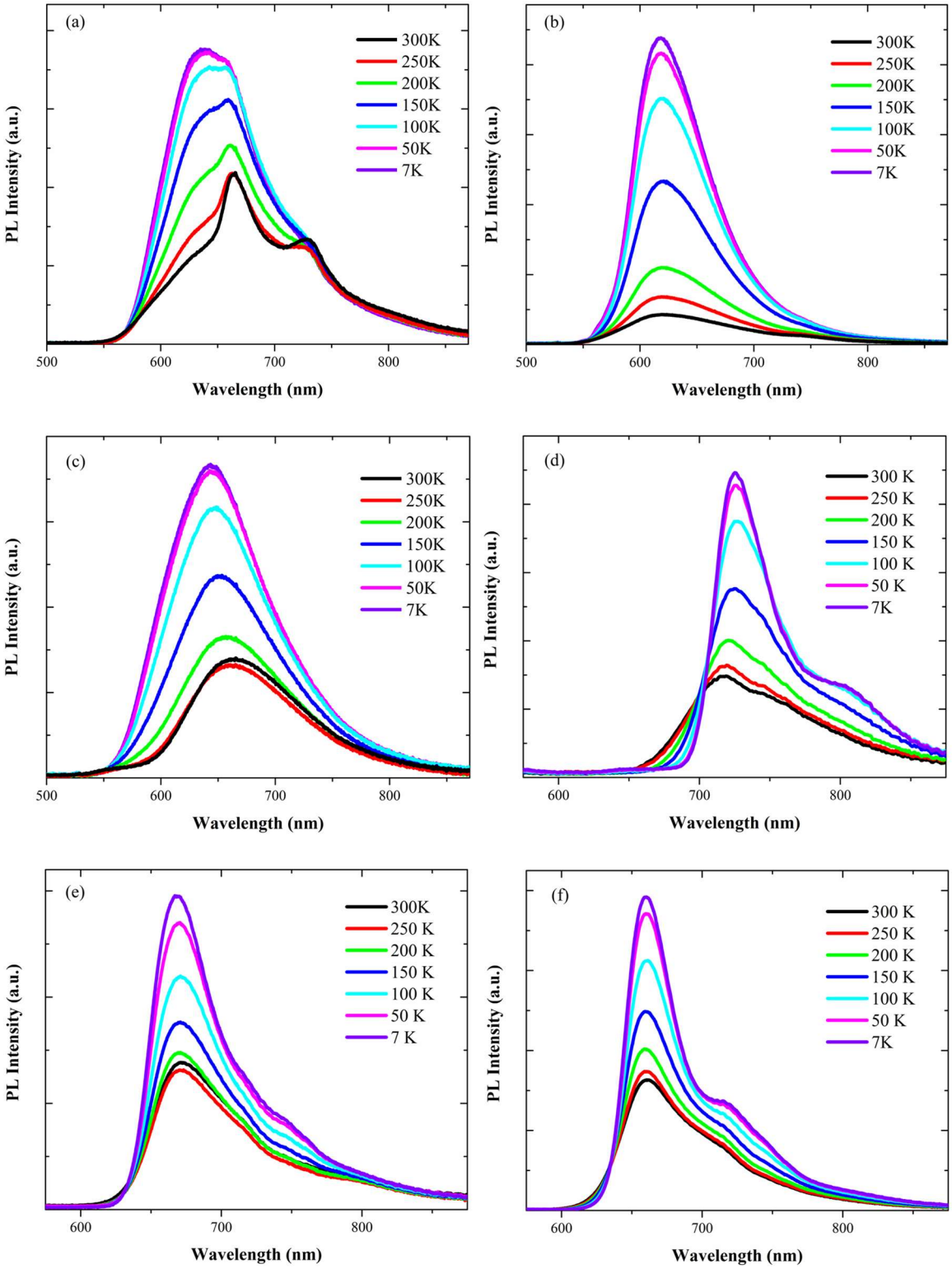

Figure 4.9 PL spectra of (a) **TPEBDP1**, (b) **TPEBDP2**, (c) **TPEBDP3**, (d) **3TPEBDP1**, (e) **3TPEBDP2**, (f) **3TPEBDP3** thin films measured at low and room temperatures in a He-cooled cryostat. Samples were excited with a 450 nm laser diode (average power < 1 mW).

4.2.5. OLEDs

Given that the highest PL efficiencies were obtained for the **3TPEBDPx** series, with **3TPEBDP2** and **3TPEBDP3** most benefitting from the AIE effect in the solid-state, it was decided to focus on these materials in the fabrication of OLEDs. Furthermore, **3TPEBDPx** molecules, presented here for the first time, are attractive since a significant fraction of their emission (78%, 43% and 35% for **3TPEBDP1, 3TPEBDP2** and **3TPEBDP3**, respectively) is in the NIR region (> 700 nm). In this spectral range, PL efficiencies up to 50 % in the solid-state (film from toluene) (Table 4.3) are, in general, difficult to achieve, mainly due to ACQ and the so-called "Energy-gap law".[28]

OLED devices were fabricated in cooperation with the group of Professor Franco Cacialli from London Centre for Nanotechnology, University College London (UCL).

As indicated in section 4.2.2.1, the homogeneity of the emitting layer is indeed an important prerequisite to fabricate efficient light-emitting devices, Therefore, toluene was used as the solvent for all OLED film preparations from this point onwards.

4.2.5.1. Photophysical properties of 3TPEBDPx:F8BT blends

For an optimization of the OLED performance of the final devices, the **3TPEBDPx** molecules were blended into poly(9,9-dioctylfluorene-*alt*-benzothiadiazole) (F8BT), which is a well-established green emitting semiconducting polymer.[3] Among the plethora of commercially available semiconducting polymers, F8BT was selected as the host polymer for mainly two reasons: first of all, its emission (Figure 4.10 (left)) perfectly overlaps with the absorption of **3TPEBDPx**, thereby allowing for an efficient energy transfer to the red/NIR emitting **3TPEBDPx** dopants. Secondly, and most importantly, the HOMO (−6.0 eV) and LUMO (−3.3 eV) of F8BT enable the formation of a 'so-called' type I or straddling heterojunction when blended with **3TPEBDPx** molecules, whose energies of the frontier molecular orbitals are listed in Table 4.3. Namely, the narrower energy bandgaps of **3TPEBDPx** are completely encompassed by the larger one of F8BT, thus forming a straddling heterojunction, which favours exciton localization and prevents exciton dissociation.

Prior to integration of the blends into OLEDs, the optical properties of such solid-state mixtures were characterized, also to identify if the AIE effect is conserved. To this aim, different concentrations of **3TPEBDPx** molecules in F8BT were investigated to find

out the best suited blend ratio in terms of quenching of the residual F8BT emission and a maximum PL efficiency. The absorption and corresponding emission spectra of such blend films are depicted in Figure 4.10 (right), whereas the Φ_F values are collected in Table 4.5.

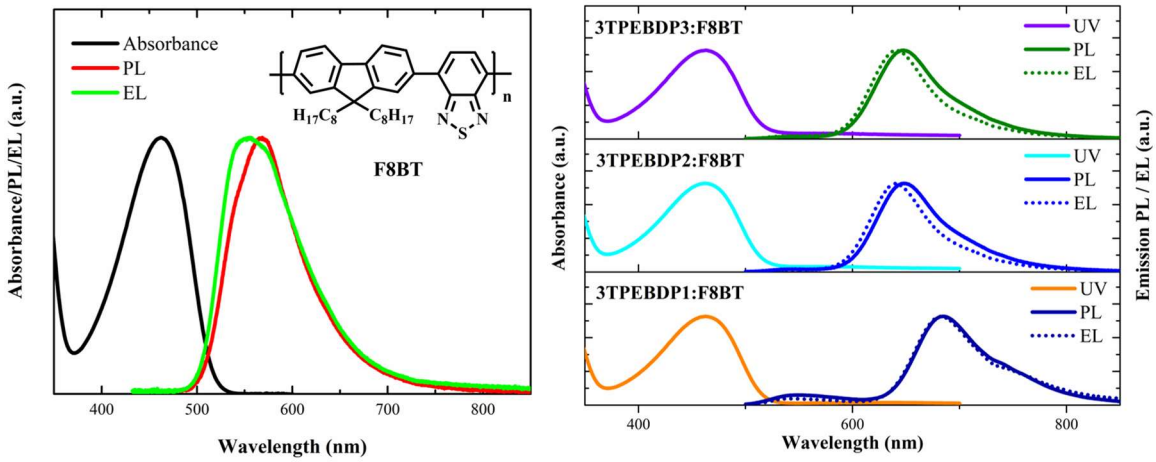

Figure 4.10 (Left) Absorption, PL, EL spectra and chemical structure of F8BT, (Right) Absorption, PL and EL spectra (dotted lines) of **3TPEBDPx:F8BT** blends with 1 w/w% of **3TPEBDPx** loading. The absorption spectra of the blends are dominated by the F8BT band peaking at 460 nm.

When looking at the absorption spectra in Figure 4.10 (right), it can be noted that the extinction profile is dominated by the F8BT absorption, as expected for a 99:1 blend. Nonetheless, at only 1 w/w% of **3TPEBDPx**, the solid-state emission of the F8BT host is almost completely quenched for all three **3TPEBDPx**, thanks to the efficient resonant energy transfer from the polymeric host to the emitters. Among the three molecules, **3TPEBDP1** is the one in which the ratio between the F8BT and acceptor emission shows the highest value, e.g. there is a significant portion of F8BT emission still present.

The **3TPEBDP1:F8BT** blend not only exhibits the most prominent portion of green emission from the host, but also, looking at Table 4.5, shows the lowest Φ_F. This means that, although the Φ_F value is increased from 10 % to 47 % after blending into F8BT (Table 4.5), some aggregation quenching affects the **3TPEBDP1** PL performance also in blends with F8BT and prevents the attainment of higher PL efficiencies. On the other hand, 1 w/w% blends of **3TPEBDP2** and **3TPEBDP3** in F8BT display Φ_F values of 96-100 %, and almost no residual green emission from the F8BT host. Also, higher doping levels were tested for **3TPEBDP2** and **3TPEBDP3** (up to 50 w/w%), but a decrease of the PL efficiency was observed when the **3TPEBDPx** content exceeds 1 %. Therefore, it has been

concluded that a concentration of 1 % **3TPEBDP2** and **3TPEBDP3** in the blend is optimal for maximizing both the PLQY and the energy transfer from F8BT to the guest molecules.

Table 4.5 PL quantum efficiency (Φ_F) of neat films and 1 w/w% **3TPEBDP1:F8BT** blends. PL efficiency values are to be considered with a 10 % uncertainty on the absolute value. For the PL efficiency experiments on the blends, samples were excited with a 450 nm laser diode (average power below 1 mW) to selectively excite the F8BT matrix. [a] The F8BT values is taken from literature.[1]

	Toluene
	Φ_F film [%]
F8BT [a]	47
Neat 3TPEBDP1	10
1% 3TPEBDP1	47
Neat 3TPEBDP2	39
1% 3TPEBDP2	96
Neat 3TPEBDP3	48
1% 3TPEBDP3	100

4.2.5.2. Fluorescence lifetime measurements of 3TPEBDPx:F8BT blends

The PL decays of both the bare **3TPEBDPx** films and the blends with F8BT were also measured. The evolution of the PL decay at varying **3TPEBDPx** concentration is illustrated in Figure 4.11, whereas the PL lifetimes (τ) and the radiative (k_R) and non-radiative (k_{NR}) decay rates are reported in Table 4.6. The k_R and k_{NR} values were obtained from the equation $\Phi_F = k_R /(k_R + k_{NR})$ and $\tau = 1/(k_R + k_{NR})$. It is noted that the k_R and k_{NR} values, as reported in Table 4.6, for the blends are probably less accurate compared to those of the neat films, as part of the emitted photons that account for the corresponding Φ_F originate from the unquenched F8BT matrix (Figure 4.10). However, such an approximation in the calculation of k_R and k_{NR} is reasonably plausible, given the substantial increase of τ and Φ_F when **3TPEBDPx** molecules are embedded into F8BT.

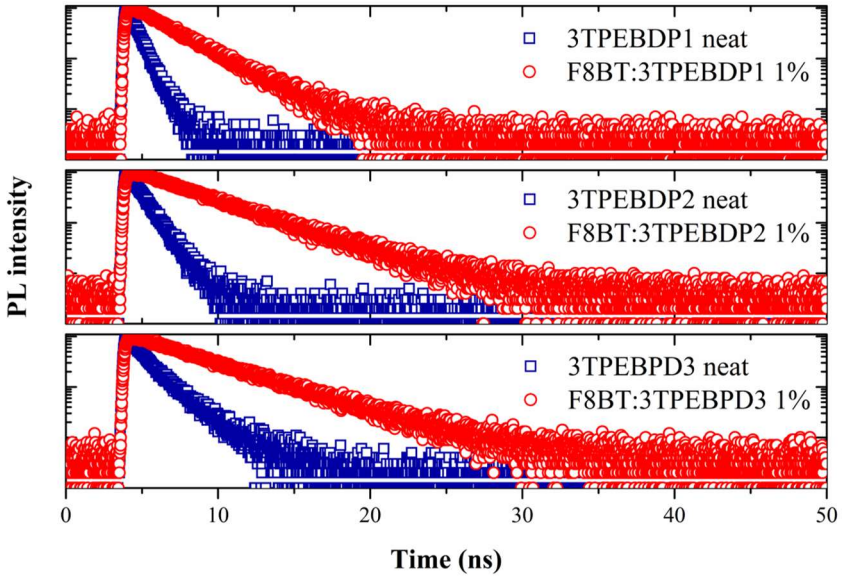

Figure 4.11 PL decays of the **3TPEBDPx** and **F8BT:3TPEBDPx** films. Decays were measured with a time-correlated single photon counting setup by exciting the films with a 445 nm picosecond pulsed laser.

Looking first at the neat **3TPEBDPx** films, (see Table 4.6) the k_R value for **3TPEBDP1** is about half compared to the ones of **3TPEBDP2** and **3TPEBDP3**. Such a lower radiative rate further supports the discussion above, confirming that intermolecular interactions, that means ACQ, are more pronounced in **3TPEBDP1** films compared to the other two system. Furthermore, the **3TPEBDP1** films also show non-radiative deactivation rates that are more than twice as high compared to the other two compounds. This suggests a limited AIE-induced PL enhancement for **3TPEBDP1**, at least in the solid-state films.

Now moving to the blends, as suggested already from the increasing Φ_F values, the AIE-effect is verified for all systems, i.e., k_{NR} is reduced to a much larger extent if compared to k_R. For **3TPEBDP2** and **3TPEBDP3**, this conclusion is somehow trivial, given that the Φ_F in F8BT is near 100 %, undoubtedly meaning that almost all non-radiative exciton recombination processes, including intermolecular rotations, are excluded, rather more efficiently than in the neat films. However, it is worth highlighting that, although $k_{NR} \sim 0$, also k_R decreases by a factor of about two, suggesting that intermolecular interactions, either in the ground state or in the excited state (excimer or exciplex formation), are probably enhanced in the blends if compared to the neat films.

Table 4.6 PL quantum efficiency (Φ_F) of neat films and 1 w/w% **3TPEBDP1:F8BT** blends, PL lifetime and calculated radiative (k_R) and non-radiative (k_{NR}) deactivation rates.

	Φ_F film [%]	τ [ns]	k_R [ns^{-1}]	k_{NR} [ns^{-1}]
Neat 3TPEBDP1	10	0.68	0.15	1.33
1% 3TPEBDP1	47	2.7	0.17	0.20
Neat 3TPEBDP2	39	1.01	0.39	0.60
1% 3TPEBDP2	96	4.29	0.22	0.01
Neat 3TPEBDP3	48	1.34	0.36	0.38
1% 3TPEBDP3	100	4.56	0.22	0

Concerning the **F8BT:3TPEBDP1** blends, k_{NR} is reduced even more dramatically from 1.3 ns^{-1} down to 0.2 ns^{-1}, meaning that the effectiveness of the non-radiative processes responsible for the reduction of Φ_F in **3TPEBDP1** where going from 47 % in solution to 10 % in film (Table 4.3) is mitigated when **3TPEBDP1** is diluted in a F8BT matrix. On the other hand, k_R exhibits only a slight increase from 0.15 to 0.17 ns^{-1} in the 1 % blend, although the residual F8BT emission might also account for such a little variation compared to the factor of two decrease of k_R observed for **3TPEBDP2** and **3TPEBDP3**. This results also mean that, in analogy to what is observed for **3TPEBDP2** and **3TPEBDP3**, dilution in F8BT does not suppress intermolecular interactions between **3TPEBDP1** molecules. Besides, electronic interactions between **3TPEBDPx** and F8BT chains cannot be ruled out either.

4.2.5.3. OLED characterization with 3TPEBDPx:F8BT blends as active, emitting layers

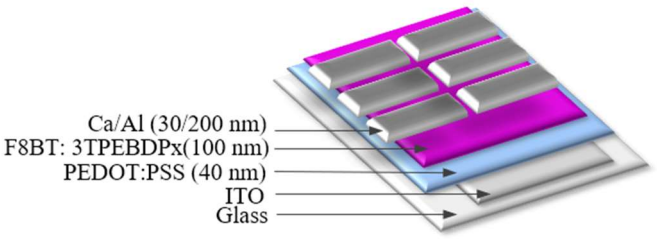

Figure 4.12 The device structure of the prepared OLEDs

OLEDs were fabricated by sandwiching the **3TPEBDPx:F8BT** blends between ITO/PEDOT:PSS anodes and Ca/Al cathodes as shown in Figure 4.12. The deposition techniques are explained in the experimental section. The electroluminescence (EL) spectra of such blends are reported in Figure 4.10, whereas the density-voltage-radiance (JVR) and external quantum efficiency (EQE) versus current density plots are reported in Figure 4.13. The OLEDs characteristics are summarised in Table 4.7.

By looking at Figure 4.10, the EL spectra of the blends show an only slight (~ 5 nm) blue-shift if compared to the PL spectra. Furthermore, as for the PL, the EL from the F8BT host is efficiently quenched in favour of the red/NIR emission from the **3TPEBDPx** dopants. In terms of device performance, the best efficiencies were obtained for the **F8BT:3TPEBDP2** blend, which exhibited an average EQE of 1.47 %, with a peak value at 1.82 %. Such values are remarkably high, considering that they are achieved from solution-processed devices, not optimized for charge injection/transport and photon out-coupling. Moreover, the maximum radiance reaches up to 2 mW/cm^2 for **F8BT:3TPEBDP2** devices, with a turn-on voltage as low as 3 V.

Although slightly less efficient (maximum EQEs up to 1.3 %), also devices incorporating **F8BT:3TPEBDP3** blends exhibited radiances up to 2 mW/cm^2, and V_{ON} ~ 3 V. Notably, whereas the EL V_{ON} of both **F8BT:3TPEBDP2** and **F8BT:3TPEBDP3** blends match the one of the neat F8BT devices[1] (Figure 1.11), the EQE and radiance values reported in Table 3 exceed those measured from the undoped F8BT OLEDs, for which maximum EQE and radiance were measured as 0.86 % and 1.1 mW/cm^2, respectively.

Table 4.7 Summary of OLEDs device data of **F8BT:3TPEBDPx** OLEDs. [a] Average maximum EQE. [b] Maximum EQE

	V_{ON} [V]	Radiance [mW/cm^2]	$<EQE_{MAX}>$ [a] [%]	EQE_{MAX} [b] [%]
1% 3TPEBDP1	4.3 ± 0.6	0.91 ± 0.55	0.51 ± 0.37	1.29
1% 3TPEBDP2	3.2 ± 0.3	1.60 ± 0.18	1.47 ± 0.21	1.82
1% 3TPEBDP3	3 ± 0.2	1.62 ± 0.41	1.16 ± 0.13	1.31

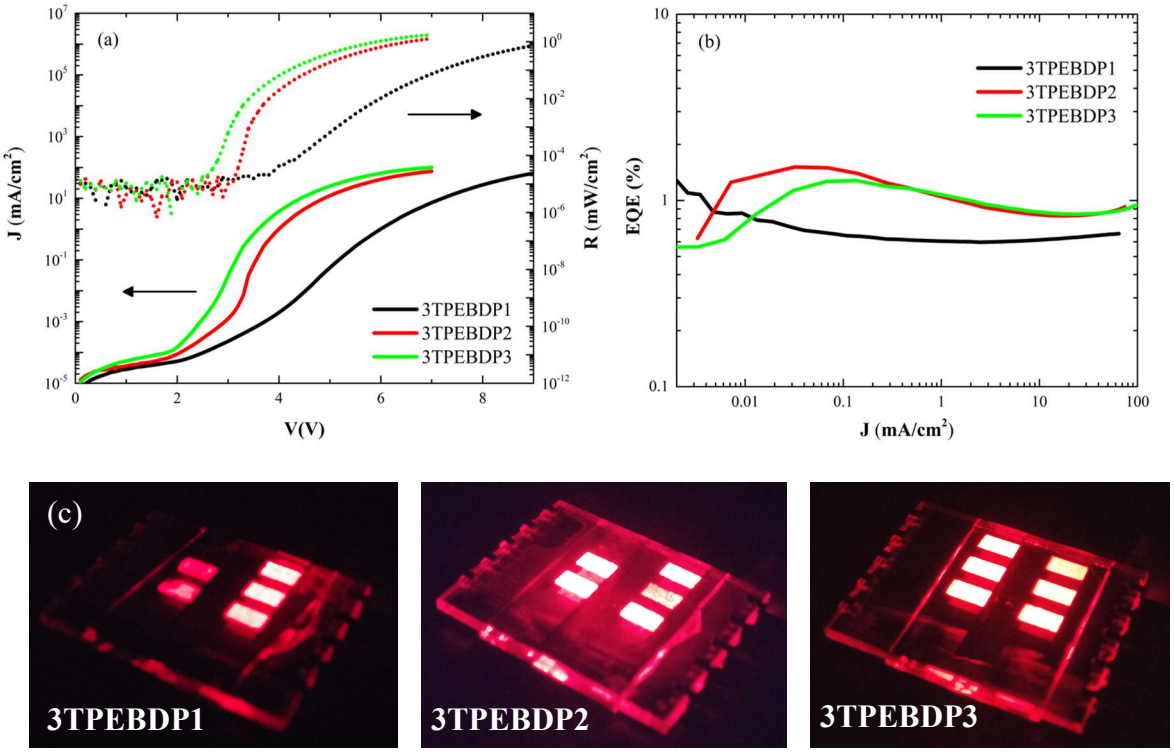

Figure 4.13 (a) JVR curves and (b) EQE versus current density plots of OLEDs incorporating **F8BT: 3TPEBDPx** (1%) blends, (c) photos of the fabricated OLEDs.

4.3. Conclusion

In summary, red/NIR emitting TPE/BODIPY- homo- and copolymers, as well as small molecule-type mono-TPE-substituted and tri-TPE-substituted BODIPY derivatives were synthesized and their AIE properties were investigated. Due to the high solid-state emission efficiency of tri-TPE-substituted materials, OLED devices were fabricated and showed EQE values exceeding 1 % for NIR-emitting **3TPEBDP2:F8BT** and **3TPEBDP3:F8BT** blends as ‘‘metal-free’’ active layers. To the best of our knowledge, such efficiencies, together with low turn-on voltage (2.5-4 V) and radiances reaching up to 2 mW/cm^2, are unprecedented for AIE OLEDs emitting in this spectral range (600-800 nm), that are fabricated by solution processing. Further optimization may lead to further progress, also for use in biomedical and communication applications.

4.4. Experimental

4.4.1. Materials and instrumentation

The starting materials (2-bromo-1,2-diphenylvinyl) benzene and 4-formylphenylboronic acid were obtained from commercial suppliers and used without further purification. All reactions were carried out under argon atmosphere by standard and Schlenk techniques, if not specified otherwise. The solvents were used as commercial p.a. quality. Dry solvents were bought from Acros.

NMR spectra were recorded on a Bruker AVANCE 400 or AVANCE III 600. APLI (Atmospheric Pressure Laser Ionization) and APCI (Atmospheric Pressure Chemical Ionization) measurements were carried out on Bruker Daltronik Bremen with micrOTOF. Gas Chromatography Mass Spectrometry (GC-MS) measurements were recorded on either a GC17AQP5050 or a 7890GC gas chromatograph by Shimadzu with 5975C MS detector by Agilent Technologies. Matrix Assisted Laser Desorption Ionisation (MALDI) measurements were carried out using a Bruker Reflex TOF at the Max Plank Institute for Polymer Research in Mainz. FD-Mass measurements were carried out using AccuTof GCX by JEOL GmbH. UV-visible absorption spectra were recorded on a Jasco V-670 spectrometer and PL spectra on a Horiba Fluoromax-4. The HOMO (highest occupied molecular orbital) levels were estimated on a Surface Analyzer MODEL AC-2 from RIKEN, given as the threshold where photoelectron emission first occurs. The TGA were recorded with TGA/DSC1 STAR^e System, Mettler Toledo. The T_m (Melting Point) determination were carried out with DigiMelt SRS MPA160 (The range 50°C-260°C). **AIE Characterization:** To understand the AIE features of the materials, their luminescent behaviour upon aggregation in aqueous media was investigated by photoluminescence (PL) spectroscopy. Photoluminescence was collected from a Horiba Fluoromax-4 spectrofluorometer, and excitation wavelength for each sample indicated in Section 4.2.2. For the preparation of samples, dry tetrahydrofuran (THF) was selected as a good solvent while water was selected as aggregation-inducing non-solvent. Stock solutions were prepared. Aliquots of the stock solution were transferred to 10 mL vials, and appropriate amounts of THF were added with a micropipette. Then, water was added dropwise to each vial with an increasing fraction (between 0–90 vol% water). The final mixture concentrations were fixed to 10^{-6} M. PL measurements of 10 samples for each compound were performed immediately. **3TPEBDPx: F8BT blend film preparation and optical**

characterization: Thin films were spin-casted onto fused silica substrates from 10 mg/mL toluene solutions. The films were deposited via spin-coating to obtain a thickness of ~100 nm, measured with a Dektak profilometer. Photoluminescence was collected from an Andor Shamrock 163 spectrograph coupled with an Andor Newton EMCCD. The PLQY measurements were carried out using an integrating sphere setup. For all PL experiments, samples were excited by using 450 nm and 520 nm laser diodes (average power below 1 mW). Time-resolved PL measurements were carried out with a time-correlated single photon counting (TCSPC) spectrometer as previously reported.[29] **OLED Fabrication and Characterization:** OLEDs were fabricated by sandwiching the polymer and blend films between ITO/PEDOT: PSS anodes and Ca/Al cathodes. ITO substrates were cleaned with acetone and isopropanol in an ultrasonic bath and treated in an O_2 plasma chamber for 10 min. A 40 nm layer of PEDOT: PSS (Sigma Aldrich) was spin-coated at 5000 rpm from a 2.8 wt.% dispersion in water and annealed at 150 ^oC for 10 min. The active layer was spin-coated on top of the annealed PEDOT: PSS in N_2 environment from the same 10 mg/mL toluene solutions used for the optical characterization in the solid-state. A Ca/Al (30/200 nm) cathode was thermally evaporated on top. The samples were then encapsulated with a UV curable epoxy resin (OSSILA E132) and measured in air using a Keithley 2400 source meter for both the current measurements and the voltage supply. The optical output of the OLEDs were measured with a calibrated silicon photodiode, and the EL spectra were collected with the same spectrometer employed for the PL experiments.

4.4.2. Synthesis of small molecules (TPEBDPx and 3TPEBDPx series) and polymers (TPEBDPx-HP and TPEBDPx-CP series)

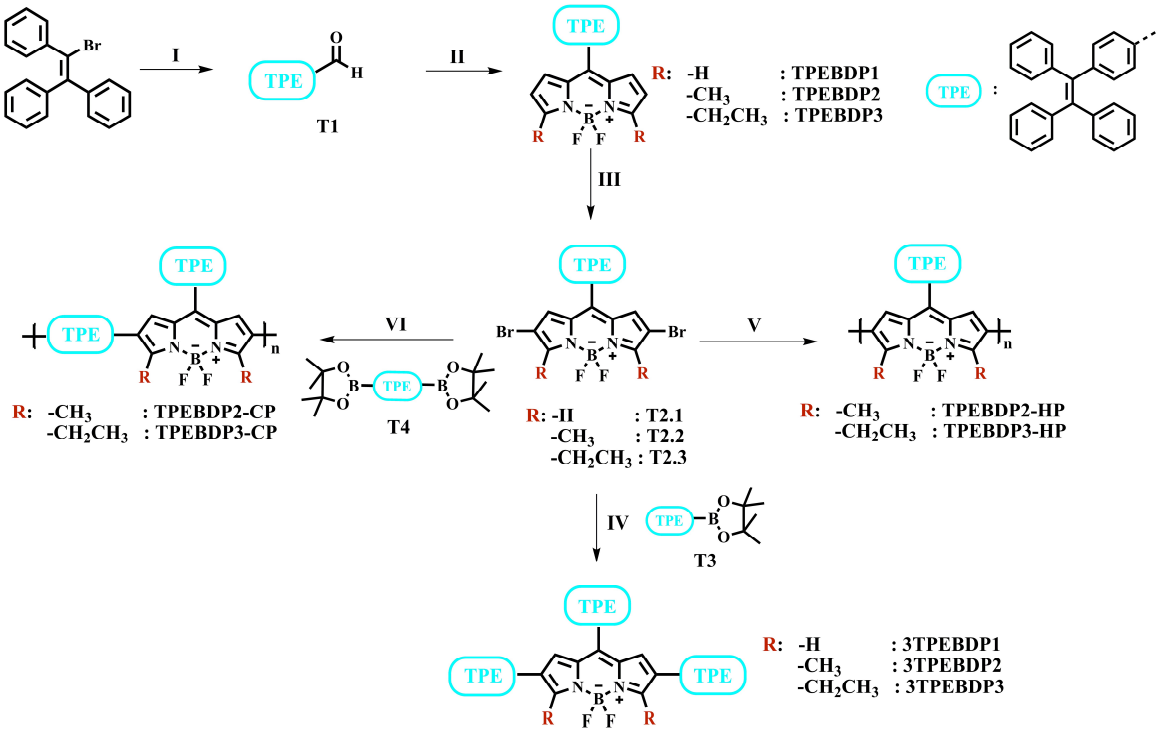

Scheme 4.2 Synthesis route for TPE-substituted BODIPY-based small molecules and polymers (I: (4-formylphenyl) boronic acid, TBAB, $Pd(PPh_3)_4$, toluene. II: corresponding pyrrole, TFA, DDQ, Et_3N, $BF_3{\cdot}OEt_2$, DCM. III: NBS, DCM:DMF(50:50). IV: K_2CO_3, $Pd(PPh_3)_4$, THF:water(80:20). V: $Ni(COD)_2$, COD, bpy, THF. VI: K_2CO_3, $Pd(PPh_3)_4$, THF:water(80:20)).

4.4.2.1. Synthesis of the TPEBDPx and 3TPEBDPx series

4.4.2.1.1. Synthesis of 4-(1,2,2-triphenylvinyl)benzaldehyde (T1)[30]

Bromotriphenylethylene (3.35 g, 10 mmol) and 4-formylphenylboronic acid (2.25 g, 15 mmol) were dissolved in a mixture of dry toluene (60 mL), TBAB (0.32 g, 1.0 mmol) and 2 M aqueous potassium carbonate solution (18 mL). The mixture was stirred at room temperature for 30 min under argon gas. $Pd(PPh_3)_4$ (0.010 g, 8.70×10^{-3} mmol) was added and the mixture was heated up to 90 °C overnight. The finalization of the reaction was checked by TLC. The mixture was poured into water and the reaction product extracted with DCM. The organic layer was dried over sodium sulfate. The solvent was removed by reduced pressure. The crude product was purified by silica gel column chromatography (toluene as the solvent) to yield (**T1**) as a pale-yellow solid (85% yield).

^{1}H NMR (400 MHz, $C_2D_2Cl_4$) δ/ppm: 9.88 (s,1H), 7.60 (d, 2H), 7.20 (d,2H), 7.09-7.16 (m, 9H), 6.98-7.07 (m, 6H).

^{13}C NMR (400 MHz, $C_2D_2Cl_4$) δ/ppm: 192.5, 150.8, 143.2, 143.2, 143.1, 143.0, 139.9, 134.3, 132.2, 131.5, 131.4, 129.4, 128.2, 128.1, 128.0, 127.2, 128.0, 128.0.

GC-MS (m/z): 360.20 (calc. 360.15).

4.4.2.1.2. General procedure for mono-TPE-substituted BODIPYs (TPEBDP1/2/3)[31]

4-(1,2,2-triphenylvinyl)benzaldehyde (**T1**) (1 eq.) and the corresponding pyrrole (2.2 eq.) were dissolved in degassed dry DCM and a drop of TFA was added. The mixture was stirred at RT for 4 h under argon gas. After consumption of the aldehyde, DDQ (1.1 eq) was added and the mixture was stirred for another 40 min. After that, triethylamine (17 eq., excess) and $BF_3 \cdot OEt_2$ (40 eq., excess) were added to the mixture. After stirring for 1 h, the solvent was removed under reduced pressure. The crude product was purified by column chromatography (silica gel, eluent DCM/PE, 2:1) to give the desired mono-TPE-substituted BODIPYs.

4.4.2.1.2.1. 4,4-difluoro-8-[4-(1,2,2-triphenylvinyl)phenyl]-4-bora-3a,4a-diaza-*s*-indacene (TPEBDP1)

Yield: 14%

^{1}H NMR (400 MHz, $C_2D_2Cl_4$) δ/ppm: 7.91 (s,2H), 7.32 (d, 2H), 7.02-7.22 (m, 17H), 6.90 (d, 2H), 6.57 (dd, 2H).

^{13}C NMR (400 MHz, $C_2D_2Cl_4$) δ/ppm: 161.4, 147.7, 147.2, 144.0, 143.4, 143.2, 143.0, 140.0, 135.0, 131.8, 131.7, 131.6, 131.6, 131.5, 130.3, 128.2, 128.0, 128.0, 127.2, 127.0, 118.8.

FD-MS (m/z): 522.20 (calc. 522.20)

TGA: 255 °C (5 % weight loss) (argon).

T_m: 255 °C

4.4.2.1.2.2. 4,4-difluoro-3,5-dimethyl-8-[4-(1,2,2-triphenylvinyl)phenyl]-4-bora-3a,4a-diaza-*s*-indacene (TPEBDP2)

Yield: 18%

^{1}H NMR (400 MHz, $C_2D_2Cl_4$) δ/ppm: 7.20 (d, 2H), 6.99-7.15 (m, 17H), 6.64 (d, 2H), 6.26 (d, 2H), 2.60 (s, 6H).

^{13}C NMR (400 MHz, $C_2D_2Cl_4$) δ/ppm:157.6, 146.2, 143.3, 131.6, 131.5, 131.5, 131.3, 130.7, 130.0, 128.1, 128.0,127.0, 126.9, 119.7, 15.3.

FD-MS (m/z): 550.23 (calc. 550.23)

TGA: 272 °C (5 % weight loss) (argon).

T_m: 260 °C

4.4.2.1.2.3. 4,4-difluoro-3,5-diethyl-8-[4-(1,2,2-triphenylvinyl)phenyl]-4-bora-3a,4a-diaza-*s*-indacene (TPEBDP3)

Yield: 17%

^{1}H NMR (400 MHz, $CDCl_3$) δ/ppm: 7.26 (d,2H), 7.12-7.22 (m,13H), 7.06-7.11 (m,4H), 6.70 (d,2H), 6.37 (d, 2H), 3.10 (q, 4H), 1.37 (t, 6H).

^{13}C NMR (400 MHz, $CDCl_3$) δ/ppm: 163.3, 145.8, 143.4,143.1, 143.0, 142.8, 142.3, 140.0, 134.1, 131.3, 131.3, 131.2, 130.9, 129.8, 127.8, 127.7, 127.7, 126.8, 126.7, 126.7, 117.0, 22.0,13.7.

FD-MS (m/z): 578.26 (calc. 578.27).

TGA: 321 °C (5 % weight loss) (argon).

T_m: 178 °C

4.4.2.1.3. General procedure for 2,6-dibrominated-8-TPE-substituted BODIPYs (T2.X)

The corresponding **TPEBDP1/2/3** (1 eq.) was dissolved in a mixture of dry DCM and dry DMF (CH_2Cl_2:DMF= 1:1). N-bromosuccinimide (NBS) (2.1 eq.) was added at RT under argon and exclusion of light. The mixture was stirred for 2 h. The reaction was carried out under TLC monitoring. Next the solvents were removed under reduced pressure and the crude product was purified by column chromatography (silica-gel, eluent DCM/PE, 2:1)

4.4.2.1.3.1. 2,6-dibromo-4,4-difluoro-8-[4-(1,2,2-triphenylvinyl)phenyl]-4-bora-3a,4a-diaza-*s*-indacene (T2.1)

Yield: 75%

^{1}H NMR (400 MHz, $C_2D_2Cl_4$) δ/ppm: 7.82 (s, 2H), 7.0-7.31(m, 19 H), 6.88 (s, 2H).

^{13}C NMR (400 MHz, $CDCl_3$) δ/ppm: 161.5, 145.7, 144.3, 142.9, 142.8, 142.7, 142.4, 139.9, 131.3, 131.2, 131.2, 131.2, 129.6, 127.9, 127.8, 127.7, 107.7.

APLI (m/z): 680.018 (calc. 680.19)

4.4.2.1.3.2. 2,6-dibromo-4,4-difluoro-3,5-dimethyl-8-[4-(1,2,2-triphenylvinyl)phenyl]-4-bora-3a,4a-diaza-*s*-indacene (T2.2)

Yield: 86%

^{1}H NMR (400 MHz, $CDCl_3$) δ/ppm: 7.03-7.26 (m, 19H), 6.74 (s, 2H), 2.65 (s, 6H).

^{13}C NMR (400 MHz, $CDCl_3$) δ/ppm: 155.4, 146.7, 143.3, 142.9, 142.7, 139.7, 131.3, 131.2, 131.2, 129.7, 127.9, 127.8, 127.7, 126.8, 108.7, 13.3.

MALDI-TOF (m/z): 707.14 (calc. 708.24)

4.4.2.1.3.3. 2,6-dibromo-4,4-difluoro-3,5-diethyl-8-[4-(1,2,2-triphenylvinyl)phenyl]-4-bora-3a,4a-diaza-*s*-indacene (T2.3)

Yield: 81%

^{1}H NMR (400 MHz, $CDCl_3$) δ/ppm: 7.04-7.25 (m, 19 H), 6.75 (s, 2H), 3.05 (q, 4H), 1.37 (t, 6H).

^{13}C NMR (400 MHz, $CDCl_3$) δ/ppm: 160.5, 146.6, 143.3, 142.9, 142.7, 142.7, 142.3, 139.8, 131.3, 131.3, 131.2, 131.2, 129.7, 127.9, 127.8, 127.8, 107.7, 21.2, 12.9.

APLI (m/z): 736.08 (calc. 736.29)

4.4.2.1.4. Synthesis of 4,4,5,5-tetramethyl-2-(4-(1,2,2-triphenylvinyl)phenyl)-1,3,2-dioxaborolane (T3)

A 2.3 M solution of *n*-BuLi (6.34 mL, 14.59 mmol) was added to a solution of bromotetraphenylethylene[32] (4 g, 9.72 mmol) in dry THF (60 mL) at -78 °C under argon. After 4 h, 2-isopropoxy-4,4,5,5-tetramethyl-1,3,2-dioxaboralane (5.95 mL, 29.2 mmol) was added. After 2 h, the mixture was warmed up slowly to RT and stirred overnight. After adding brine, the mixture was extracted with DCM. The organic layer was dried over sodium sulfate. After filtration, the solvents were reduced under pressure. The crude product was purified by column chromatography (silica gel, eluent PE/DCM, 5:1). The product was yielded as white powder (58%).

^{1}H NMR (400 MHz, $CDCl_3$) δ/ppm: 7.56 (m, 2H), 7.00-7.14 (m, 17H), 1.34 (s, 12H).

^{13}C NMR (400 MHz, $CDCl_3$) δ/ppm: 143.8, 143.5, 134.0, 131.3, 131.3, 130.6, 127.7, 127.6, 126.2, 83.6, 24.8.

GC-MS (m/z): 458.30 (calc. 458.39)

4.4.2.1.5. General Procedure of tri-TPE-substituted BODIPYs (3TPEBDP1/2/3)

The corresponding dibromo-BODIPY (**T2.1-3**) (1 eq.) and 4,4,5,5-tetramethyl-2-(4-(1,2,2-triphenylvinyl)phenyl)-1,3,2-dioxaborolane (**T3**) (2 eq.) were placed into a microwave vial together with 12 mL of dry and degassed THF under argon gas. Aqueous 2 M K_2CO_3 (3 mL) solution and $Pd(PPh_3)_4$ (0.1 eq.) were added and the mixture was heated to 110 °C in the microwave reactor for 20 min. The reaction mixture was quenched by the addition of water, then extracted with DCM and the organic phase dried over magnesium sulfate. The solvents were removed under reduced pressure. The products were purified by column chromatography (silica-gel, eluent toluene).

4.4.2.1.5.1. 4,4-difluoro-2,6,8-tris[4-(1,2,2-triphenylvinyl)phenyl]-4-bora-3a,4a-diaza-s-indacene (3TPEBDP1)

Yield: 38%

^{1}H NMR (400 MHz, $C_2D_2Cl_4$) δ/ppm: 8.8 (s, 2H), 7.00-7.38 (m, 57H), 6.93 (s, 2H).

^{13}C NMR (400 MHz, $CDCl_3$) δ/ppm: 147.5, 145.8, 143.8, 143.8, 143.6, 143.5, 141.5, 140.6, 132.3, 131.7, 131.6, 131.6, 130.4, 130.3, 128.2, 128.1, 128.0, 128.0, 127.9, 127.1, 126.7, 124.8.

APCI (m/z): 1182.49 (calc. 1182.48)

TGA: 139 °C (5 % weight loss) (argon).

T_m: Cannot be detected (Over 260 °C).

4.4.2.1.5.2. 4,4-difluoro-3,5-dimethyl-2,6,8-tris[4-(1,2,2-triphenylvinyl)phenyl]-4-bora-3a,4a-diaza-s-indacene (3TPEBDP2)

Yield: 70%

^{1}H NMR (400 MHz, $C_2D_2Cl_4$) δ/ppm: 7.24 (s, 2H), 6.95-7.17 (m, 55H), 6.65 (s, 2H), 2.67 (s, 6H).

^{13}C NMR (400 MHz, $CDCl_3$) δ/ppm: 144.1, 143.8, 143.5, 143.5, 141.5, 140.6, 132.3, 131.7, 131.6, 131.6, 130.4, 130.3, 128.2, 128.1, 128.0, 128.0, 127.9, 127.1, 126.7, 124.8, 119.7, 15.3.

FD-MS (m/z): 1210.51 (calc. 1210.52)

TGA: 132 °C (5 % weight loss) (argon).

T_m: Cannot be detected (Over 260 °C).

4.4.2.1.5.3. 4,4-difluoro-3,5-diethyl-2,6,8-tris[4-(1,2,2-triphenylvinyl)phenyl]-4-bora-3a,4a-diaza-s-indacene (3TPEBDP3)

Yield: 55%

^{1}H NMR (400 MHz, $C_2D_2Cl_4$) δ/ppm: 7.24 (d, 2H), 6.95-7.13 (m, 55H), 6.65 (s, 2H), 3.08 (q, 4H), 1.20 (t, 6H).

^{13}C NMR (400 MHz, $CDCl_3$) δ/ppm: 155.3, 144.0, 143.8, 143.5, 143.5, 141.5, 140.6, 132.3, 131.7, 131.6, 131.6, 130.4, 130.3, 128.2, 128.1, 128.0, 128.0, 127.8, 127.1, 126.6, 124.8, 117.0, 22.0,13.7.

APLI (m/z): 1238.56 (calc. 1238.55)

TGA: 368 °C (5 % weight loss) (argon).

T_m: Cannot be detected (Over 260 °C).

4.4.2.2. Synthesis of TPEBDPx-HP and TPEBDPx-CP series

4.4.2.2.1. Synthesis of (E)-1,2-diphenyl-1,2-bis(4-(4,4,5,5-tetramethyl-1,3,2-dioxaborolan-2-yl) phenyl) ethene (T4)

Dibrominated-TPE[33] (3 g, 6.12 mmol) was dissolved in dry THF (120 mL) under argon atmosphere. 2.3 M *n*-BuLi (7.58 mL, 17.44 mmol) was added dropwise to the solution at -78 °C and stirred for 2 h. 2-isopropoxy-4,4,5,5-tetramethyl-1,3,2-dioxaborolane (5.47 g, 29.4 mmol) was added in one portion to solution and stirred for another 2 h. The resulting mixture was warmed up to RT and left for overnight. Later the reaction mixture quenched with water and extracted with $CHCl_3$. The organic layer was dried over Na_2SO_4 and the solvent was removed under reduced pressure. The crude product was purified by column chromatography (silica-gel, eluent PE/DCM, 5:1). The product was yielded as white powder (42% yield).

^{1}H NMR: (400 MHz, $C_2D_2Cl_4$) δ/ppm: 7.53 (d, 4H), 7.13-6.99 (m, 14H), 1.32 (s, 24H).

^{13}C NMR: (100 MHz, $CDCl_3$) δ/ppm: 146.8, 143.5, 141.4, 134.2, 131.5, 130.8, 128.0, 126.9, 84.0, 30.0, 25.2.

APCI (m/z): 585.33 (calc. 585.37)

4.4.2.2.2. General procedure for homopolymer synthesis (TPEBDPx-HP) by Yamamoto-type polymerization

The corresponding 2,6-dibrominated-8-TPE-substituted BODIPY (**T2.X**) (1 eq), bis(1,5-cyclooctadiene)nickel(0) ($Ni(COD)_2$) (2.8 eq), 2-2'-bipyridine (2.8 eq) and 1,5-cyclooctadiene (2.6 eq) was placed in a microwave vial under argon atmosphere. The mixture was dissolved in THF (15 mL) and heated to 110 °C in the microwave for 30 min. After irradiation, the mixture was precipitated in cold methanol and the solid product was collected by filtration. The crude product was further purified by successive Soxhlet extraction with acetone, hexane, and ethyl acetate, respectively. The product was collected by extraction with chloroform. The final polymers were precipitated in cold methanol. The products were obtained as dark green powders.

4.4.2.2.2.1. TPEBDP2-HP

T2.2 (167 mg, 0.236 mmol), bis(1,5-cyclooctadiene)nickel(0) ($Ni(COD)_2$) (182 mg, 0.660 mmol), 2-2'-bipyridine (103 mg, 0.660 mmol) and 1,5-cyclooctadiene (66.3 mg, 0.613 mmol) was dissolved in 15 mL of THF.

Yield: $CHCl_3$ fraction (90 mg, 66%) as dark green powder.

^{1}H NMR (400 MHz, $C_2D_2Cl_4$) δ/ppm:7.45-7.01 (m, 19H), 6.82-6.74 (m, 2H), 2.86-2.69 (m, 6H).

^{13}C NMR (100 MHz, $C_2D_2Cl_4$) δ/ppm: 160.2, 156.4, 147.5, 143.6, 143.4, 143.1, 142.8, 140.1, 133.3, 131.7, 131.6, 131.5, 131.4, 131.1, 130.8, 130.0, 128.3, 128.1, 128.0, 127.3, 127.1, 13.8.

GPC (THF, PS standard): M_n= 29.0 kg/mol, M_w= 53.1 kg/mol

TGA: 188 °C (5 % weight loss) (argon).

4.4.2.2.2.2. TPEBDP3-HP

T2.3 (300 mg, 0.407 mmol), bis(1,5-cyclooctadiene)nickel(0) ($Ni(COD)_2$) (314 mg, 1.141 mmol), 2-2'-bipyridine (178 mg, 1.141 mmol) and 1,5-cyclooctadiene (115 mg, 1.059 mmol) was dissolved in 15 mL of THF.

Yield: $CHCl_3$ fraction (134 mg, 54%) as dark green powder.

^{1}H NMR (400 MHz, $C_2D_2Cl_4$) δ/ppm: 7.41-6.90 (m, 19H), 6.81-6.74 (m, 2H), 3.10-3.0 (m, 4H), 1.39-1.29 (m, 6H).

^{13}C NMR (100 MHz, $C_2D_2Cl_4$) δ/ppm: 162.5, 146.5, 143.5, 143.2, 143.1, 143.0, 142.4, 140.4, 131.3, 131.3, 131.2, 130.0, 128.0, 127.9, 126.9, 120.6, 21.1, 13.9.

GPC (THF, PS standard): M_n= 21.4 kg/mol, M_w= 67.3 kg/mol

TGA: 362 °C (5 % weight loss) (argon).

4.4.2.2.3. General procedure for copolymer synthesis (TPEBDPx-CP) by Suzuki-type polymerization

The corresponding 2,6-dibrominated-8-TPE-substituted BODIPY (**T2.X**) (1 eq), (E)-1,2-diphenyl-1,2-bis(4-(4,4,5,5-tetramethyl-1,3,2-dioxaborolan-2-yl)phenyl)ethane (diboronicester-TPE) (**T4**) (1 eq), tetrakis(triphenylphosphine)palladium(0) ($Pd(PPh_3)_4$) (0.1 eq) were placed in microwave vial and dissolved in 12 mL of THF under argon atmosphere. Aqueous 2 M K_2CO_3 (3mL) solution was added and the reaction mixture was heated to 110 °C in the microwave reactor for 30 min. After irradiation, the mixture was precipitated into cold methanol and the solid product was collected by filtration. The crude product was further purified by successive Soxhlet extractions with acetone, hexane, and ethyl acetate, respectively. The product was collected by extraction with chloroform. The final polymers were reprecipitated into cold methanol. The products were obtained as purple powders.

4.4.2.2.3.1. TPEBDP2-CP

T2.2 (242 mg, 0.342 mmol), **T4** (200 mg, 0.342 mmol), and tetrakis (triphenylphosphine)palladium(0) ($Pd(PPh_3)_4$) (39.5 mg, 0.034 mmol) were placed in a microwave vial and dissolved in 12 mL of THF under argon atmosphere. Aqueous 2 M K_2CO_3 (3 mL) (1.324 g, 9.58 mmol) solution was added to the reaction mixture.

Yield: $CHCl_3$ fraction (180 mg, 58%) as purple powder.

^{1}H NMR (400 MHz, $C_2D_2Cl_4$) δ/ppm: 7.39-7.01 (m, 37H), 6.80-6.75 (m, 2H), 2.85-2.70 (m, 6H).

^{13}C NMR (100 MHz, $C_2D_2Cl_4$) δ/ppm: 158.0, 147.0, 145.2, 143.3, 140.3, 140.3, 140.3, 138.7, 138.6, 138.6, 138.6, 135.8, 135.7, 133.9, 128.7, 128.7, 128.7, 128.7, 128.7, 128.6, 126.3, 126.2, 126.2, 125.7, 125.7, 110.9, 16.0, 13.2.

GPC (THF, PS standard): M_n= 5.2 kg/mol, M_w= 40.0 kg/mol

TGA: 257 °C (5 % weight loss) (argon).

4.4.2.2.3.2. TPEBDP3-CP

T2.3 (252 mg, 0.342 mmol), **T4** (200 mg, 0.342 mmol), and tetrakis (triphenylphosphine)palladium(0) ($Pd(PPh_3)_4$) (39.5 mg, 0.034 mmol) were placed in a microwave vial and dissolved in 12 mL of THF under argon atmosphere. Aqueous 2 M K_2CO_3 (3 mL) (1.324 g, 9.58 mmol) solution was added to the reaction mixture.

Yield: $CHCl_3$ fraction (160 mg, 50%) as purple powder.

^1H NMR (400 MHz, $C_2D_2Cl_4$) δ/ppm:7.45-7.10 (m, 37H), 6.84-6.75 (m, 2H), 3.15-3.05 (m, 4H), 1.40-1.30 (m, 6H).

^{13}C NMR (100 MHz, $C_2D_2Cl_4$) δ/ppm: 168.6, 155.4, 142.3, 121.1, 140.9, 140.3, 140.3, 138.6, 138.6, 138.5, 135.8, 135.6, 134.0, 128.8, 128.8, 128.7, 128.7, 128.6, 128.6, 128.6, 126.5, 126.5, 125.6, 125.6, 119.3, 107.0, 21.1, 14.0.

GPC (THF, PS standard): M_n= 4.5 kg/mol, M_w= 5.6 kg/mol

TGA: 355 °C (5 % weight loss) (argon).

4.5. References

1. S. Baysec, A. Minotto, P. Klein, S. Poddi, A. Zampetti, S. Allard, F. Cacialli, U. Scherf, *Sci. China Chem*. **2018**, *61*, 932.
2. N. Boens, W. Leen, W. Dehaen, *Chem. Soc. Rev*. **2012**, *41*, 1130.
3. A. Zampetti, A. Minotto, B. M. Squeo, V. G. Gregoriou, S. Allard, U. Scherf, C. L. Chochos, F. Cacialli. *Sci. Rep*. **2017**, *7*,1611.
4. P. Murto, A. Minotto, A. Zampetti, X. Xu, M. R. Andersson, F. Cacialli, E. Wang, *Adv. Opt. Mater*. **2016**, *4*, 2068.
5. E. Marechal, *Prog. Org. Coat*. **1982**, *10*, 251.
6. G. Ullrich, R. Ziessel, A. Harriman, *Angew. Chem. Int. Ed*. **2008**, *47*, 1184.
7. A. Louder, K. Burgess, *Chem. Rev*. **2007**, *107*, 4891.
8. R. Ziessel, G. Ulrich, A. Harriman, *New J. Chem*. **2007**, *31*, 496.
9. M. Chen, L. Li, H. Nie, J. Tong, L. Yan, B. Xu, J. Z. Sun, W. Tian, Z. Zhao, A. Qin, B. Z. Tang, *Chem. Sci*. **2015**, *6*, 1932.
10. W. Dong, J. Pina, Y. Pan, E. Preis, J. S. Melo, U. Scherf, *Polymer* **2015**, *76*, 173.
11. Z. Zhao, S. Chen, J. W. Y. Lam, Z. Wang, P. Lu, F. Mahtab, H. H. Y. Sung, I. D. Williams, Y. Ma, H. S. Kwok, B. Z. Tang, *J. Mater. Chem*. **2011**, *21*, 7210.
12. Z. Zhao, S. Chen, J. W. Y. Lam, P. Lu, Y. Zhong, K. S. Wong, H. S. Kwok, B. Z. Tang, *Chem. Commun*. **2010**, *46*, 2221.
13. Q. Zhao, S. Zhang, Y. Liu, J. Mei, S. Chen, L. Ping, A. Qin, Y. Ma, J. Z. Sun, B. Z. Tang, *J. Mater. Chem.* **2012**, *22*, 7387.
14. W. Z. Yuan, P. Lu, S. Chen, J. W. Y. Lam, Z. Wang, Y. Liu, H. S. Kwok, Y. Ma, B. Z. Tang, *Adv. Mater*. **2010**, *22*, 2159.
15. J. Luo, J. Xie, J. W. Y. Lam, L. Cheng, H. Chen, C. Qiu, H. S. Kwok, X. Zhan, Y. Liu, D. Zhu, B. Z. Tang, *Chem. Commun*. **2001**, *18*, 1740.
16. J. Mei, Y. Hong, J. W. Y. Lam, A. Qin, Y. Tang, B. Z. Tang, *Adv. Mater*. **2014**, *26*, 5429.
17. C. F. A. Gomez-Duran, R. Hu, G. Feng, T. Li, F. Bu, M. Arseneault, B. Liu, E. Pena-Cabrera, B. Z. Tang, *ACS Appli. Mater. Interfaces* **2015**, *7*, 15168.
18. R. Hu, E. Lager, A. Aguilar-Aguilar, J. Liu, J. W. Y. Lam, H. H. Y. Sung, I. D. Williams, Y. Zhong, K. S. Wong, E. Pena-Cabrera, B. Z. Tang, *J. Phys. Chem. C* **2009**, *113*, 15845.

19. M. Baglan, S. Ozturk, B. Gur, K. Meral, U. Bozkaya, O. A. Bozdemir, S. Atilgan, *RSC Advances* **2013**, *3*, 15866.
20. Q. Li, Y. Qian, *New J. Chem*. **2016**, *40*, 7095.
21. L. Zhensheng, Y. Chen, X. Lv, W. F. Fu, *New J. Chem*. **2013**, *37*, 3755.
22. R. Hu, G. F. A. Gomez-Duran, J. W. Y. Lam, J. L. Belmonte-Vazquez, C. Deng, S. Chen, R. Ye, E. Pena-Cabrera, Y. Zhong, K. S. Wong, B. Z. Tang, *Chem. Commun*. **2012**, *48*, 10099.
23. Z. Zhao, B. Chen, J. Geng, Z. Chang, L. Aparicio-Ixta, H. Nie, C. C. Goh, L. G. Ng, A. Qin, G. Ramos-Ortiz, B. Liu, B. Z. Tang, *Part. Part. Syst. Charact*. **2014**, *31*, 481.
24. H. Gao, Y. Gao, C. Wang, H. Dehua, Z. Xie, L. Liu, B. Yang, Y. Ma, *ACS. Appl. Mater. Int.* **2018**, *10*, 14956.
25. Y. Zhao, S. He, J. Yang, H. Sun, X. Shen, X. Han, Z. Ni, *Opt. Mater*. **2018**, *81*,102.
26. K. Tram, H. Yan, H. A. Jenkins, S. Vassiliev, D. Bruce, *Dyes Pigm*. **2009**, *82*, 392.
27. J. Chen, C. C. W. Law, J. W. Y. Lam, Y. Dong, S. M. F. Lo, I. D. Williams, D. Zhu, B. Z. Tang, *Chem. Mater*. **2003**, *15*, 1535.
28. R. Englman, J. Jortner, *Mol. Phys*. **1970**, *18*, 145.
29. A. Petrozza, S. Brovelli, J. J. Michels, H. L. Anderson, R. H. Friend, C. Silva, F. Cacialli, *Adv. Mater*. **2008**, *20*, 3218.
30. X. Q. Zhang, Z. G. Chi, H. Y. Li, B. J. Xu, X. F. Li, W. Zhou, S. W. Liu, Y. Zhang, J. R. Xu. *Chem. Asian J*. **2011**, *6*, 808.
31. L. Zeng, C. Jiao, X. Huang, K. W. Huang, W. S. Chin, J. Wu, *Org. Lett*. **2011**,*13*, 6026.
32. Y. Wang, I. Zhang, B. Yu, X. Fang, X. Su, Y. M. Zhang, T. Zhang, B. Yang, M. Li, S. X. A. Zhang, *J. Mater. Chem. C* **2015**, *3*, 12328.
33. W. Bai, Z. Wang, J. Tong, J. Mei, A. Qin, J. Z. Sun, B. Z. Tang, *Chem. Commun*. **2015**, *51*,1089.

CHAPTER 5

SUMMARY AND OUTLOOK

5.1. Summary of Chapters 2-4

Herein, synthesis, characterization and application of small molecules and polymers which were designed according to various structural modification strategies were demonstrated.

Among the chromophores, BODIPY gained significant attention due to its facile synthesis, structural versatility, excellent spectroscopic property and a wide range of potential applications in various research fields such as organic lasers, biosensors, bioimaging, photosensitizers, photovoltaic devices etc. However, major drawbacks such as low solid-state emission, mostly in the visible part of the spectrum, limits its usage in many applications. With this motivation, NIR absorbing organic materials were synthesized, based on anthracene-fused BODIPY units that are incorporated into novel copolymers with different types of electron-rich linker groups, made by Stille-type cross-couplings. All copolymers studied are low band gap materials and exhibited absorption bands up to 1200 nm. Optical and electronic properties of the D-A type copolymers were investigated as well as their use as semiconducting layer in n-type OFET devices. Hereby, only **P2** showed a homogeneous film morphology with a very moderate electron mobility of ~10^{-9} cm^2/Vs.

One of the critical issues that limit the solid-state application of organic materials is the aggregation-caused quenching (ACQ). However, aggregation-induced emission (AIE) as anti-ACQ photophysical phenomenon may overcome the common aggregation problem in some practical applications. In the third chapter of this thesis, polymers based on TPE units as prominent AIE-active molecules were investigated. Five different linear poly(TPE)s were synthesized by reductive polyolefination with dicobalt octacarbonyl as condensing agent. The resulting polymers showed absorption and emission in the UV-VIS region of the spectrum with high solid-state photoluminescence quantum yields of 32% - 72%. In addition to the optical and AIE properties, applications in OLEDs and for the

fluorometric detection of nitroaromatic compounds were investigated. **P4** with diphenyl ether side groups (rotors) prove itself as a promising candidate for a solid-state PL sensor for nitroaromatic analytes due to its amplified PL quenching behaviour to trinitrobenzene (TNB) as analyte. The Stern-Volmer quenching constant was calculated as 4.75 x 10^{-3} M^{-1} for the linear part of the Stern-Volmer plot for TNB concentrations up to 80 µM. Among OLEDs with the polymers **P1**, **P4** and **P5**, as active emitting layer, **P4**, showed the best EQE with 0.05% while **P5** showed the lowest turn-on voltage with 6.13 V.

The experience on two previous important topics, brought us to the point; if we can combine AIE and NIR, extension of efficiencies in the solid-state emission can be achievable while conserving the NIR-emission properties of chromophore species. With this motivation small molecules based on BODIPY cores that are functionalized with TPE unit at different positions, as well as polymers (homo- and copolymers) were synthesized. Small molecules and polymers showed absorption and emission in the red/NIR regions. For the small molecules solid-state PLQYs up to 50% were observed while for the polymers, only PLQYs of up to 3% resulted. In addition to the investigation of optical and AIE properties, the high solid-state emissive tri-TPE-substituted BODIPY molecules were used as active emissive component in OLED. Remarkably, we observed an enhancement of photoluminescence efficiencies up to ~100% by blending the TPE-substituted BODIPY fluorophores into a F8BT matrix. By incorporating these blends into OLEDs, electroluminescence spectra peaking in the range 650–700 nm are obtained, with up to 1.8% external quantum efficiency and ~2 mW/cm^2 radiance. This is a remarkable result for red/NIR emitting and solution-processed OLEDs.

5.2. Outlook

Regarding the last strategy of combining NIR photoluminescence and aggregation-induced emission, further optimization can lead to a progress in the utilization of tri-TPE-substituted BODIPY molecules for biomedical and communication purposes. In addition to this, combining the strategy of AIE and thermally activated delayed fluorescence (TADF), efficient solid-state electroluminescence with up to 100% internal quantum efficiency (IQE) could be achievable. After the fluorescent and phosphorescent materials, TADF materials are considered as third generation light emitting materials for OLEDs.[1,2] Typical TADF materials comprise D-A type structures which exhibits a relative orientation

near orthogonality. As a consequence, a small energy gap between the S_1 and T_1 states is provided which induces the activation of the reverse intersystem crossing (RISC) from T_1 to S_1 and radiative relaxation as fluorescence. One potential approach was reported by Hatakeyama et al.[3] The energy gap between S_1 and T_1 states was reduced to ~0.2 eV and allowed RISC by substituting the para-position relative to the central boron atom with nitrogen atoms (Figure 5.1, **DABNA-2**) which exhibits the opposite resonance effect of boron atoms. The incorporation of the material into OLEDs resulted in 25% EQE and ~100% IQE. Another potential approach reported by Ji et al.[4] presented an asymmetric thiophene fusion to BODIPY chromophore (Figure 5.1, **BDP-1**) promoted ISC and displayed a large triplet state quantum yield of 63.7%.

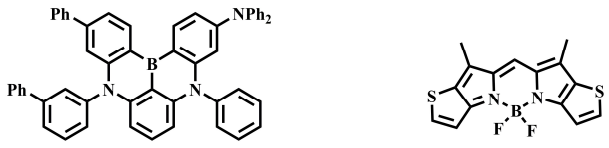

DABNA-2 BDP-1

Figure 5.1 Chemical structures showed TADF properties.[3,4]

5.3. References

1. H. Uoyama, K. Goushi, K. Shizu, H. Nomura, C. Adachi, *Nature* **2012**, *492*, 234.
2. S. Xu, T. Liu, Y. Mu, Y.-F. Wang, Z. Chi, C.-C. Lo, S. Liu, Y. Zhang, A. Lien, J. Xu, *Angew. Chem. Int. Ed*. **2015**, *54*,874.
3. T. Hatakeyama, K. Shiren, K. Nakajima, S. Nomura, S. Nakatsuka, K. Kinoshita, J. Ni, Y. Ono, T. Ikuta, *Adv. Mater*. **2016**, *28*, 2777.
4. S. Ji, J. Ge, D. Escudero, Z. Wang, J. Zhao, D. Jacquemin, *J. Org. Chem*. **2015**, *80*, 5958.

LIST OF ABBREVIATIONS

ABS	Absorbance
ACQ	Aggregation-Caused Quenching
AIE	Aggregation-Induced Emission
AIEE	Aggregation-Induced Emission Enhancement
APCI	Atmospheric Pressure Chemical Ionization
APLI	Atmospheric Pressure Laser Ionization
BDT	Benzodithiophene
BGBC	Bottom-gate bottom-contact
BGTC	Bottom-gate top-contact
BODIPY	Boron-dipyrromethene or 4,4-Difluoro-4-bora-3a,4a-diaza-*s* indacene
BTh	Bithiophene
BzT	Benzothiadiazole
ca.	*circa* (approximately)
$CHCl_3$	Chloroform
CP	Copolymer
CT	Charge Transfer
CV	Cyclic Voltammogram
D	Drain
D	Emissive Defect
D-A	Donor-Acceptor
DCM	Dichloromethane
DDQ	2,3-Dichloro-5,6-dicyano-1,4-benzoquinone
DMF	Dimethylformamide
DNT	Dinitrotoluene
DSA	Distyreneanthracene
DTP	Dithienopyrrole
E_C	Conduction band
E_g	Band gap
E_g^{EL}	Electrical band gap
E_g^{OPT}	Optical Band Gap
E_V	Valence Band
EL	Electroluminescence
Em	Emission
ET	Electron Transfer
ETL	Electron Transfer Layer
EQE	External Quantum Efficiency
ε	Molar Absorptivity
F8BT	Poly(9,9-dioctylfluorene-*alt*-benzothiadiazole)
FET	Field Effect Transistor
FMO	Frontier Molecular Orbital
FWHM	Full width at half maximum
GC-MS	Gas Chromatography Mass Spectrometry
GPC	Gel Permeation Chromatography

HH	Head to head
HOMO	Highest Occupied Molecular Orbital
HP	Homopolymer
HPS	1,1,2,3,4,5-Hexaphenyl-1H-silole
HTL	Hole Transport Layer
I	Current
IC	Internal Conversion
ICT	Intersystem crossing
I_{DS}	Drain-source current
I_{ON}/I_{OFF}	Current on/off ratio
IPA	Isopropyl alcohol
IQE	Internal Quantum Efficiency
ITO	Indium Tin Oxide
IUPAC	Internal Union of Pure and Applied Chemistry
J	Current Density
JVR	Current Density-Voltage-Radiance
k_{NR}	Non-radiative decay rate
k_R	Radiative decay rate
K_{SV}	Stern-Volmer quenching constant
LUMO	Lowest Unoccupied Molecular Orbital
MALDI	Matrix Assisted Laser Desorption Ionisation
MMA	Methyl Methacrylate
MPN	Microporous Network
μ	Mobility
μ_e	Electron Mobility
μ_h	Hole Mobility
NDI	Naphthalene-Tetracarboxylic Diimide
NIR	Near-Infrared
NMR	Nuclear Magnetic Resonance
OFET	Organic Field Effect Transistor
OLED	Organic Light Emitting Diode
OPV	Organic Photovoltaic Device
OTS	Octadecyltrichlorosilane
Ox.	Oxidation
PA	Picric Acid
PEDOT:PSS	Poly(3,4-ethylenedioxythiophene)-poly(styrenesulfonate)
pH	Power of Hydrogen
PDI	Perylene-Tetracarboxylic Diimide
PL	Photoluminescence
PLED	Polymer Light Emitting Diode
PLQY or Φ	Photoluminescence Quantum Yield
Pt	Platinum
Q	Fluorescence Quenching Defect or Analyte
Qx	Quinoxaline
R	Radiance
Red.	Reduction
RIM	Restriction of Intramolecular Motion
RIR	Restriction of Intramolecular Rotation

RISC	Reverse Intersystem Crossing
RIV	Restriction of Intramolecular Vibration
S	Source
S_0	Ground state
S_1	Singlet state
SCE	Standard Calomel Electrode
T_1	Triplet state
TADF	Thermally Activated Delayed Fluorescence
TBAP	Tetrabutylammonium perchlorate
TFA	Trifluoroacetic acid
TFT	Thin Film Transistor
TGBC	Top-gate bottom-contact
TGTC	Top-gate top-contact
THBA	10,10′,11,11′-Tetrahydro-5,5′-bidibenzo[*a,d*][7]annulenylidene
THF	Tetrahydrofuran
TICT	Twisted Intramolecular Charge Transfer
TMS	Tetramethylsilane
TNB	Trinitrobenzene
TNT	Trinitrotoluene
TPA	Triphenylamine
TPE	Tetraphenylethylene
TPP	Tetraphenylpyrazine
TT	Tail to tail
τ	Decay lifetimes
UV	Ultraviolet
V	Voltage
V_{DS}	Drain-source voltage
V_{GS}	Gate voltage
V_{OC}	Open Circuit Voltage
V_T	Threshold Voltage
Vis.	Visible
Vol.	Volume
w/w	Weight to weight

LIST OF PUBLICATIONS

1. S. Baysec, A. Minotto, P. Klein, S. Poddi, A. Zampetti, S. Allard, F. Cacialli, U. Scherf, Tetraphenylethylene-BODIPY Aggregation-Induced Emission Luminogens for Near-Infrared Polymer Light-Emitting Diodes. *Sci. China Chem.* **2018**, *61*, 932. (Chapter 4)

2. N. Gasparini, A. Garcia-Rodriguez, M. Prosa, S. Baysec, A. Palma-Cando, A. Katsouras, A. Avgeropoulos, G. Pagona, V. G. Gregoriou, C. L. Chochos, S. Allard, U. Scherf, C. J. Brabec and T. Ameri, Indacenodithienothiophene-based Ternary Organic Solar Cells. *Front. Energy Res*. **2017**, *4*, 40.

3. B. M. Squeo, V. G. Gregoriou, A. Avgeropoulos, S. Baysec, S. Allard, U. Scherf, C. L. Chochos, BODIPY-based Polymeric Dyes as Emerging Horizon Materials for Biological Sensing and Organic Electronic Applications. *Prog. Polym. Sci*. **2017**, *71*, 26.

4. S. Baysec, E. Preis, S. Allard, U. Scherf, Very High Solid-State Photoluminescence Quantum Yields of Poly(tetraphenylethylene) Derivatives. *Macromol. Rapid Commun*. **2016**, *37*, 1802. (Chapter 3)

5. S. Baysec, N. A. Unlu, S. O. Hacioglu, Y. A. Udum, A. Cirpan, L. Toppare, Electrochemical Properties of Perylene Diimide (PDI) and Benzotriazole (Btz) Bearing Conjugated Polymers to Investigate the Effect of π-Bridge on Electrochemical Properties. *J. Macromol. Sci., Pure Appl. Chem*. **2015**, *52*, 1.

LIST OF CONFERENCE PUBLICATIONS

1. S. Baysec, A. Minotto, S. Allard, F. Cacialli, U. Scherf; BODIPY-based far-red/NIR chromophores with Aggregation-Induced Emission; Poster; European Materials Research Society Fall Meeting, 2017 Warsaw, Poland.

2. S. Baysec, S. Allard, U. Scherf; Synthesis of Near-IR Absorbers as Sensitizers for Organic Electronics Devices; Poster; 19th International Krutyn Summer School 2016 Krutyn, Poland.

3. S. Baysec, S. Allard, U. Scherf; Synthesis of Near-IR Absorbers as Sensitizers for Organic Electronics Devices; Oral Poster Presentation and Poster; Macromolecular Colloquium Freiburg 2016, Freiburg, Germany.

4. S. Baysec, S. Allard, U. Scherf; Synthesis of Near-IR Sensitizers for Organic Electronics; Poster; 13th European Conference on Molecular Electronics, 2015 Strasbourg, France.

5. S. Baysec, S. Allard, U. Scherf; Synthesis of Near-IR Sensitizers for Organic Electronics; Poster; International School-Synthesis and Characterization of Conjugated Materials for Near-IR Applications, 2014 Gothenburg, Sweden.

6. S. Baysec, S. Allard, U. Scherf; Synthesis of Near-IR Sensitizers for Organic Electronics; Oral presentation and Poster; Young Polymer Scientist Forum-DWI Leibniz Institut fur Interactive Materalien, 2014 Aachen, Germany.

The CV is not included in the online version for privacy reasons.